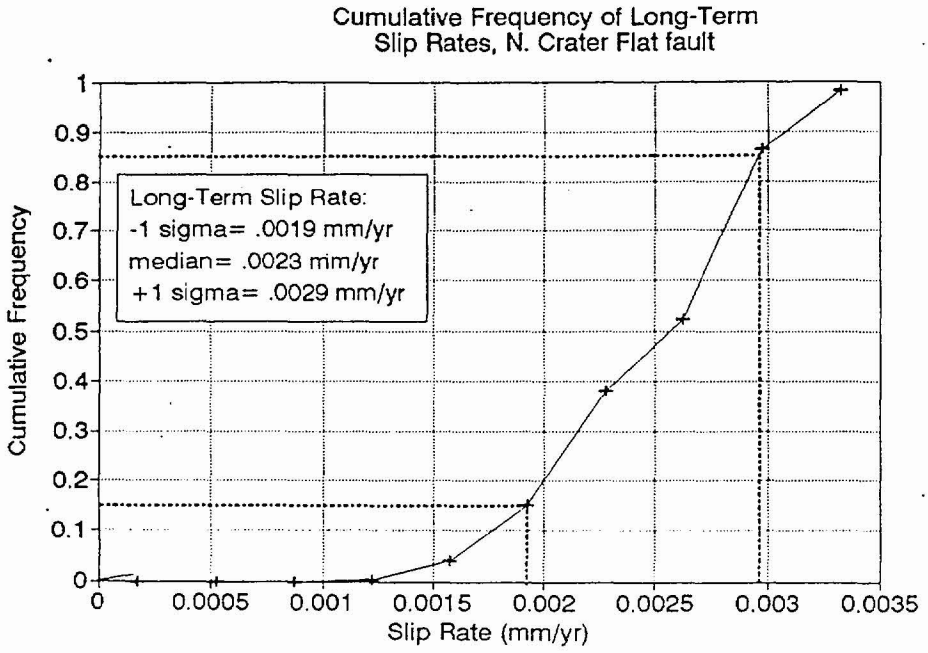
Cumulative Frequency of Long-Term Slip Rates, N. Crater Flat fault
Long-Term Slip Rate:
-1 sigma= .0019 mm/yr
median= .0023 mm/yr
+1 sigma= .0029 mm/yr
Cumulative Frequency
Slip Rate (mm/yr)
0
0.1
0.2
0.3
0.4
0.5
0.6
0.7
0.8
0.9
1
0.0005
0.001
0.0015
0.002
0.0025
0.003
0.0035

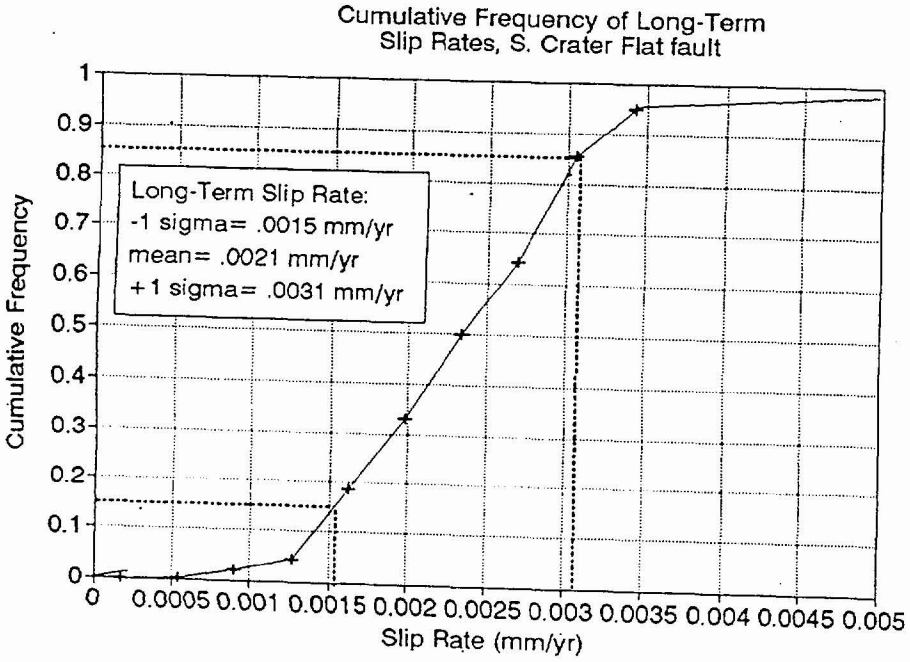
Cumulative Frequency of Long-Term Slip Rates, S. Crater Flat fault
Long-Term Slip Rate:
-1 sigma= .0015 mm/yr
mean= .0021 mm/yr
+1 sigma= .0031 mm/yr
Cumulative Frequency
Slip Rate (mm/yr)
0
0.1
0.2
0.3
0.4
0.5
0.6
0.7
0.8
0.9
1
0.0005
0.001
0.0015
0.002
0.0025
0.003
0.0035
0.004
0.0045
0.005

ASM-A1-3

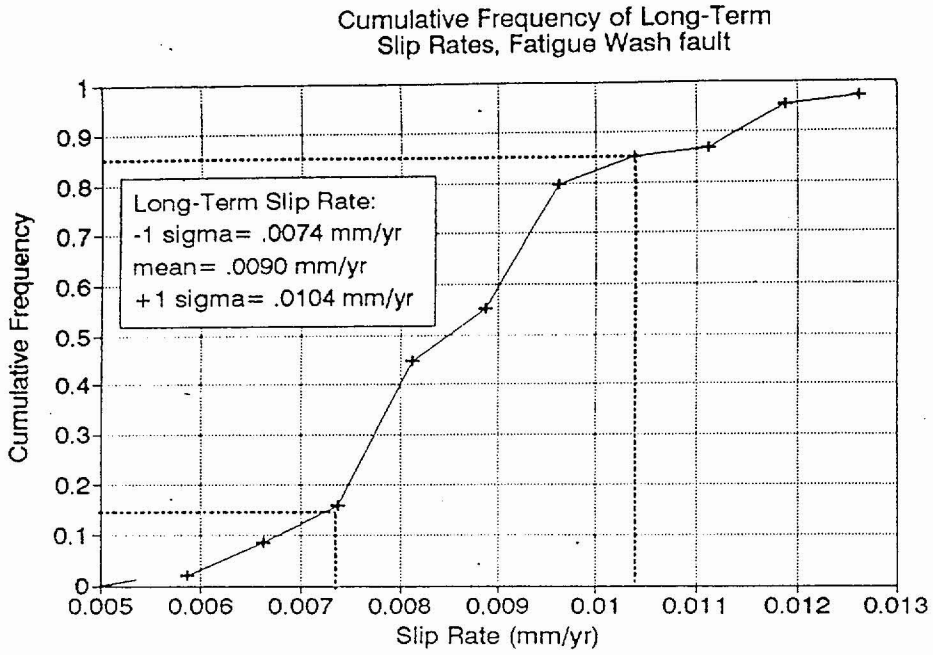
Cumulative Frequency of Long-Term Slip Rates, Fatigue Wash fault
Long-Term Slip Rate:
-1 sigma= .0074 mm/yr
mean= .0090 mm/yr
+1 sigma= .0104 mm/yr
Cumulative Frequency
Slip Rate (mm/yr)
0
0.1
0.2
0.3
0.4
0.5
0.6
0.7
0.8
0.9
1
0.005
0.006
0.007
0.008
0.009
0.01
0.011
0.012
0.013

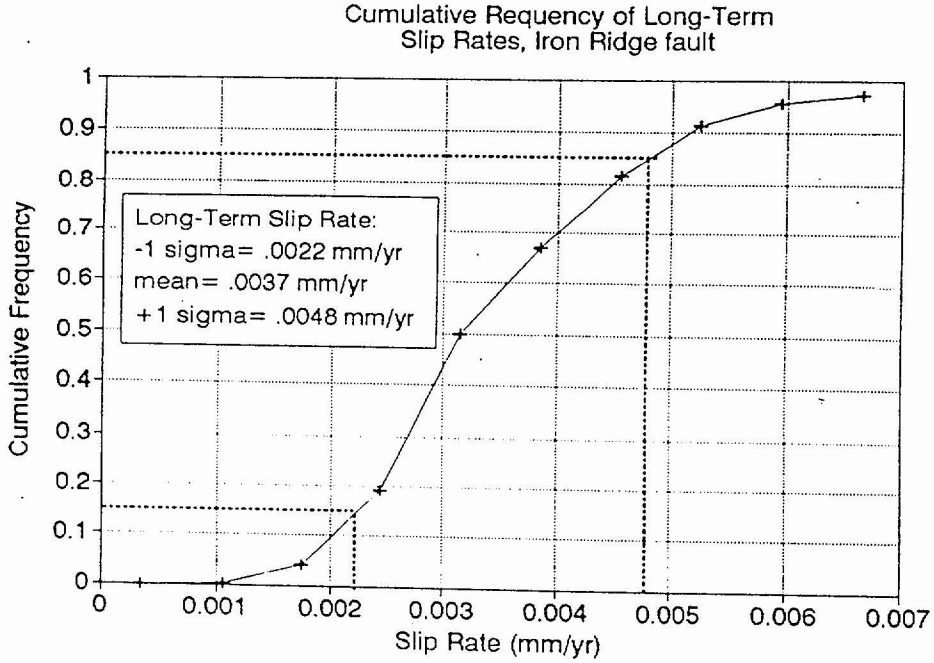
Cumulative Requency of Long-Term Slip Rates, Iron Ridge fault
Long-Term Slip Rate:
-1 sigma= .0022 mm/yr
mean= .0037 mm/yr
+1 sigma= .0048 mm/yr
Cumulative Frequency
Slip Rate (mm/yr)
0
0.1
0.2
0.3
0.4
0.5
0.6
0.7
0.8
0.9
1
0
0.001
0.002
0.003
0.004
0.005
0.006
0.007

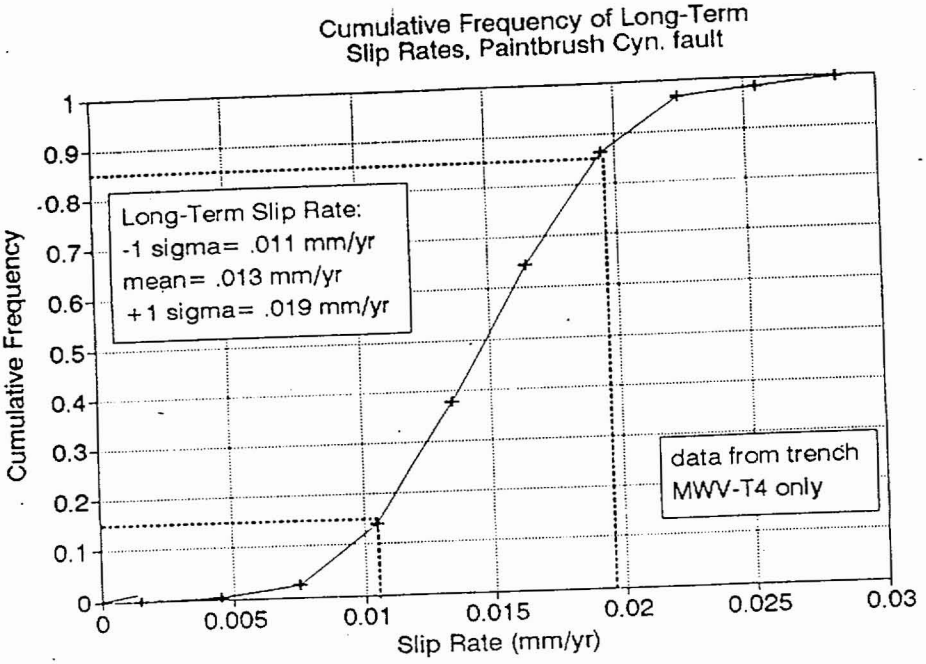
Cumulative Frequency of Long-Term Slip Rates, Paintbrush Cyn. fault
Long-Term Slip Rate:
-1 sigma= .011 mm/yr
mean= .013 mm/yr
+1 sigma= .019 mm/yr
data from trench MWV-T4 only
Cumulative Frequency
Slip Rate (mm/yr)
0
0.1
0.2
0.3
0.4
0.5
0.6
0.7
0.8
0.9
1
0.005
0.01
0.015
0.02
0.025
0.03

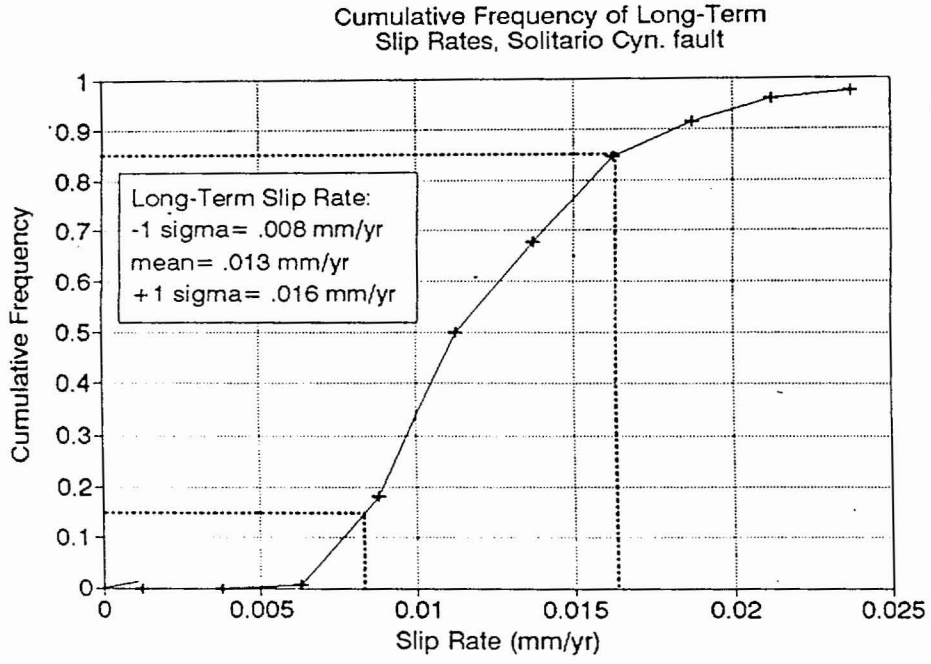
Cumulative Frequency of Long-Term Slip Rates, Solitario Cyn. fault
Long-Term Slip Rate:
-1 sigma= .008 mm/yr
mean= .013 mm/yr
+1 sigma= .016 mm/yr
Cumulative Frequency
Slip Rate (mm/yr)
0
0.1
0.2
0.3
0.4
0.5
0.6
0.7
0.8
0.9
1
0.005
0.01
0.015
0.02
0.025

ASM-A1-5

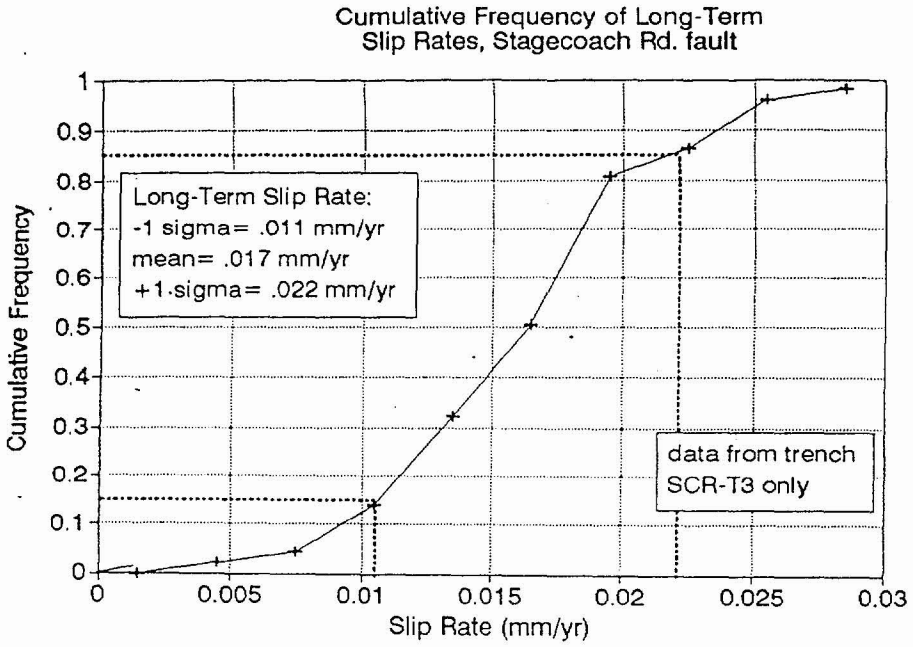
Cumulative Frequency of Long-Term Slip Rates, Stagecoach Rd. fault
Long-Term Slip Rate:
-1 sigma= .011 mm/yr
mean= .017 mm/yr
+1 sigma= .022 mm/yr
data from trench SCR-T3 only
Cumulative Frequency
Slip Rate (mm/yr)
0
0.1
0.2
0.3
0.4
0.5
0.6
0.7
0.8
0.9
1
0.005
0.01
0.015
0.02
0.025
0.03

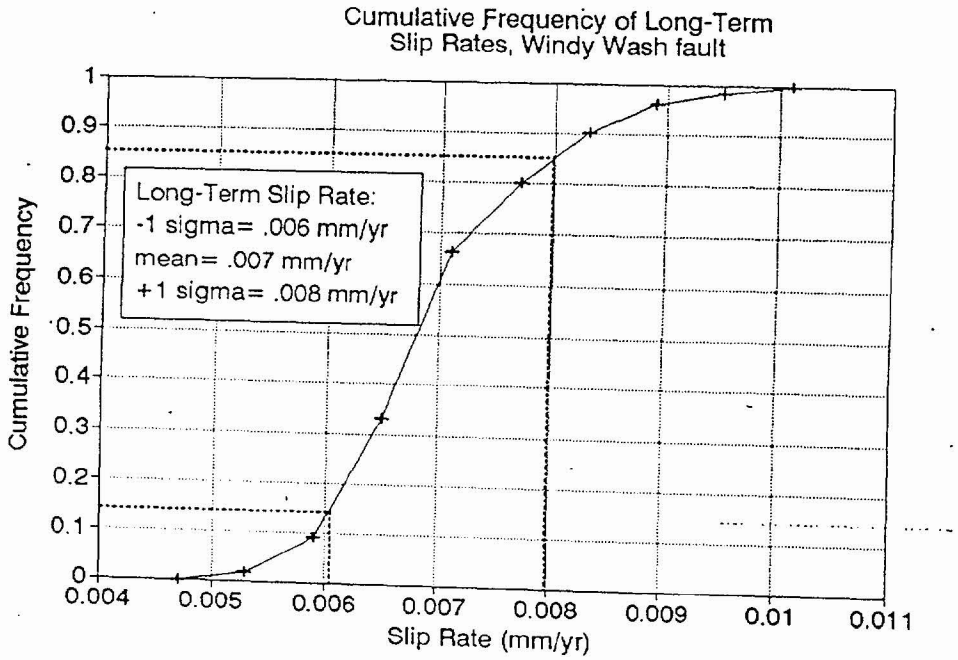
Cumulative Frequency of Long-Term Slip Rates, Windy Wash fault
Long-Term Slip Rate:
-1 sigma= .006 mm/yr
mean= .007 mm/yr
+1 sigma= .008 mm/yr
Cumulative Frequency
Slip Rate (mm/yr)
0
0.1
0.2
0.3
0.4
0.5
0.6
0.7
0.8
0.9
1
0.004
0.005
0.006
0.007
0.008
0.009
0.01
0.011

APPENDIX ASM-2

Graphs showing the cumulative frequency of interval slip rates for 10 local Yucca Mountain faults.

Note: these CDFs were computed by creating a normalized-grouped dataset of all interval slip rates on all Yucca Mountain faults, using the method of McCalpin (1995). Then for each of the 10 faults, that CDF was scaled to the long-term slip rate (from Appendix ASM-1) to yield these CDFs.

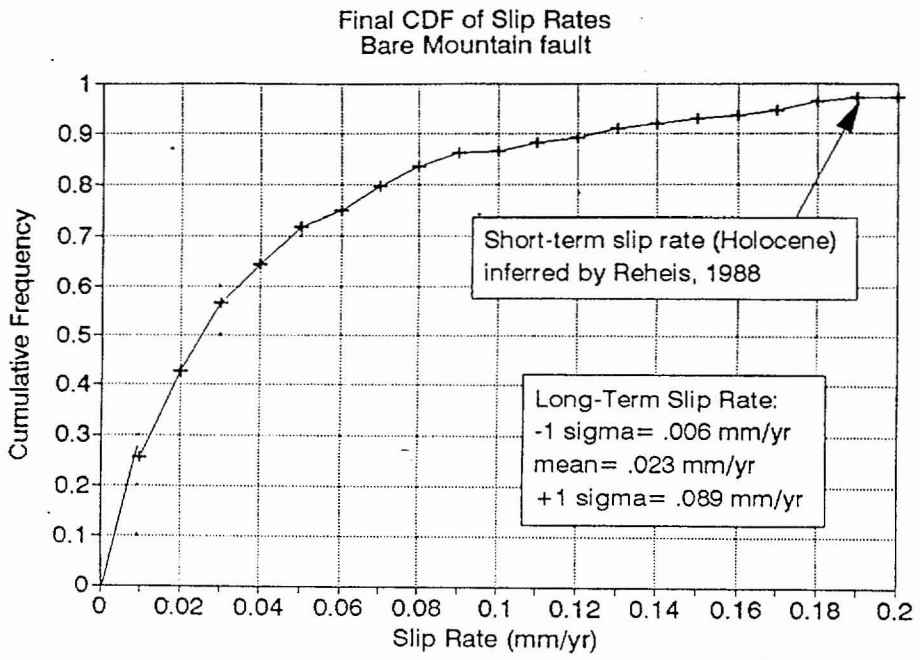
Final CDF of Slip Rates
Bare Mountain fault
Cumulative Frequency
Slip Rate (mm/yr)
Short-term slip rate (Holocene)
inferred by Reheis, 1988
Long-Term Slip Rate:
-1 sigma= .006 mm/yr
mean= .023 mm/yr
+1 sigma= .089 mm/yr

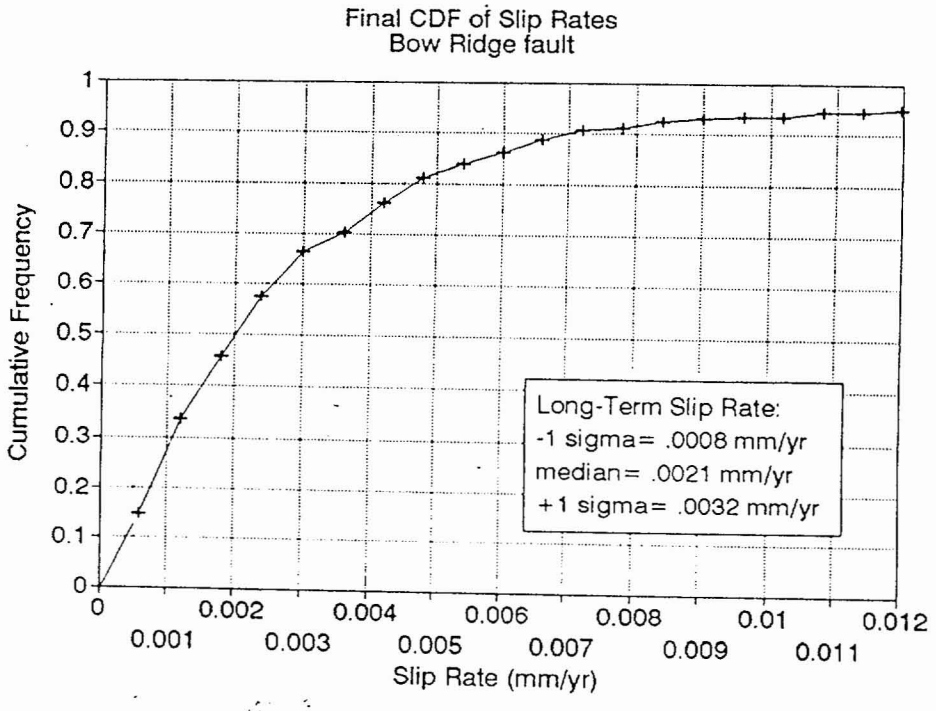
Final CDF of Slip Rates
Bow Ridge fault
Cumulative Frequency
Slip Rate (mm/yr)
Long-Term Slip Rate:
-1 sigma= .0008 mm/yr
median= .0021 mm/yr
+1 sigma= .0032 mm/yr

ASM-A2-2

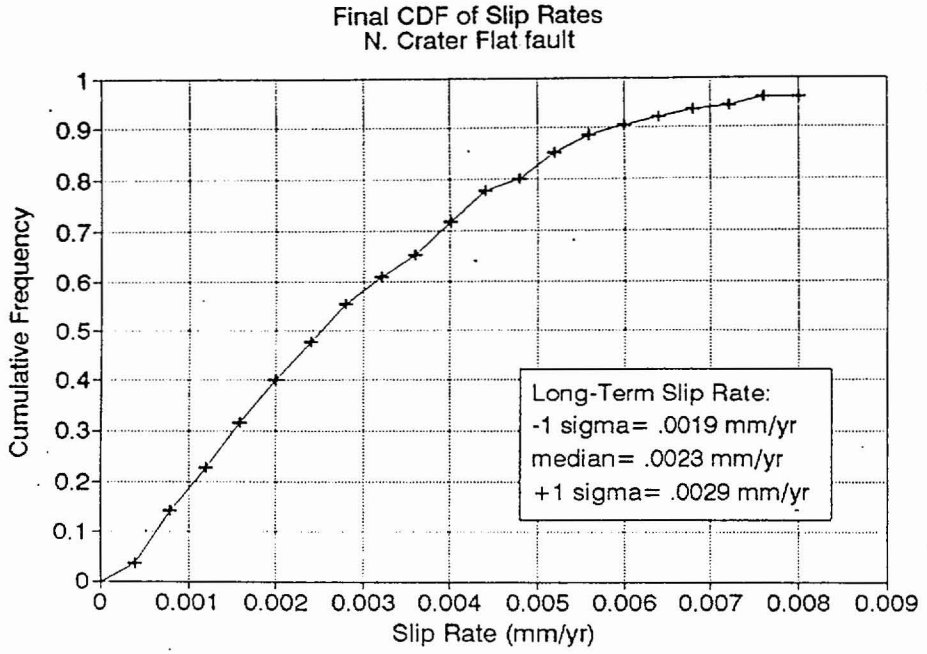
Final CDF of Slip Rates
N. Crater Flat fault
Cumulative Frequency
Slip Rate (mm/yr)
Long-Term Slip Rate:
-1 sigma= .0019 mm/yr
median= .0023 mm/yr
+1 sigma= .0029 mm/yr
0
0.1
0.2
0.3
0.4
0.5
0.6
0.7
0.8
0.9
1
0.001
0.002
0.003
0.004
0.005
0.006
0.007
0.008
0.009

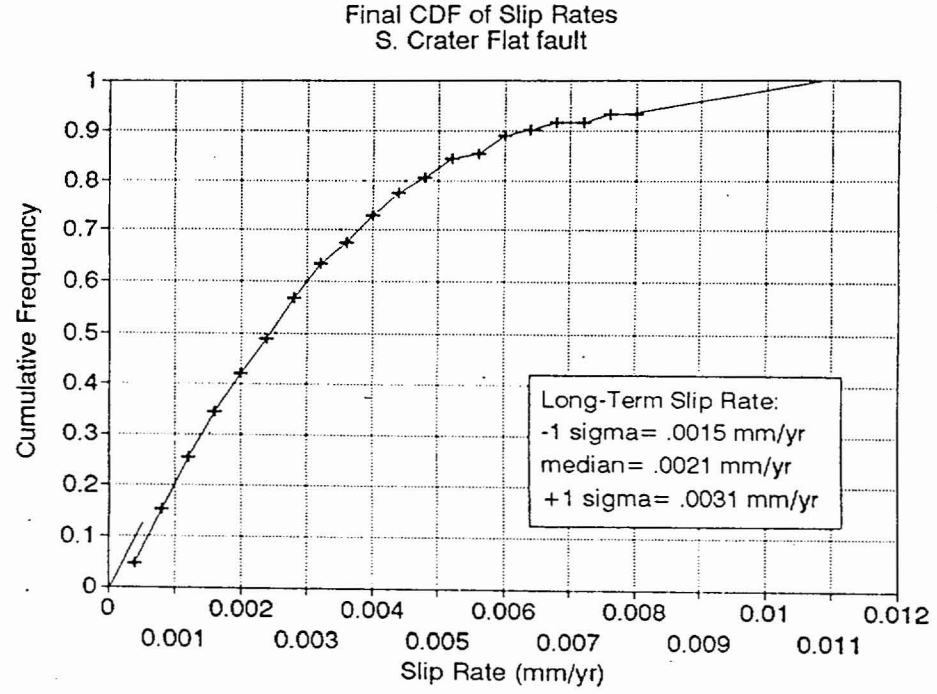
Final CDF of Slip Rates
S. Crater Flat fault
Cumulative Frequency
Slip Rate (mm/yr)
Long-Term Slip Rate:
-1 sigma= .0015 mm/yr
median= .0021 mm/yr
+1 sigma= .0031 mm/yr
0
0.1
0.2
0.3
0.4
0.5
0.6
0.7
0.8
0.9
1
0.001
0.002
0.003
0.004
0.005
0.006
0.007
0.008
0.009
0.01
0.011
0.012

ASM-A2-3

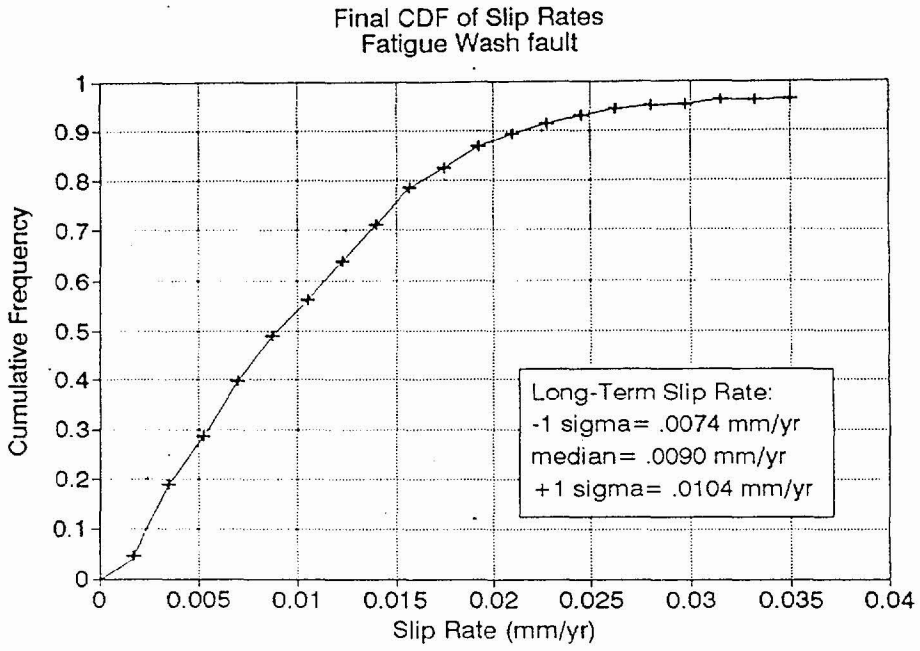
Final CDF of Slip Rates
Fatigue Wash fault
Cumulative Frequency
Slip Rate (mm/yr)
Long-Term Slip Rate:
-1 sigma= .0074 mm/yr
median= .0090 mm/yr
+1 sigma= .0104 mm/yr

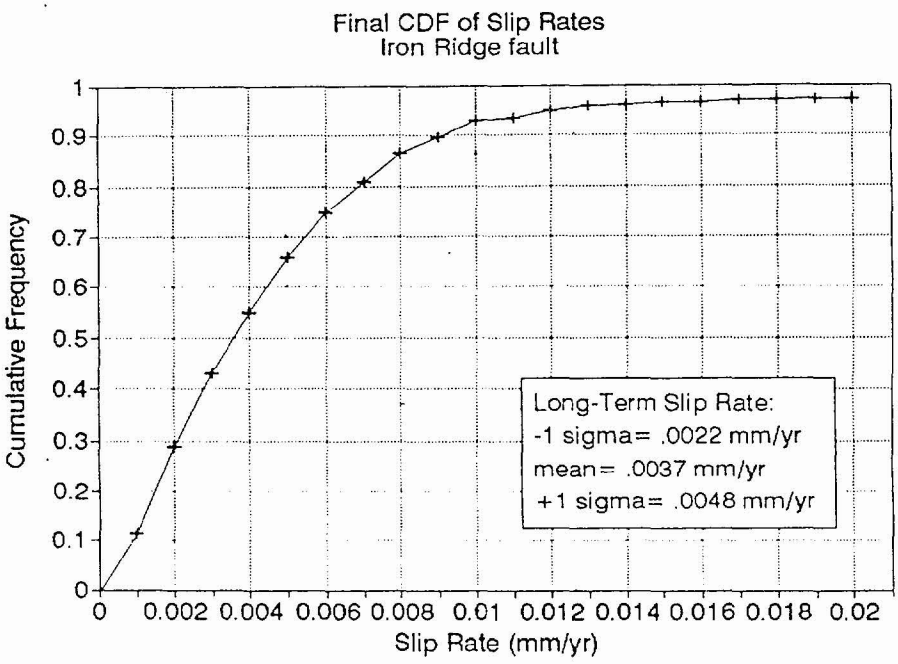
Final CDF of Slip Rates
Iron Ridge fault
Cumulative Frequency
Slip Rate (mm/yr)
Long-Term Slip Rate:
-1 sigma= .0022 mm/yr
mean= .0037 mm/yr
+1 sigma= .0048 mm/yr

ASM-A2-4

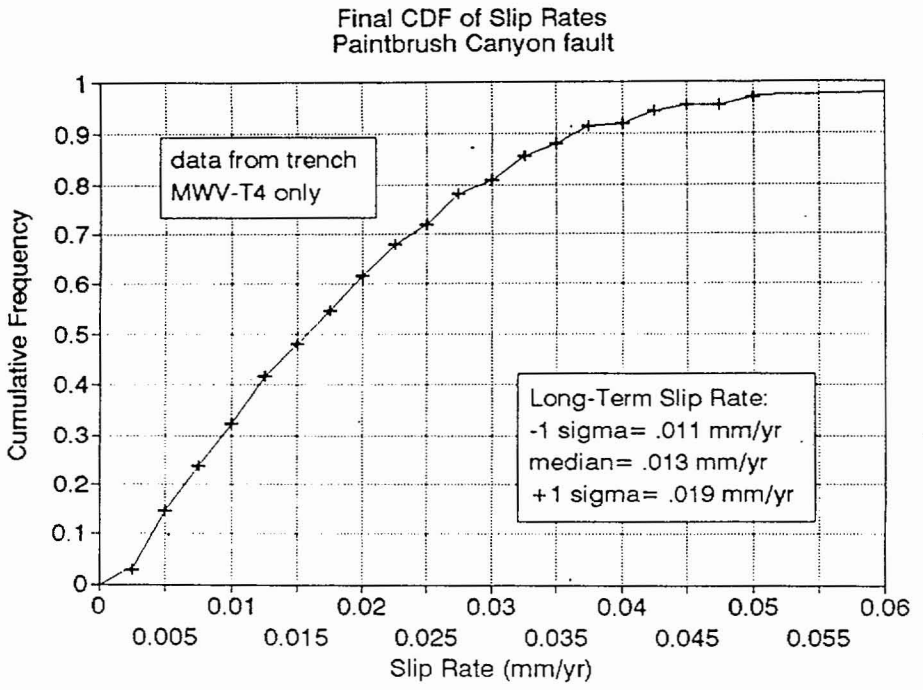
Final CDF of Slip Rates
Paintbrush Canyon fault
data from trench
MWV-T4 only
Long-Term Slip Rate:
-1 sigma= .011 mm/yr
median= .013 mm/yr
+1 sigma= .019 mm/yr
Cumulative Frequency
Slip Rate (mm/yr)
0
0.1
0.2
0.3
0.4
0.5
0.6
0.7
0.8
0.9
1
0.005
0.01
0.015
0.02
0.025
0.03
0.035
0.04
0.045
0.05
0.055
0.06

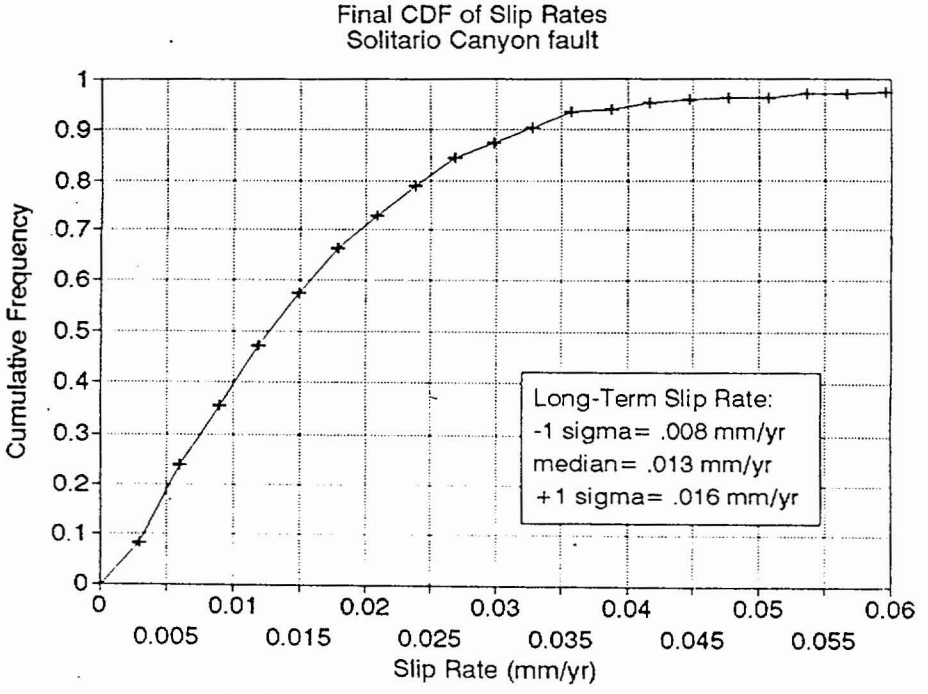
Final CDF of Slip Rates
Solitario Canyon fault
Long-Term Slip Rate:
-1 sigma= .008 mm/yr
median= .013 mm/yr
+1 sigma= .016 mm/yr
Cumulative Frequency
Slip Rate (mm/yr)
0
0.1
0.2
0.3
0.4
0.5
0.6
0.7
0.8
0.9
1
0.005
0.01
0.015
0.02
0.025
0.03
0.035
0.04
0.045
0.05
0.055
0.06

ASM-A2-5

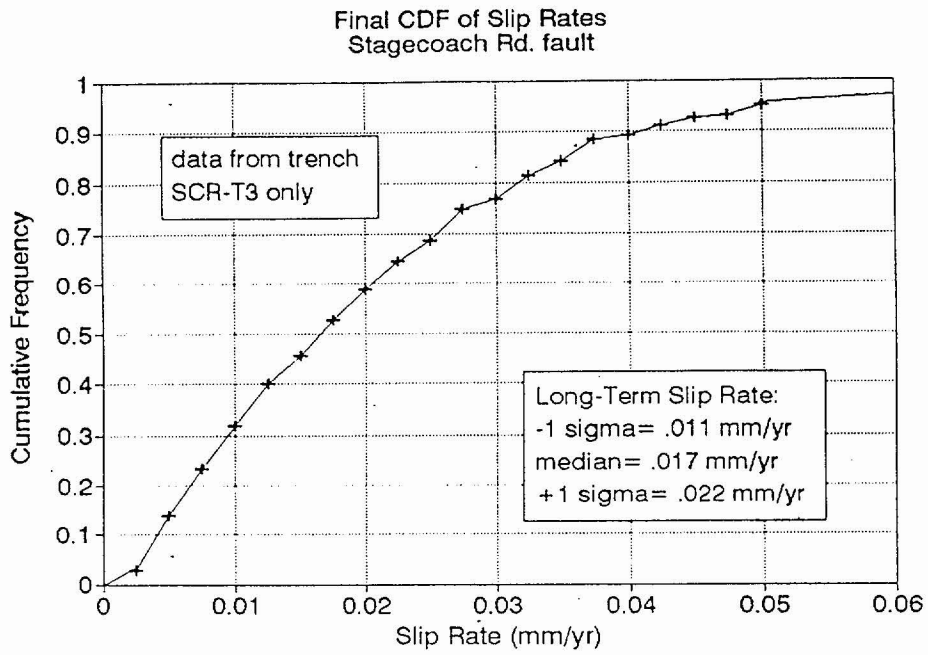
Final CDF of Slip Rates
Stagecoach Rd. fault
data from trench
SCR-T3 only
Long-Term Slip Rate:
-1 sigma= .011 mm/yr
median= .017 mm/yr
+1 sigma= .022 mm/yr
Cumulative Frequency
Slip Rate (mm/yr)
0
0.1
0.2
0.3
0.4
0.5
0.6
0.7
0.8
0.9
1
0.01
0.02
0.03
0.04
0.05
0.06

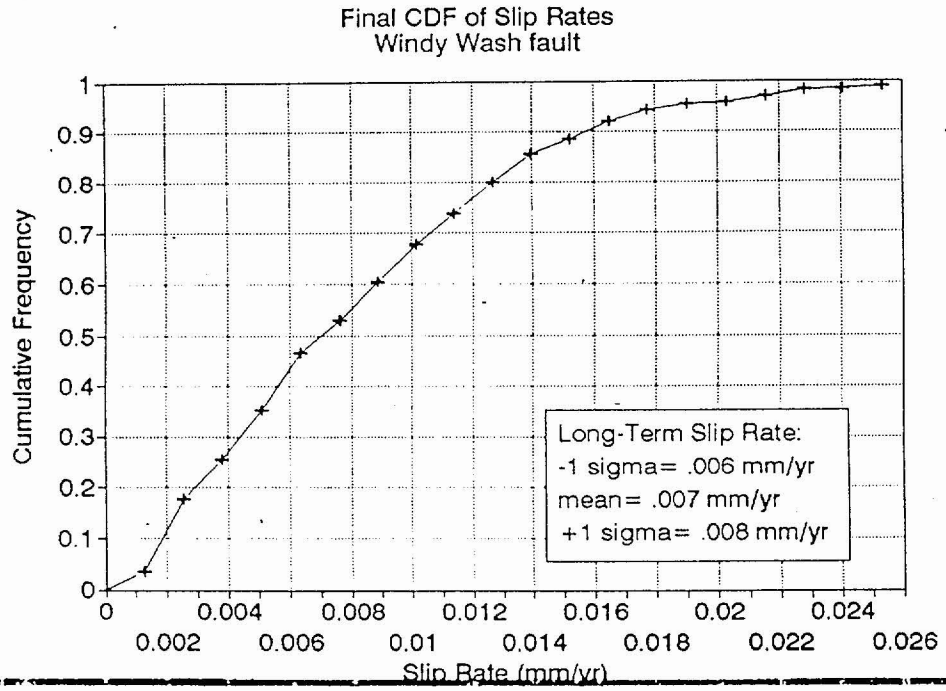
Final CDF of Slip Rates
Windy Wash fault
Long-Term Slip Rate:
-1 sigma= .006 mm/yr
mean= .007 mm/yr
+1 sigma= .008 mm/yr
Cumulative Frequency
Slip Rate (mm/yr)
0
0.1
0.2
0.3
0.4
0.5
0.6
0.7
0.8
0.9
1
0.002
0.004
0.006
0.008
0.01
0.012
0.014
0.016
0.018
0.02
0.022
0.024
0.026

ASM-AZ-6

APPENDIX ASM-3

Graphs showing frequency histograms of long-term mean recurrence interval for 10 local Yucca Mountain faults.

Note: these histograms show 36 permutations of long-term mean recurrence interval, based on 6 estimates each of the age of the oldest and youngest dated paleoearthquakes, and the number of seismic cycles between those dates. We assumed that the minimum, preferred, and maximum ages for paleoearthquakes in Table 5-1 of USGS (written communication, 1996) represented ± 1 sigma limits. We then split these age values up into a six-part frequency distribution (with symmetrical probabilities of 0.025, 0.125, and 0.35) by linear interpolation (see spreadsheet RI-[fault name].WQZ for actual calculations.)

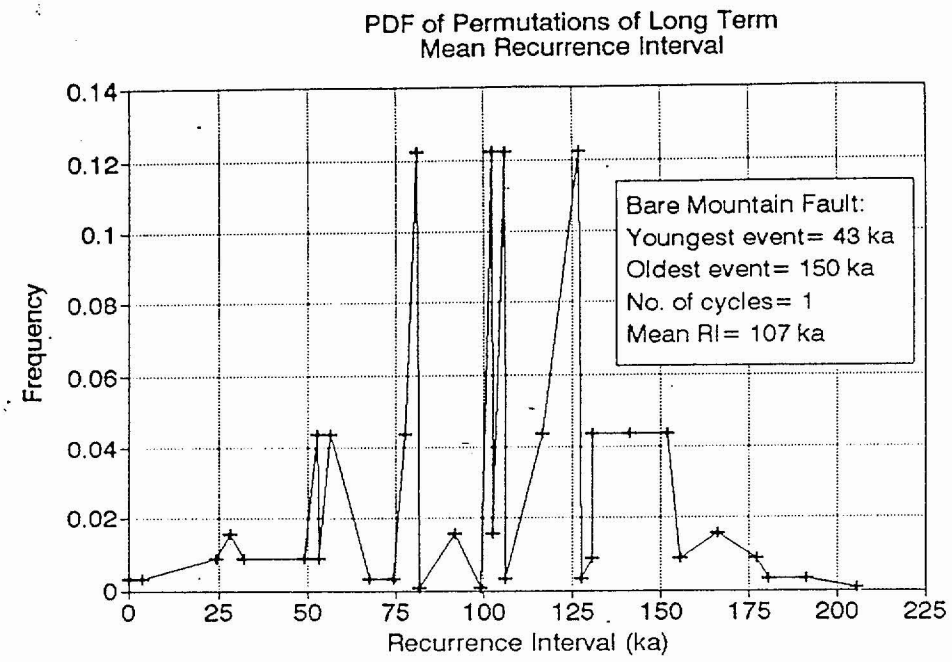
PDF of Permutations of Long Term
Mean Recurrence Interval
Frequency
Recurrence Interval (ka)
Bare Mountain Fault:
Youngest event= 43 ka
Oldest event= 150 ka
No. of cycles= 1
Mean RI= 107 ka
0.14
0.12
0.1
0.08
0.06
0.04
0.02
0
0 25 50 75 100 125 150 175 200 225

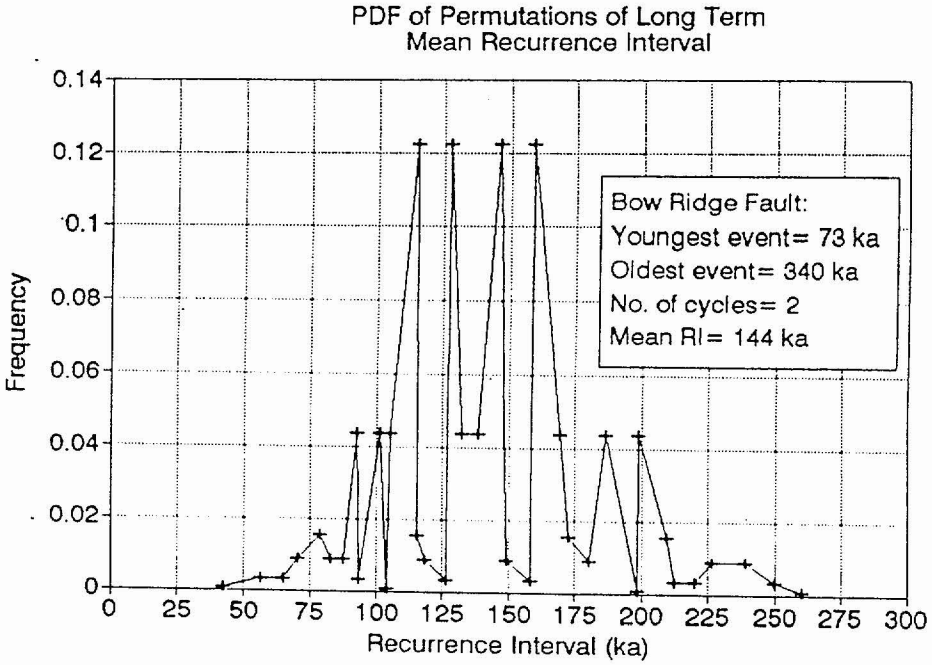
PDF of Permutations of Long Term
Mean Recurrence Interval
Frequency
Recurrence Interval (ka)
Bow Ridge Fault:
Youngest event= 73 ka
Oldest event= 340 ka
No. of cycles= 2
Mean RI= 144 ka
0.14
0.12
0.1
0.08
0.06
0.04
0.02
0
0 25 50 75 100 125 150 175 200 225 250 275 300

ASM - A3 - 2

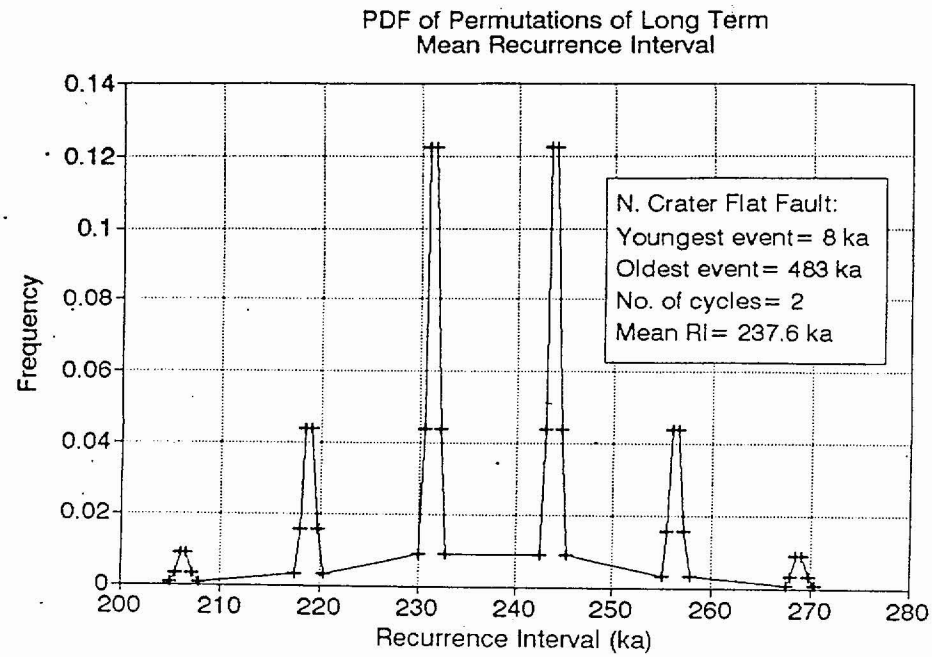
PDF of Permutations of Long Term
Mean Recurrence Interval
Frequency
0.14
0.12
0.1
0.08
0.06
0.04
0.02
0
200
210
220
230
240
250
260
270
280
Recurrence Interval (ka)
N. Crater Flat Fault:
Youngest event= 8 ka
Oldest event= 483 ka
No. of cycles= 2
Mean RI= 237.6 ka

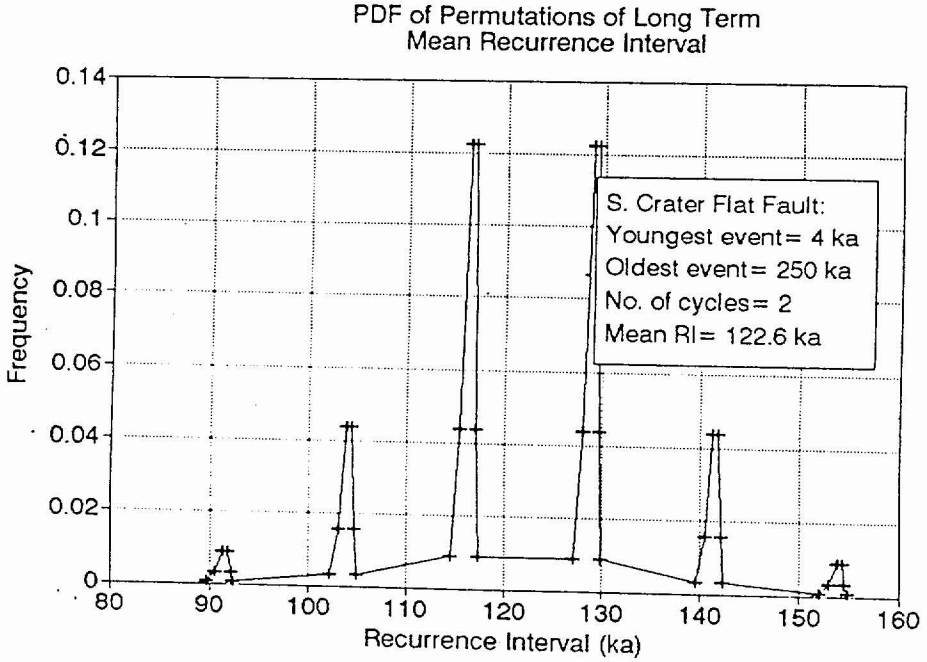
PDF of Permutations of Long Term
Mean Recurrence Interval
Frequency
0.14
0.12
0.1
0.08
0.06
0.04
0.02
0
80
90
100
110
120
130
140
150
160
Recurrence Interval (ka)
S. Crater Flat Fault:
Youngest event= 4 ka
Oldest event= 250 ka
No. of cycles= 2
Mean RI= 122.6 ka

ASM-A3-3

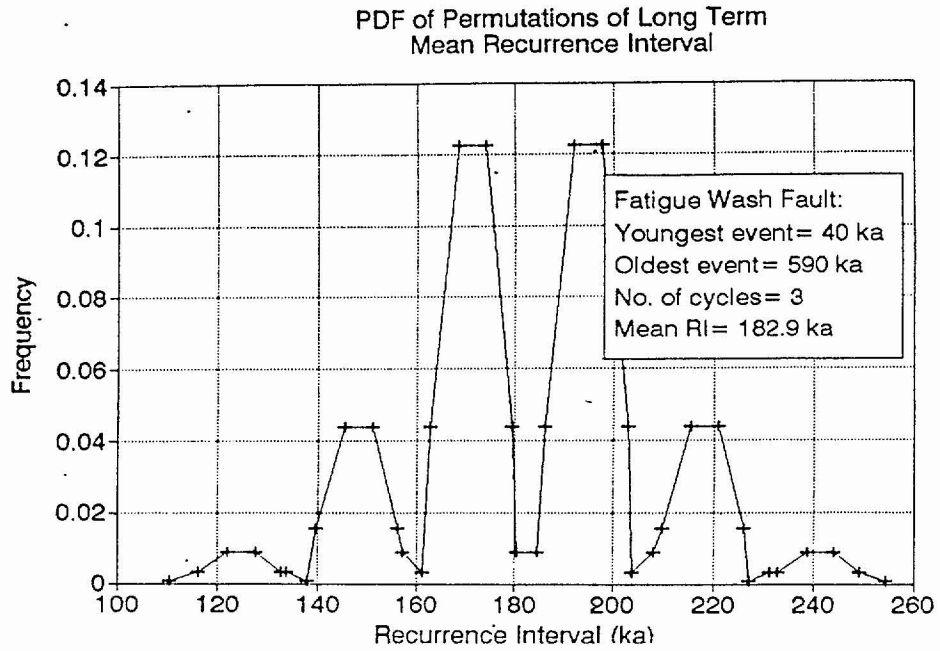
PDF of Permutations of Long Term
Mean Recurrence Interval
Frequency
0.14
0.12
0.1
0.08
0.06
0.04
0.02
0
100
120
140
160
180
200
220
240
260
Recurrence Interval (ka)
Fatigue Wash Fault:
Youngest event= 40 ka
Oldest event= 590 ka
No. of cycles= 3
Mean RI= 182.9 ka

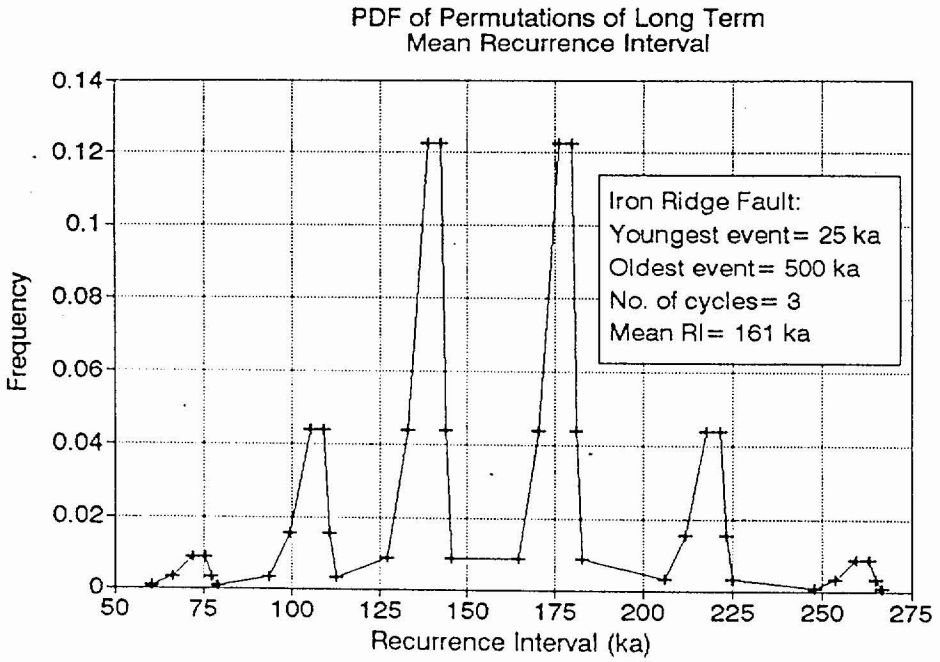
PDF of Permutations of Long Term
Mean Recurrence Interval
Frequency
0.14
0.12
0.1
0.08
0.06
0.04
0.02
0
50
75
100
125
150
175
200
225
250
275
Recurrence Interval (ka)
Iron Ridge Fault:
Youngest event= 25 ka
Oldest event= 500 ka
No. of cycles= 3
Mean RI= 161 ka

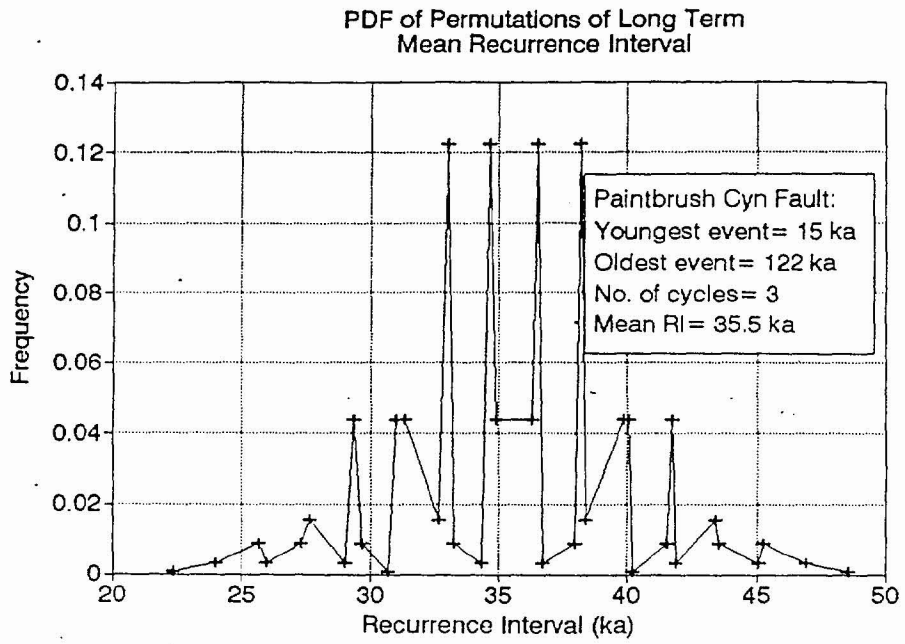
PDF of Permutations of Long Term
Mean Recurrence Interval
Paintbrush Cyn Fault:
Youngest event= 15 ka
Oldest event= 122 ka
No. of cycles= 3
Mean RI= 35.5 ka
Frequency
Recurrence Interval (ka)
0.14
0.12
0.1
0.08
0.06
0.04
0.02
0
20
25
30
35
40
45
50

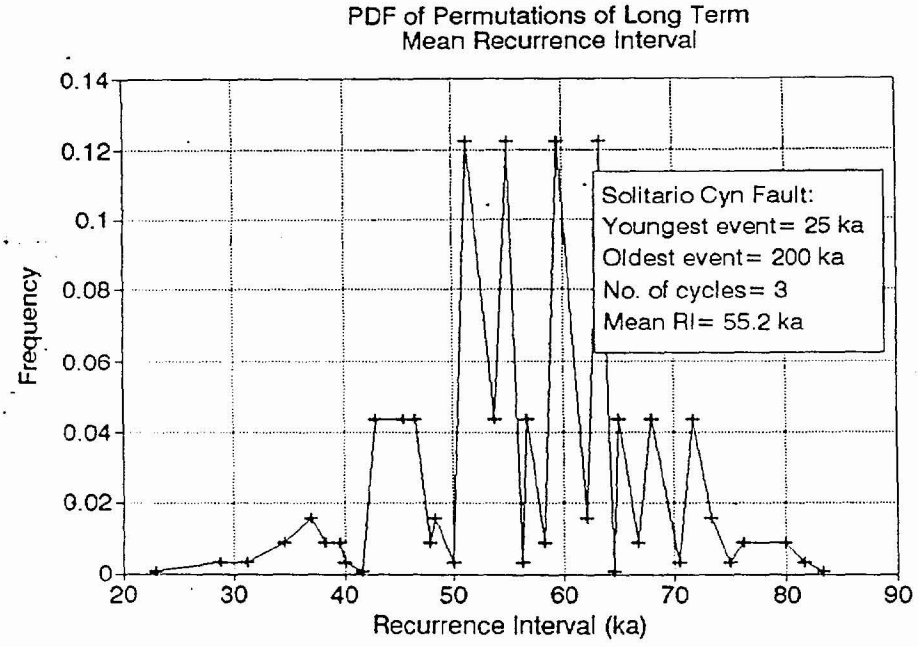
PDF of Permutations of Long Term
Mean Recurrence Interval
Solitario Cyn Fault:
Youngest event= 25 ka
Oldest event= 200 ka
No. of cycles= 3
Mean RI= 55.2 ka
Frequency
Recurrence Interval (ka)
0.14
0.12
0.1
0.08
0.06
0.04
0.02
0
20
30
40
50
60
70
80
90

ASM-A3-5

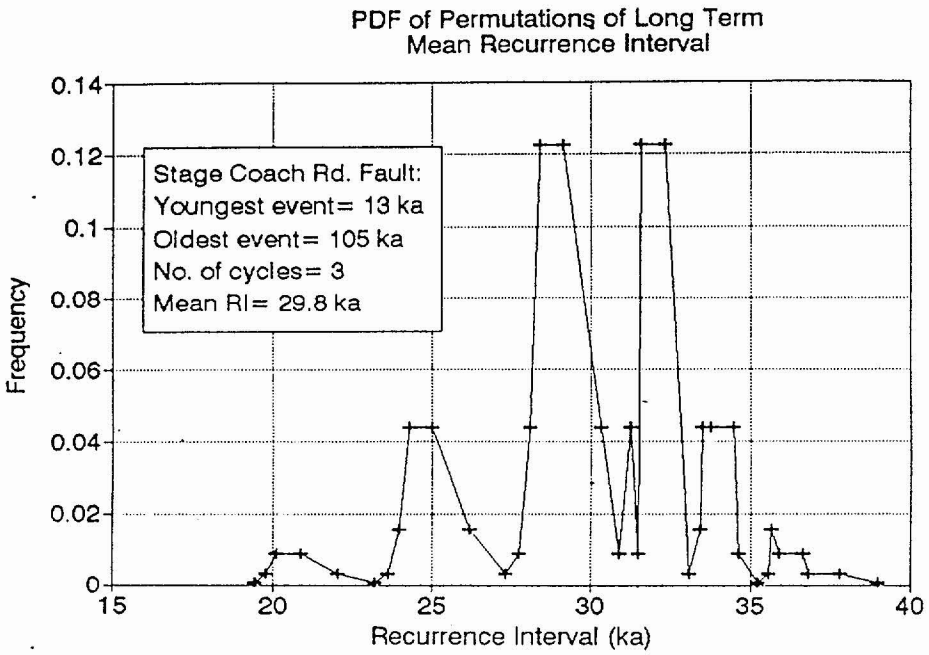
PDF of Permutations of Long Term
Mean Recurrence Interval
Stage Coach Rd. Fault:
Youngest event= 13 ka
Oldest event= 105 ka
No. of cycles= 3
Mean RI= 29.8 ka
Frequency
0.14
0.12
0.1
0.08
0.06
0.04
0.02
0
15
20
25
30
35
40
Recurrence Interval (ka)

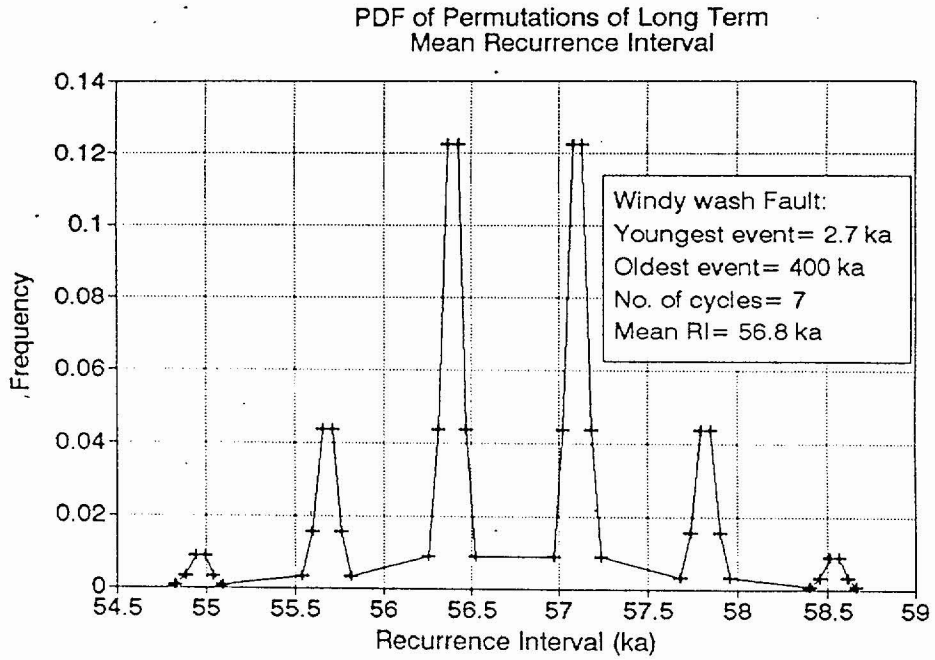
PDF of Permutations of Long Term
Mean Recurrence Interval
Windy wash Fault:
Youngest event= 2.7 ka
Oldest event= 400 ka
No. of cycles= 7
Mean RI= 56.8 ka
Frequency
0.14
0.12
0.1
0.08
0.06
0.04
0.02
0
54.5
55
55.5
56
56.5
57
57.5
58
58.5
59
Recurrence Interval (ka)

APPENDIX ASM-4

Graphs showing cumulative frequency distributions of long-term mean recurrence interval for 10 local Yucca Mountain faults.

Note: these CDFs were derived from the PDFs of Appendix ASM-3.

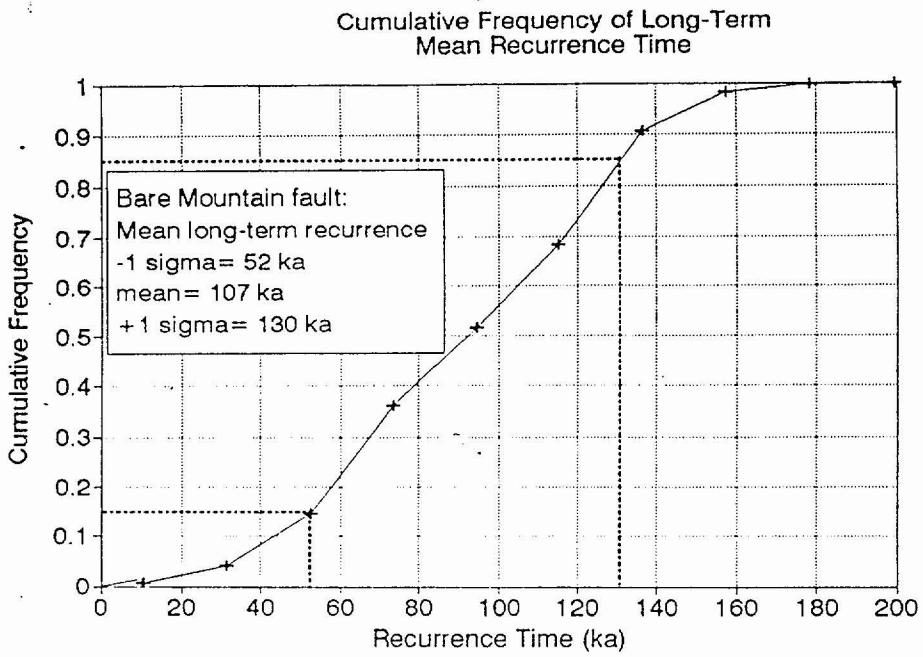
Cumulative Frequency of Long-Term
Mean Recurrence Time
Bare Mountain fault:
Mean long-term recurrence
-1 sigma= 52 ka
mean= 107 ka
+1 sigma= 130 ka
Cumulative Frequency
Recurrence Time (ka)
0
0.1
0.2
0.3
0.4
0.5
0.6
0.7
0.8
0.9
1
0
20
40
60
80
100
120
140
160
180
200

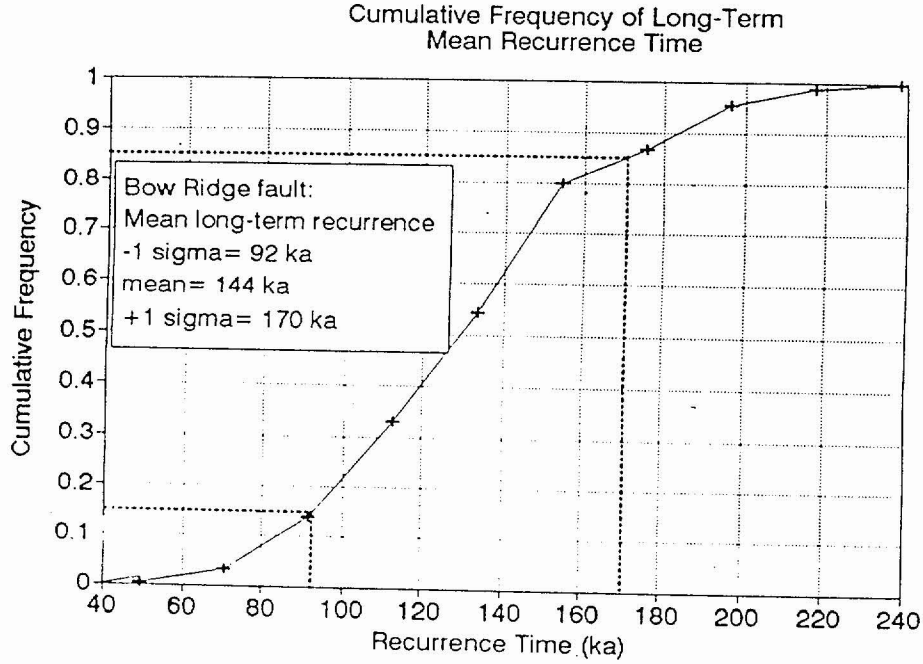
Cumulative Frequency of Long-Term
Mean Recurrence Time
Bow Ridge fault:
Mean long-term recurrence
-1 sigma= 92 ka
mean= 144 ka
+1 sigma= 170 ka
Cumulative Frequency
Recurrence Time (ka)
0
0.1
0.2
0.3
0.4
0.5
0.6
0.7
0.8
0.9
1
40
60
80
100
120
140
160
180
200
220
240

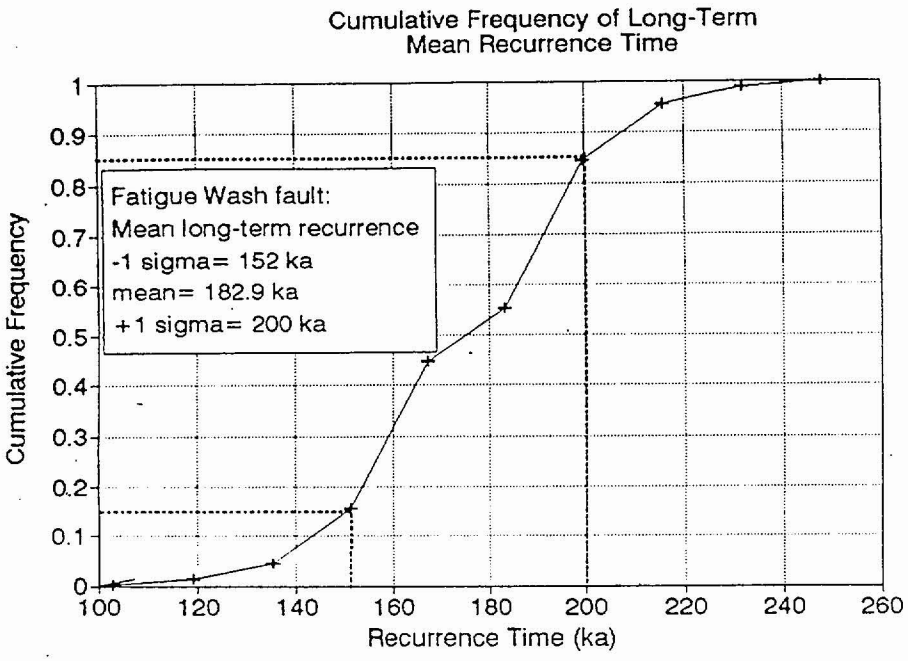
Cumulative Frequency of Long-Term
Mean Recurrence Time
Fatigue Wash fault:
Mean long-term recurrence
-1 sigma= 152 ka
mean= 182.9 ka
+1 sigma= 200 ka
Cumulative Frequency
Recurrence Time (ka)
0
0.1
0.2
0.3
0.4
0.5
0.6
0.7
0.8
0.9
1
100
120
140
160
180
200
220
240
260

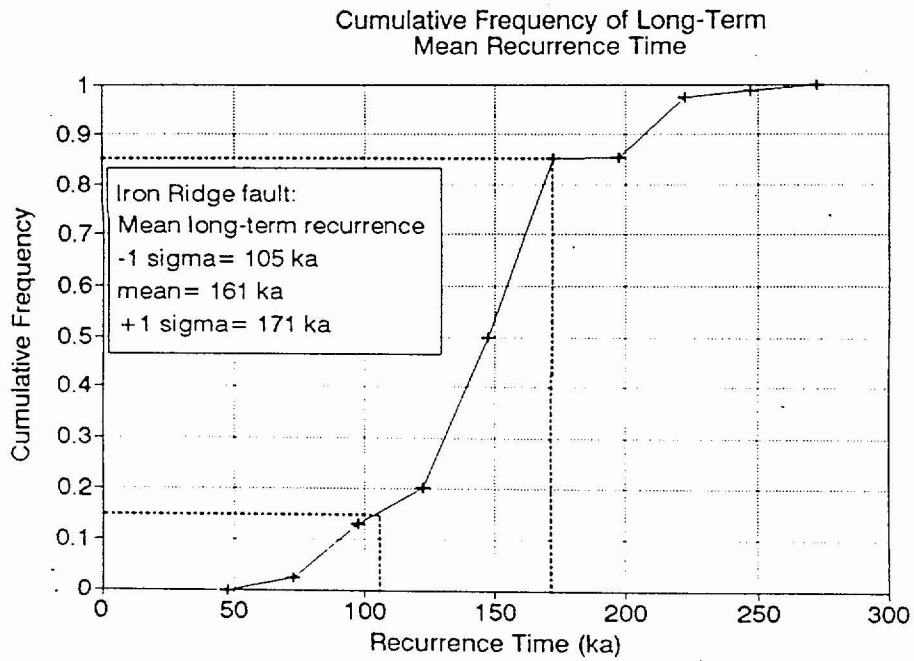
Cumulative Frequency of Long-Term
Mean Recurrence Time
Iron Ridge fault:
Mean long-term recurrence
-1 sigma= 105 ka
mean= 161 ka
+1 sigma= 171 ka
Cumulative Frequency
Recurrence Time (ka)
0
0.1
0.2
0.3
0.4
0.5
0.6
0.7
0.8
0.9
1
0
50
100
150
200
250
300

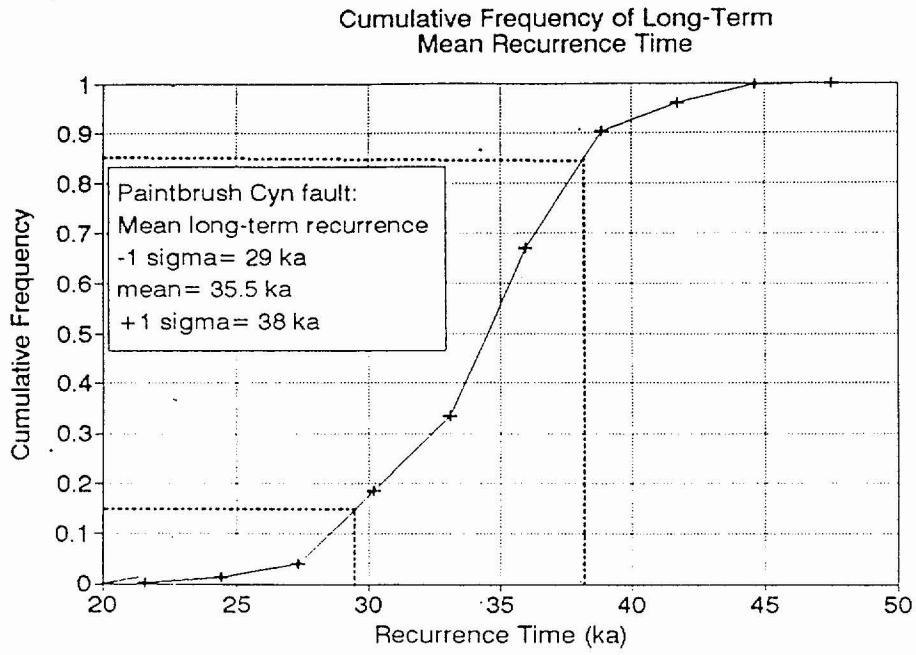
Cumulative Frequency of Long-Term
Mean Recurrence Time
Paintbrush Cyn fault:
Mean long-term recurrence
-1 sigma= 29 ka
mean= 35.5 ka
+1 sigma= 38 ka
Cumulative Frequency
Recurrence Time (ka)
0
0.1
0.2
0.3
0.4
0.5
0.6
0.7
0.8
0.9
1
20
25
30
35
40
45
50

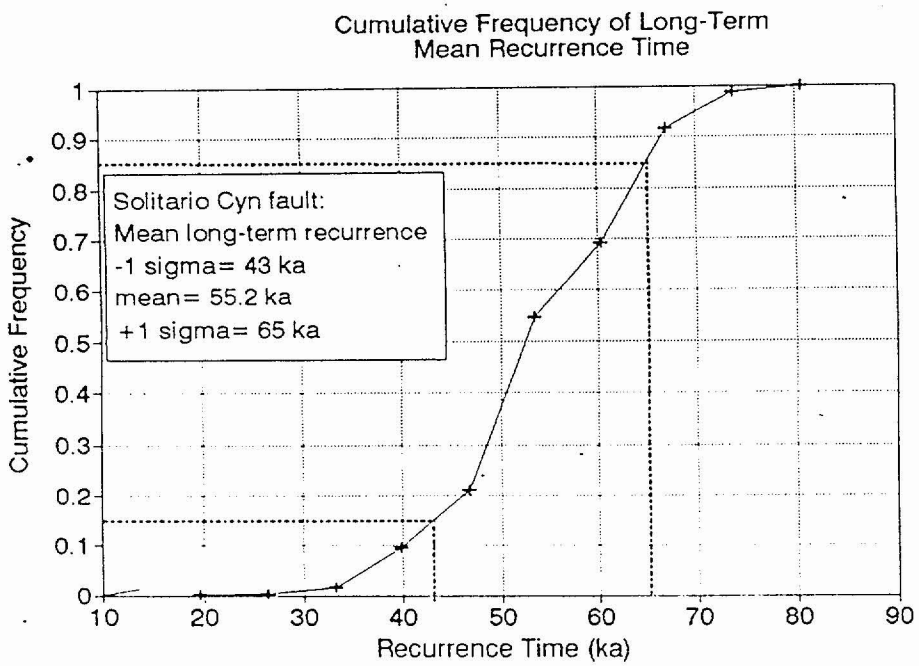
Cumulative Frequency of Long-Term
Mean Recurrence Time
Solitario Cyn fault:
Mean long-term recurrence
-1 sigma= 43 ka
mean= 55.2 ka
+1 sigma= 65 ka
Cumulative Frequency
Recurrence Time (ka)
0
0.1
0.2
0.3
0.4
0.5
0.6
0.7
0.8
0.9
1
10
20
30
40
50
60
70
80
90

ASM-A4-4

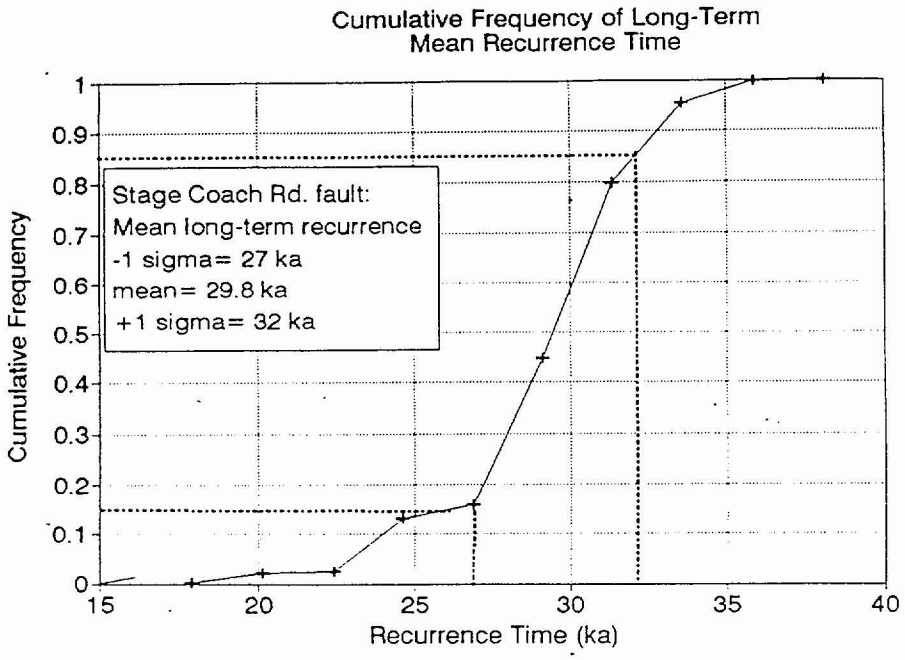
Cumulative Frequency of Long-Term
Mean Recurrence Time
Stage Coach Rd. fault:
Mean long-term recurrence
-1 sigma= 27 ka
mean= 29.8 ka
+1 sigma= 32 ka
Cumulative Frequency
Recurrence Time (ka)
0
0.1
0.2
0.3
0.4
0.5
0.6
0.7
0.8
0.9
1
15
20
25
30
35
40

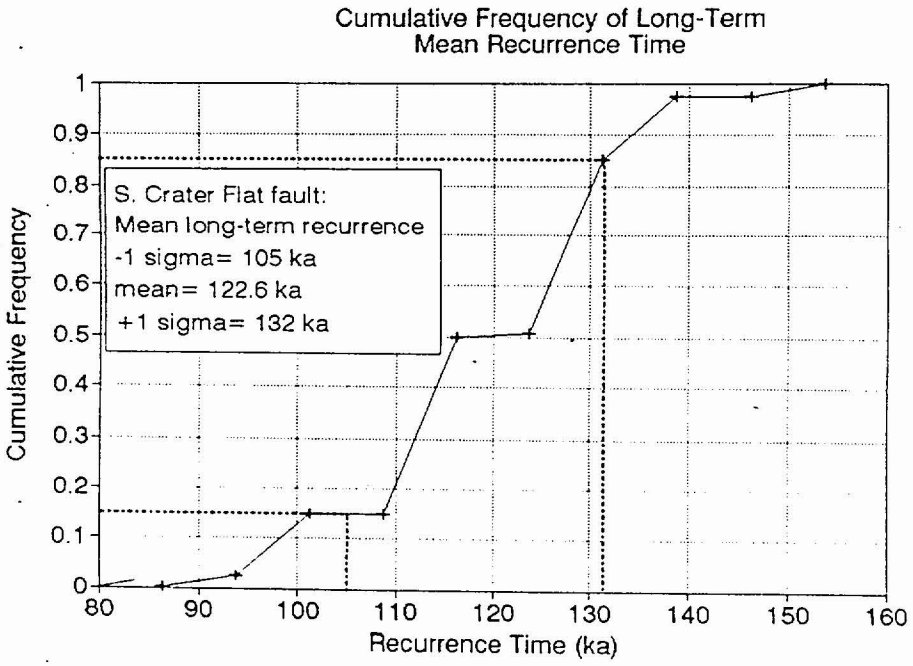
Cumulative Frequency of Long-Term
Mean Recurrence Time
S. Crater Flat fault:
Mean long-term recurrence
-1 sigma= 105 ka
mean= 122.6 ka
+1 sigma= 132 ka
Cumulative Frequency
Recurrence Time (ka)
0
0.1
0.2
0.3
0.4
0.5
0.6
0.7
0.8
0.9
1
80
90
100
110
120
130
140
150
160

ASM-A4-5

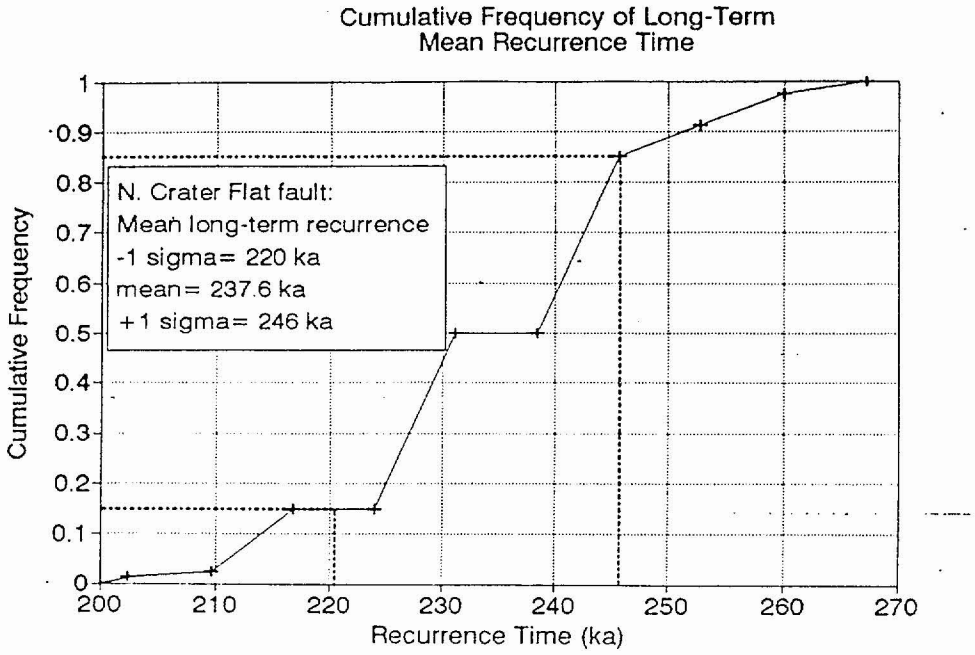
Cumulative Frequency of Long-Term
Mean Recurrence Time
N. Crater Flat fault:
Mean long-term recurrence
-1 sigma= 220 ka
mean= 237.6 ka
+1 sigma= 246 ka
Cumulative Frequency
Recurrence Time (ka)
0
0.1
0.2
0.3
0.4
0.5
0.6
0.7
0.8
0.9
1
200
210
220
230
240
250
260
270

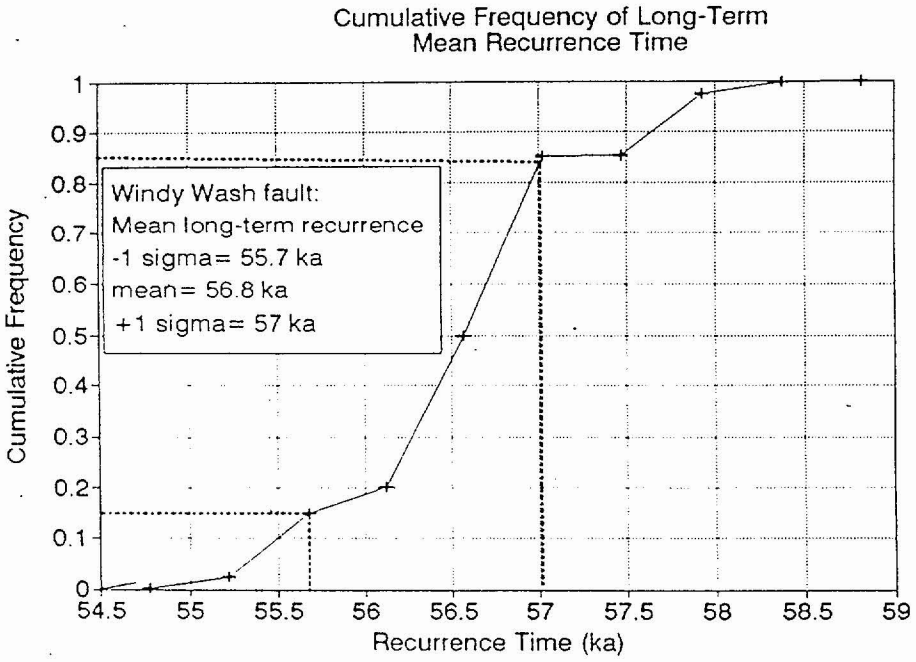
Cumulative Frequency of Long-Term
Mean Recurrence Time
Windy Wash fault:
Mean long-term recurrence
-1 sigma= 55.7 ka
mean= 56.8 ka
+1 sigma= 57 ka
Cumulative Frequency
Recurrence Time (ka)
0
0.1
0.2
0.3
0.4
0.5
0.6
0.7
0.8
0.9
1
54.5
55
55.5
56
56.5
57
57.5
58
58.5
59

APPENDIX ASM-5

Graphs showing cumulative frequency distributions of individual recurrence intervals for 10 local Yucca Mountain faults.

Note: these CDFs were created by scaling the normalized-grouped CDF of recurrence to the long-term mean recurrence interval of each fault, in the same manner as done for slip rates (Appendix ASM-2).

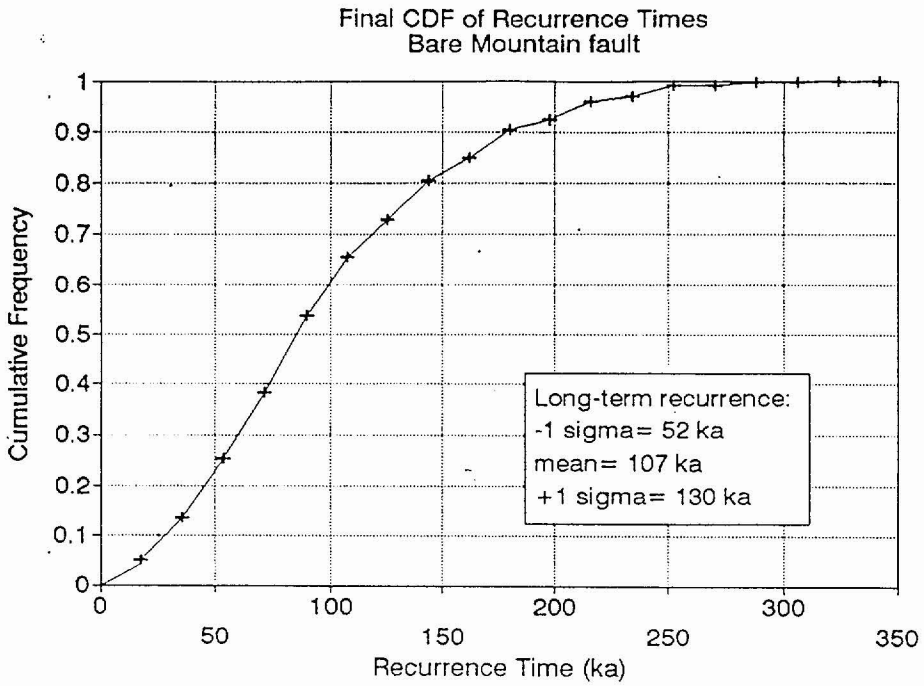
Final CDF of Recurrence Times
Bare Mountain fault
Cumulative Frequency
Recurrence Time (ka)
Long-term recurrence:
-1 sigma= 52 ka
mean= 107 ka
+1 sigma= 130 ka

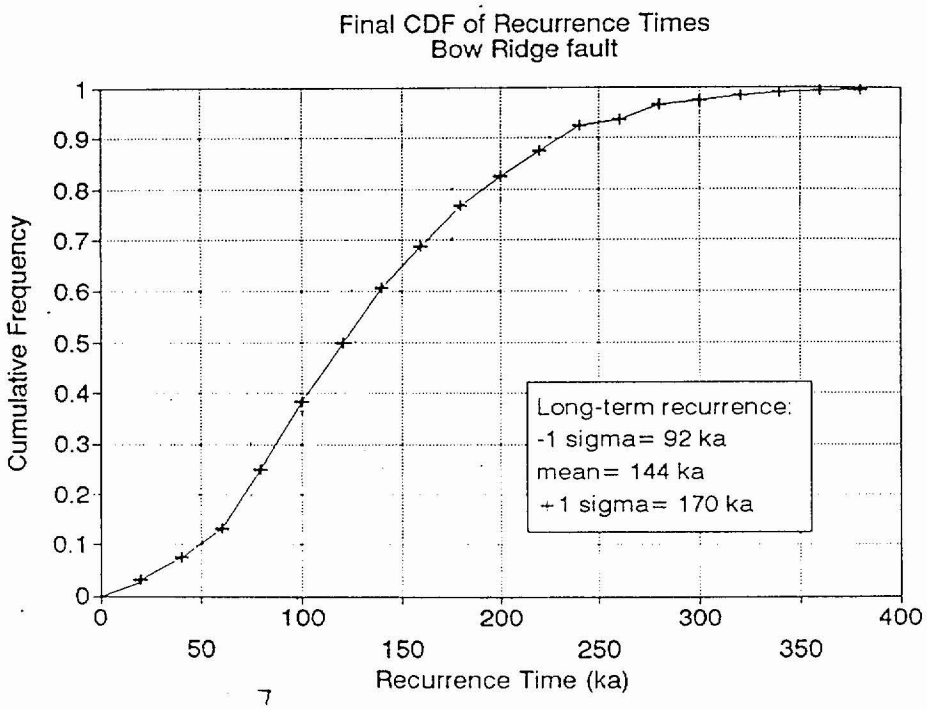
Final CDF of Recurrence Times
Bow Ridge fault
Cumulative Frequency
Recurrence Time (ka)
Long-term recurrence:
-1 sigma= 92 ka
mean= 144 ka
+1 sigma= 170 ka

ASM-AS-2

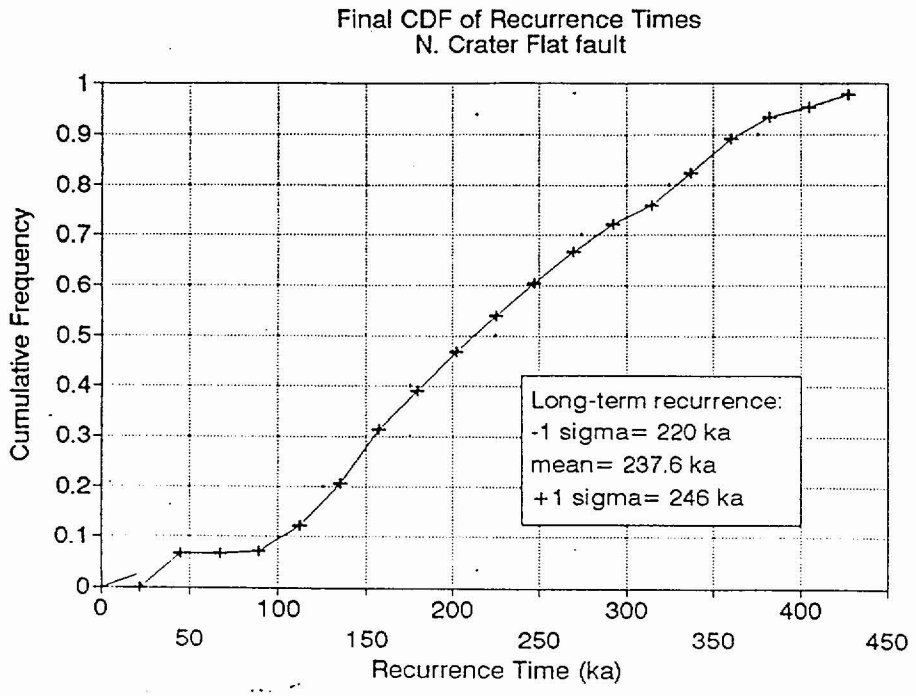
Final CDF of Recurrence Times
N. Crater Flat fault
Cumulative Frequency
Recurrence Time (ka)
Long-term recurrence:
-1 sigma= 220 ka
mean= 237.6 ka
+1 sigma= 246 ka

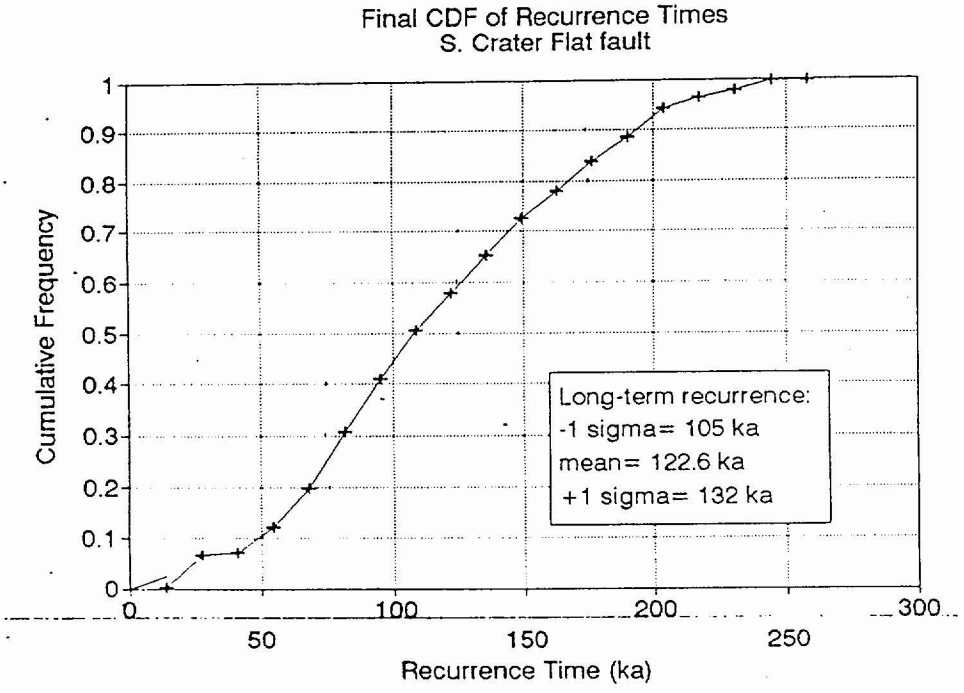
Final CDF of Recurrence Times
S. Crater Flat fault
Cumulative Frequency
Recurrence Time (ka)
Long-term recurrence:
-1 sigma= 105 ka
mean= 122.6 ka
+1 sigma= 132 ka

ASM-A5 - 3

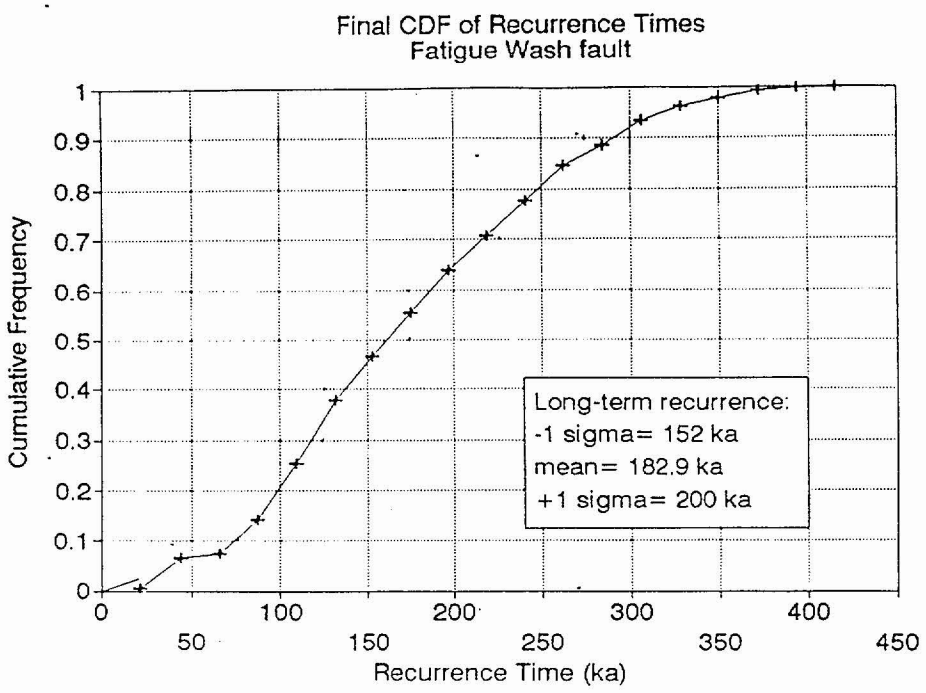
Final CDF of Recurrence Times
Fatigue Wash fault
Cumulative Frequency
Recurrence Time (ka)
Long-term recurrence:
-1 sigma= 152 ka
mean= 182.9 ka
+1 sigma= 200 ka

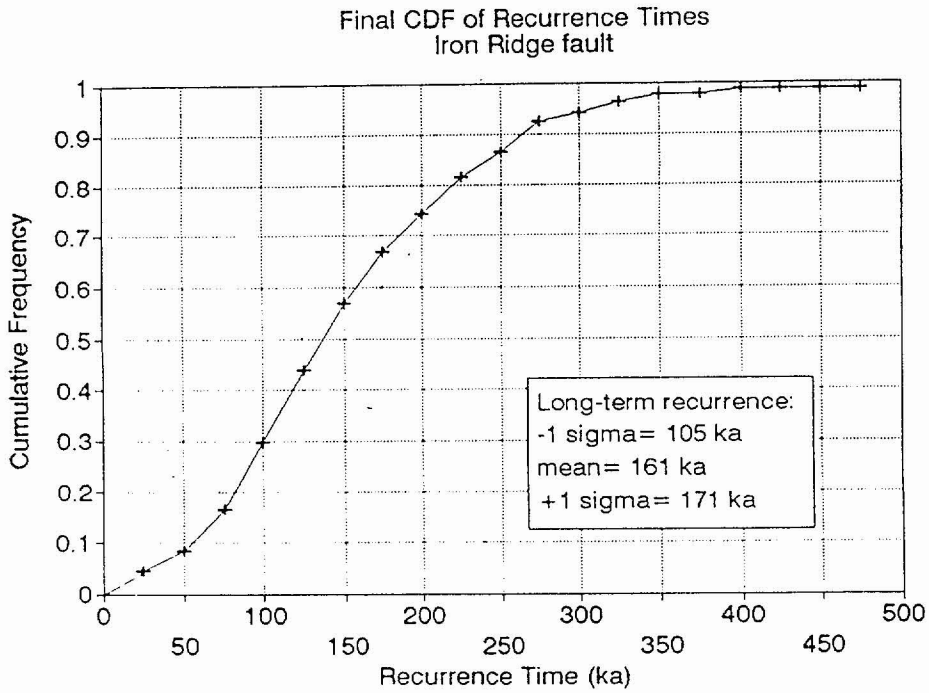
Final CDF of Recurrence Times
Iron Ridge fault
Cumulative Frequency
Recurrence Time (ka)
Long-term recurrence:
-1 sigma= 105 ka
mean= 161 ka
+1 sigma= 171 ka

ASM-AS-4

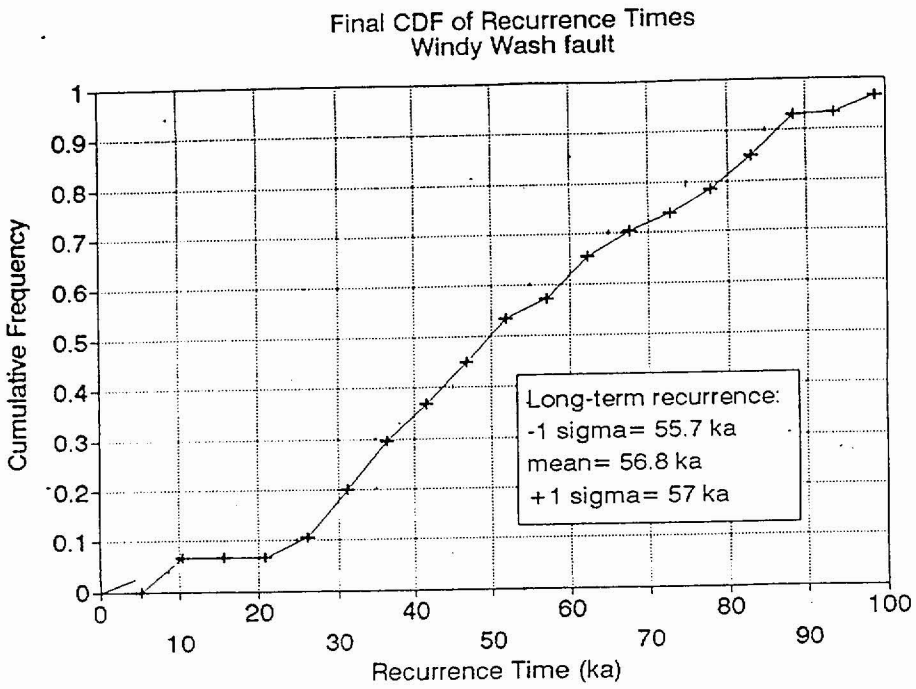
Final CDF of Recurrence Times
Windy Wash fault
Cumulative Frequency
Recurrence Time (ka)
Long-term recurrence:
-1 sigma= 55.7 ka
mean= 56.8 ka
+1 sigma= 57 ka

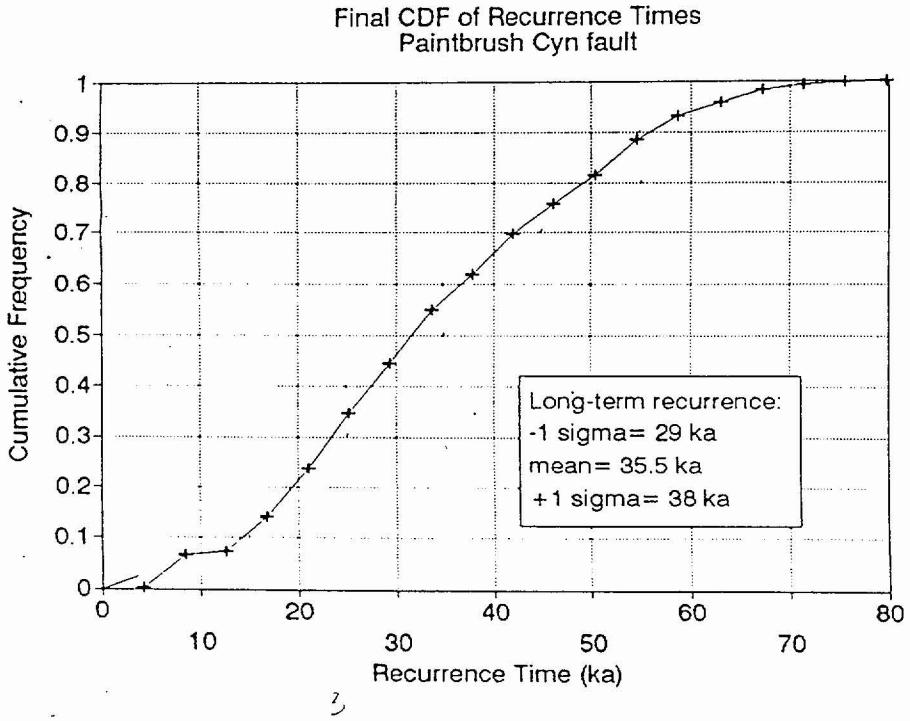
Final CDF of Recurrence Times
Paintbrush Cyn fault
Cumulative Frequency
Recurrence Time (ka)
Long-term recurrence:
-1 sigma= 29 ka
mean= 35.5 ka
+1 sigma= 38 ka

ASM-AS-5

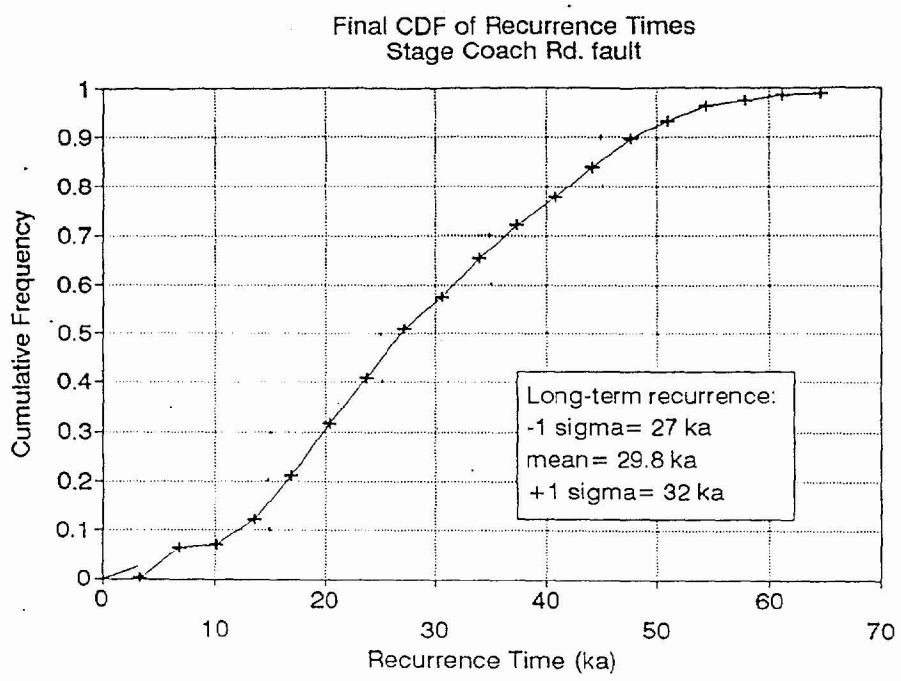
Final CDF of Recurrence Times
Stage Coach Rd. fault
Cumulative Frequency
Recurrence Time (ka)
Long-term recurrence:
-1 sigma= 27 ka
mean= 29.8 ka
+1 sigma= 32 ka

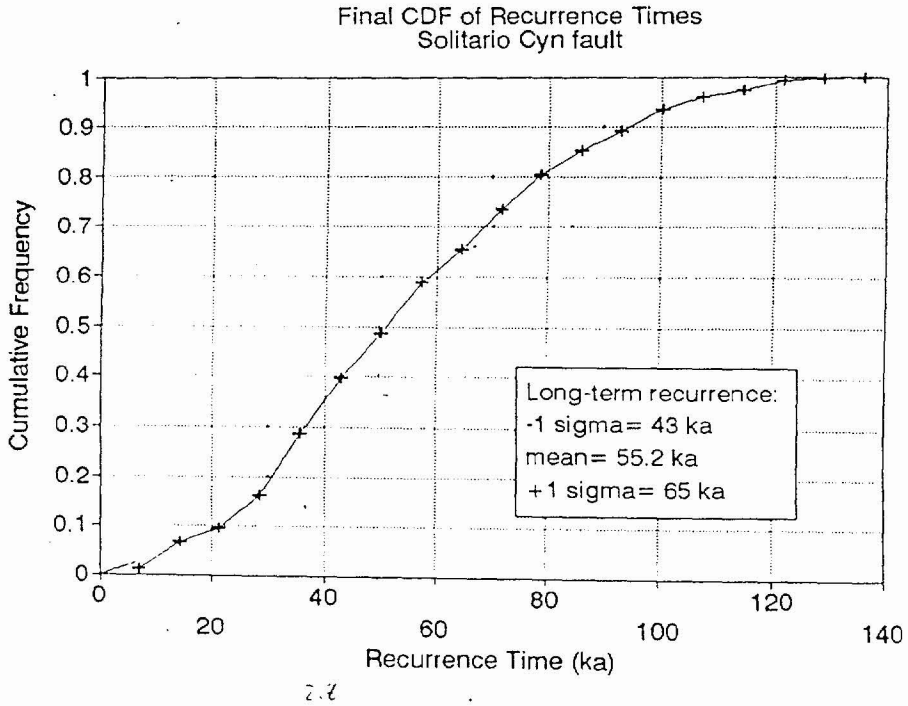
Final CDF of Recurrence Times
Solitario Cyn fault
Cumulative Frequency
Recurrence Time (ka)
Long-term recurrence:
-1 sigma= 43 ka
mean= 55.2 ka
+1 sigma= 65 ka

ASM - A5 - 6

APPENDIX ASM-6
REGIONAL SEISMIC SOURCE CHARACTERIZATION

The following notes document decisions on the fault characteristics and probabilities for 24 faults listed in Table ASM-6, which summarizes the relevant regional earthquake sources for the Yucca Mountain region. The 15 faults having names shown in *italic font* have substantial field data, or correlate with faults that have substantial field data, for estimating slip rate (SR), recurrence interval (RI), and approximate surface rupture length (SRL). The 9 faults having names shown in normal font have sparse characterization data; for these we use the method described in Sections 3.5.3 and 3.5.4 to estimate SR from SRL and RI from the estimated age of the faulted geomorphic surfaces summarized in Piety (1995), Reheis (1992), Reheis and Noller (1991), and Dohrenwend *et al.* (1992a,b).

1. H95, Carrara, or U.S. 95. The Carrara fault (also referred to as the Highway 95 fault) is informally characterized. It is not referred to in the main documentation available to the team, but is described briefly in the letter of David B. Slemmons (DBS) to Richard Quittmeyer of February 3, 1997. This document lists geologic, geomorphologic, and geophysical features that indicate that it is a Quaternary fault, including the following.

   (1) W.D. Nichols' (1987) description of drill holes and geophysical surveys indicates Pleistocene fault deformation along an unnamed northwest structure.

   (2) Low-angle aerial reconnaissance by DBS showed many features that appeared to result from Quaternary faulting.

   (3) The horizontal gravity gradients shown at SSC Workshop 3 exhibit a linearity that appears to be fault-controlled.

   (4) The feature is within 2 km of the Lathrop Cone.

   (5) The feature may explain vertical axis rotation at the south end of Yucca Mountain, and Bullfrog Hills.

   (6) Gilmore's geodetic profile as summarized by Pezzopane (SSC Workshop 2) shows an anomalous segment of the Beatty-Las Vegas geodetic level line that coincides with the Carrara feature.

(7) Ken Smith (SSC Workshop 2) showed that it is aligned along a belt of higher seismicity.

(8) Brocher *et al.* (SSC Workshop 3) showed a seismic reflection profile, aeromagnetic map, and isostatic gravity map had a NW-trending fault at U.S. Highway 95.

(9) The M&O Geophysics Synthesis Report (1996) showed a prominent arcuate structure along the Carrara feature, which appears to curve into the Rock Valley structural zone near Skull Mountain.

(10) Fridrich and Price (1992) inferred this fault south of Bare Mountain and Yucca Mountain on the basis of geologic and geophysical data.

(11) Quade *et al.* (1995) and oral discussions with Quade indicate the Carrara/Highway 95 feature is at the 13,100 ^{14}C yr (and earlier Quaternary) diatomaceous spring deposits, which appear to be from deeply circulating groundwater that emerged at a Pleistocene groundwater barrier just west of the southward extension of the Crater Flat fault.

We assign a high probability (0.85) for the Carrara fault being seismogenic based on these factors. We assign a low probability (0.15) of the fault being non-seismogenic, since the fault has not been thoroughly characterized. The abrupt truncation of all of the seismogenic, NS-trending faults between the Bare Mountain fault and the southeast end of Yucca Mountain at the Carrara fault also suggests that it is an active Quaternary fault. Two total fault lengths (20 and 42 km) are considered with equal weight. The shorter length of 20 km represents the northwest part of the fault (from the Amargosa River to U.S. Highway 95 and the southward projection of Windy Wash fault) that exhibits greater geomorphic expression. Extension of the fault an additional 22 km to east of Lathrop Wells (Amargosa Valley) is less certain. A lower probability of 0.5 is assigned to the 42-km length, which extends the fault eastward from the 20-km section that has geomorphic expression. The 10-km-long extension at the south end of Yucca Mountain lacks documented geomorphic evidence of Quaternary activity, but is marked by the abrupt truncation of Yucca Mountain. The change to a more east-west trend east of the Windy Wash intersection could indicate a decrease in rate of activity. The additional 12-km extension east of Yucca Mountain is an assumed feature that is based on the geophysical map showing depth to bedrock. The Mwmax values depend on SRL and are:

Mwmax=6.94 (for SRL= 42 km), Mwpref=6.64 (SRL=20 km, with a high probability of 0.7), and Mwmin=6.24 (SRL=10 km, with a low probability of 0.2). Although there is a component of vertical slip, the Carrara fault is characterized as a strike-slip fault. The uplifted block has a relief of about 22 m at U.S. Ecology, where Jim Yount reports that the upper surface appears to have a late Pleistocene soil (128 ka), which corresponds to a vertical separation rate >0.1 mm/yr. The estimates for the horizontal component of SR of 0.013 (0.2), 0.05 (0.6), and 0.12 (0.2) mm/yr are from the Crater Flat subparallel extension rate used for our detachment model.

2. MM, Mine Mountain. This fault is characterized as a strike-slip fault. This fault is truncated by Yucca Lake fault (YCL) and possibly by a fault at the boundary with Jackass Flat. Mw=6.64 for SRL= 20 km (based on Plate 1 of Piety (1995). Based on the northern truncation by YCL and an inferred fault along the northern edge of Jackass Flat, a total fault length of 20 km is used. Two SRL values (10 and 20 km) are given equal weight. Reheis and Noller (Y-238) list the 3-km segment as "a weakly to moderately expressed lineament or scarp on surfaces of Quaternary deposits and as a topographic lineament along a range front or in bedrock." SR and RI are inferred from SRL and assumption of three pre-Holocene surface rupturing earthquakes.

3. WAH, Wahmonie. This fault is characterized as an oblique-slip fault. Mw=6.42 for SRL=14.5, based on Plates 1 and 2 in Piety (1995). Data primarily from Plate 1. Based on the truncation by the Cane Springs fault (CS), a single value of SRL (14.5) is used (weight 1.0). Reheis and Noller (1991) report "weakly expressed to prominent scarps and lineaments." Oral discussions with Jim Yount indicate late Pleistocene activity at the north end of the fault. SR and RI are inferred from SRL and assumption of three pre-Holocene surface rupturing earthquakes.

4. AM, Ash Meadow. This fault is characterized as a west-dipping normal fault. Mw=6.24, 6.91, and 6.94, respectively for SRLs=10, 38, and 40 km. This fault was at a shallow water table during Pleistocene, and the surface effects may be by partly plastic behavior. Revised on Figure 13 of Anderson *et al.* (1995b). Preferred length is 38 km from north end near Amargosa River (AR); scarp about 14 km SE of Nevada Highway 373 and Stateline, which Anderson *et al.* (1995b) notes may be a northern extension of West

Resting Spring Range (WRSR) fault. The fault has fair, but incomplete, characterization data. Although the original mapping of Donovan shows three segments, the displacement values tabulated in Anderson *et al.* (1995b) suggest that there is no segmentation. The average surface offset values from Table 5 of Anderson *et al.* (1995b) for the three fault segments are similar, which suggests that average displacement (AD) = 0.8 m; MS = 2 m; and for 35,000 years the average slip rate = 0.02 mm/yr. This corresponds to M = 6.91. The report of Anderson *et al.* includes a series of more active ruptures along the west side of Resting Springs Range, which could make the length too long, the slip rate too high, and recurrence interval too short for the entire zone. On the other hand, the late Quaternary surface fault shown by Anderson *et al.* (1995b) north of U.S. Highway 95 was verified by observations of DBS during a recent aerial flight, which is suggested by the surface scarp pattern. Their data do not clearly show whether there was one or more than one event.

5. RV, Rock Valley. This appears to be one of the most important strike-slip faults near Yucca Mountain. This fault appears to be truncated on the west end by the Amargosa River fault, and on the east end by the Buried Hills and/or Spotted Range faults, and to the southeast by distributed northeast-trending short faults. Data were derived from Piety (1995) and Chapter 4.13 of USGS (written communication,1996). The maximum earthquake is Mw=7.1+/-0.4 from Mw=6.69+0.74 MD, or Mw=7.23 from Mw=5.08 + log 72. Exploratory Studies Facility (ESF) dip is 70, 80, or 90 with left oblique. SRL is based on Plate 1 of Piety (1995); SR and RI are from Chapter 6.12 of USGS (written communication, 1996).

6. WSR, West Specter Range. This fault is characterized as a west-dipping normal fault. Based on shadows observed along this fault during low-sun-angle (LSA) aerial reconnaissance in early morning and late afternoon illumination, D.B. Slemmons (DBS) estimated that the maximum slope of the scarps in alluvium are approximately 15 to 18 degrees. Scarps with similar slopes normally indicate that the most recent displacement was early Holocene or late Pleistocene. The activity rates observed by Anderson *et al.* (1995b) appear to be correct, although DBS observations at Amargosa Flat indicate that there may be one or two Holocene to late Quaternary events. The fault probably is truncated by the Rock Valley fault and may cross the valley on the west side of West

Specter Range. No surface trace is visible toward the Last Chance Range fault. The fault appeared to connect northward with ESR (Anderson *et al.*, 1995b), and may extend northward to join or terminate against the Rock Valley fault zone for a maximum length of 25 km. DBS observed that the scarp extends south for a total length of about 18 km from north of Highway 95 to the south edge of Amargosa Flat. Several aerial observations with low-sun angle illumination did not show any offsets in active alluvial fans to the south toward Last Chance. DBS observed this zone several times with LSA, and observed a 15-km gap in late Quaternary faulting south of Amargosa Flat in bedrock and recent alluvium. There also is a possibility that it connects southward under young alluvium and bedrock units to the Last Chance Range fault discussed in Anderson *et al.* (1995a), to Y- 938, and to the North Pahrump fault zone at the northeast end of the Stewart Valley Playa. The ASM team did not characterize the Last Chance fault because it has a low rate of activity, is a short segment with a low rate of activity, and an interconnection to the West Specter Range fault would require faulting across a 20-km gap with no known Quaternary faulting. Anderson *et al.* (1995a) estimate a slip rate of 0.004 mm/yr and a recurrence interval of at least 113 ka, based on one event. Their descriptions suggest two events, which concurs with an observation of DBS for the scarp in Amargosa Flat. The observation of DBS of about 2 m of Holocene and late Quaternary offset led to higher SR estimates of 0.004, 0.01, and 0.02 mm/yr.

7. CS. Cane Springs. This fault is characterized as a strike-slip fault. Mw= 6.61 for SRL=21 and Mw=6.68 for 26 km based on interpretation of Plate 1 of Piety (1995). The fault appears to merge with three splays at the southwest end, and truncates against the curving end of Yucca Lake fault at the northeast end; accordingly, the length has a small uncertainty range. SR and RI are inferred from SRL and assumption of three pre-Holocene surface rupturing earthquakes.

8. AR, Amargosa River. This fault is characterized as a strike-slip fault. This fault has unresolved relations to other faults. Map revised from Fig. 8 of Anderson *et al.* (1995b) and Piety (1995), Mw=6.34 for SRL=12.4 km (Anderson *et al.*, 1995a), and Mw=6.70 for SRL=24.8 km (Anderson *et al.*, 1995a) and D.B. Slemmons field and LSA aerial observations of a late Quaternary fault scarp at location noted on map, and L=48 km from +north end of Y-238 to NE corner of Stewart Valley playa. DBS observations of two

other unmapped Quaternary scarps between the scarp noted above and Stewart playa. SR is poorly constrained from the small 1.1-m surface offset (Anderson *et al.*, 1995b) /12 to 128 ka, with preferred value at 0.05 mm/yr. The values, higher than those implied in Anderson *et al.* (1995b), are based on aerial reconnaissance. The RIs are estimated at >10 ka, 128 ka, and preferred value at a mid-value of 69 ka. Most of the fault zone is at or near the water-table level, and the surface deformation appears to be partly from warping. RI data are not available. The proposed maximum length of 48 km is from the northeast end of Stewart Valley playa to Y-238 on Plate 2 of Piety (1995) to the southeast of Big Dune, but a more likely scenario is segmentation into two segments. The latter possibility could include the activation of the northwest edge of Montgomery Range and springs including Devil's Hole. DBS has several LSA Ektachrome slides, and the 1:24,000 scale quadrangle map suggests that there are at least three active Quaternary faults in the 10- to 20-km gap between Stewart Valley and the south end of AR as suggested in Anderson *et al.* (1995b). However, the faults are distributed over a width of several kilometers, which appears to preclude a simple throughgoing fault. These short (2- to 3-km-long) oblique fault scarps are between the east edge of Stewart Valley, the Devil's Hole spring area, and the Grapevine Spring area. Their presence suggests that there is no gap between Amargosa River (AR) and Ash Meadow (AM) and N Pahrump-Stateline fault zones, and that the two zones may be connected by a complex, segmented zone.

9. YCL, Yucca Lake. This fault is characterized as a strike-slip fault. Mw=6.49 from SRL= 16.3 km based on extension to the south as mentioned in Piety (1995); Mw=6.63 from SRL=20.6 includes Y-238 (Plate 1, Piety, 1995) near CS. Comment in Piety (1995), "only youthful-appearing...fault." SR and RI are inferred from SRL and assumption of three pre-Holocene surface rupturing earthquakes.

10. ER, Eleana Range. This fault is characterized as an east-dipping normal fault. Length=10.6 and 12.7, based on Piety (1995, Plate 1). The database has ambiguous late to mid-Pleistocene dating and no displacement data. Piety (1995) reports that one unit with scarps is 160 to 800 ka, and one date suggests that the faulting is post-128 ka. SR and RI are inferred from SRL and assumption of three pre-Holocene surface rupturing earthquakes.

11. ESR, East Specter Range. This fault is characterized as an east-dipping normal fault. SRL=9 km (minimum) and 15 km (maximum) based on Plate 2 of Piety (1995). The length is defined by scattered scarps in alluvium and by the topography. Anderson *et al.* (1995a) and observations noted in the letter of DBS to Richard Quittmeyer of February 3, 1997, suggested similar characteristics to West Specter Range fault (WSR) when viewed with LSA. The appearance is similar, and the West Specter Range does not appear to be tilted from long-term paleoseismic activity, so parameters similar to WSR are used. SR and RI are inferred from SRL and assumption of three pre-Holocene surface rupturing earthquakes.

12. YC, Yucca. This fault is characterized as a strike-slip fault. Mw=6.66 and 6.83 for SRL=23 and 33 km, respectively. SR lengths are based on the estimated total length of distributed surface rupture. No significant measurements of displacement from multiple events is reported. Oblique slip is suggested by en echelon pattern. SR and RI are inferred from SRL and assumption of three pre-Holocene surface rupturing earthquakes.

13. WSM, West Spring Mountains. This fault is characterized as a west-dipping normal fault. Fault extends northward from Hidden Hills Ranch to scarp near Grapevine Springs, and probably to near U.S. Highway 95 at the northwest corner of Spring Mountains (LSA aerial reconnaissance and tilted Pliocene/Pleistocene surfaces). Slip rate and recurrence interval data are from Anderson *et al.* (1995a). The Wells and Coppersmith (1994) regressions suggest that the large displacements noted by Anderson *et al.* (1995a) are from multiple offsets of >2.2 m. Smaller offsets suggest an average for 17 measurements of SO of 1.33 m, or using AD/MD =0.38, the MD should be 3.5 m, and M=7.05. This is similar to M=7.09 for a rupture length from Grapevine Springs scarps to the PVFZ at Hidden Hills along a narrow and linear N17W eastern boundary of the 3- to 4-km-thick Pahrump Tertiary half-graben. Anderson *et al.* (1995b) estimate of AD=1.8-2.0 may be somewhat too high (40%). Anderson *et al.* (1995a) estimated the RI and SR at more than 28 ka to as much as 120 ka, and less than 0.02 mm/yr to as much as 0.07 mm/yr. They suggest that there were two, or possibly three, events.

14. FC, Furnace Creek. This fault is characterized as a strike-slip fault. Mw=7.49 (based on >120 km length and similarity to M=7.5 Owens Valley fault scarp of 1872). The south end is defined as the abrupt change in strike at the north end of EDV, and extends northward without apparent segmentation to the north end of the Fish Lake Valley fault (Piety [1995] and Reheis and Sawyer [1996]). FC had average displacements (ADs) of about 2.5 to 3.5 m per event along several fault strands. Table 5 of K. E. Klinger and L. A. Piety (USBR, written communication, 1996) indicates AD=4.5 m of strike-slip offset. Owens Valley is assumed to be an analogous event with M=7.5, Dmax=9+/-2 m, Davg=~4-5 m, slip rate ~2.0 m, 0.45+/- 0.75. The unpublished data of Strom and Nikonov and of Slemmons show the AD = 0.38, or approximately 0.4 x Dmax, which gives an AD of about 3.4 m for M=7.5. This is reasonably close to the 4.5 value estimated by R. E. Klinger and L. A. Piety (USBR, written communication, 1996). Accordingly, the values of R. E. Klinger and L. A. Piety (USBR, written communication, 1996) will be used. The slip rate is approximately two to four times higher than that of Owens Valley fault, and about two to three times higher than the 2.42+/-0.7 m in Panamint Valley.

15. EDV, East Death Valley. This fault is characterized as a west-dipping normal fault. Mw=7.21 (based on L=75 km, scaled from maps of Brogan *et al.* [1991]). The maximum net displacement (5.0 m at mileage 38.1 of Table A1 in R. E. Klinger and L. A. Piety, USBR, written communication, 1996) corresponds to Mw=7.21, using the regression of Wells and Coppersmith (1994). These values are consistent with the somewhat higher magnitude 1872 Owens Valley earthquake of Mw=7.5, which had a length of 100 to 108 km and MD=9.1 ± 2 m (Beanland and Clark [1994]). The north end of the fault zone is shown on Plate 2 of Piety (1995) as an abrupt strike change of Holocene scarps at California Highway 190 near Salt Springs in the middle of Section 21 of T28E, R1E. The south end is truncated by the Southern Death Valley (SDV) fault system at Shoreline Butte. The vertical component for surface fault slip rate and RI data are based on R. E. Klinger and L. A. Piety (USBR, written communication, 1996). Klinger and Piety, Tables 4 and 5, indicate a mainly vertical separation of 3 to 5 mm/yr, which should be increased by 15.5% for a 60-degree dip for use of the Wells and Coppersmith (1994) regressions. The Tertiary extension direction is about N60W in a N12S-trending Death Valley graben, as suggested by striae on fault surfaces in the bedrock (oral

communication by Martin Miller, University of Wisonsin-Eau Claire). Only a few strike-slip offsets are shown in Figure 5 of R. E. Klinger and L. A. Piety (USBR, written communication, 1996); their report did not include deformation at Cinder Hill. Accordingly, our analysis characterizes the EDV as a normal fault that is assumed to dip 60 degrees westward, and places the strike-slip component to a subparallel outboard fault, the inferred MDV, which is assumed to be a vertical strike-slip fault about 3 to 5 km west of EDV. A vector analysis of EDV of N12W orientation, and a vertical slip rate of 4 mm/yr for N50W extension (parallel to the FC and SDV right-slip faults), would be 4.62 mm/yr net normal-slip component on a frontal fault dipping 60 degrees. The dip-slip component for a normal fault dipping 60 degrees (EDV) would have net components 3.46, 4.62, and 5.77 mm/yr, for vertical separation rates of 3, 4, and 5 mm/yr, respectively. The AD (average displacement) from R. E. Klinger and L. A. Piety (USBR, written communication, 1996) is 2.5 to 3.5 m; using a 1/0.38=2.63 multiplier suggests AD=3.0 m, MD=7.9 m, or from Wells and Coppersmith (1994), Mw=7.35.

16. BLR, Belted Range. This fault is characterized as a west-dipping normal fault. Mw=7.04 for SRLmax=49 km and Mw=6.61 for SRLmin=21 km as reported in Anderson *et al.* (1995a) and Piety (1995). The scarps that Anderson *et al.* (1995a) studied are in the middle segment of BLR (Piety, 1995) opposite the highest part of the range; they did not evaluate the activity rates of the other parts of the fault. Anderson *et al.* (Table 3, 1995a) infer an AD=0.675 m based on profiles of single-event scarps at four data points; this corresponds to MD=1.8, which is close to the 1.5 m observed value. Multiple-event scarps average 2.7 m in height, which suggests four events in 118 ka. Displacements are as great as 2.5 m; they estimated SR of 0.01-0.1 mm/yr on a fault with a long-term SR of about 0.05 since 12.5 to 11.5 Ma. Examination of the data in Figures 7 and 8 (Anderson *et al.*, 1995a) indicates steep scarp slopes of 11 to 19 degrees, which suggests that for all but one profile, there were two, three, or four faulting events, with MD= 1 to 2 m and Mw=6.6-6.9 during the last 128 ka. Anderson *et al.* (1995a) report that the RI is poorly constrained. They suggest that it is greater than 10 ka, but with multiple events in less than 100 ka, perhaps much less than 100 ka. Based on multiple events (2 to 4) during the past approximately 128 ka, a range of RI (20 to 69 kyr) is used in this analysis.

17. MDV, Mid Death Valley. This fault is characterized as a strike-slip fault. The fault length is assumed to be 72 km from near Cinder Hill to an intersection with the southern segment of the Furnace Creek fault zone (DBS): Mmax=7.23 (based on L=72 km, and the regression for all fault types of Wells and Coppersmith, 1994). A mid-valley fault zone includes all of the strike-slip component of EDV as shown by vector diagrams from the striation direction shown in places along the frontal fault plane, the extension direction shown in bedrock by the Miocene and Pliocene extension in Black Mountains, and geometry of extension from the valley opening, which is subparallel to the N50W Furnace Creek and Southern Death Valley strike-slip faults. MDV is demonstrated geologically by the Cinder Hill right-lateral offset, which is variously reported to be 80 m and 100 to 200 m (as reported by Larry Anderson at Stop 5 in DOE/Participant Management Field Trip Guide Book, dated January 28-31, 1992). The earlier radiometric date of Cinder Hill is 680 ka, but a new radiometric date is reported to be 100 ka to no more than 200 ka. This suggests a geologic strike-slip rate at Cinder Hill that is about 0.15 to 2 mm/yr, with a preferred rate of about 1 mm/yr, which is the minimum value in Table ASM-6. At the north end of the EDV near Salt Creek, a strike-slip fault with associated folded Quaternary to Pliocene sediments was mapped by Lauren Wright and Bennie Troxel. Martin Miller (telephone conversation of 4/24/97) reports that the Miocene (~15 Ma) to Pliocene direction of extension for the basement rocks of Black Mountains was N60W. The slip vector diagrams indicate that the strike-slip component is about 40 percent of the rate observed for the frontal fault. The minimum slip rate is based on the ca. 1 mm/yr rate observed at Cinder Hill; the maximum rate of 3 mm/yr is based on a vector diagram for the N50W extension of the valley noted under discussion of the East Death Valley fault (EDV); and the preferred slip rate is the average of the minimum and maximum values.

18. GV, Grapevine. This fault is characterized as a strike-slip fault. Mw=6.72 for SRL=29 km, which is similar to the 23 km estimated by Reheis (1992). It appears to extend 8 km on Piety (1995), Plate 1, and 17 km on Plate 2 to a possible connection with FC, or a similar distance on strike to Y-239. The low uncertainty in length is the apparent connection at both ends to the more active Furnace Creek fault zone. Quaternary displacements are implied by topographic lineaments (subtle to prominent) on surfaces of

Quaternary deposits. SR and RI are inferred from SRL and assumption of three pre-Holocene surface rupturing earthquakes.

19. WDV, West Death Valley. This fault is characterized as an east-dipping normal fault. Mw=7.13 (based on L=62 km as mapped by Brogan *et al.* [1991] in Death Valley). The minimum and preferred SRLs of 25 and 39 km are based on the two shorter groupings. This zone appears to have a very low slip rate, demonstrated by tilted fans that appear to be middle to early Pleistocene (oral comments at SSC Workshop 5 by Charles D. Harrington) along the Panamint Mountains and that have a thin veneer of younger Quaternary alluvium. Brogan (telephone conversation) reported that the scarps are only a few meters high, and the longest continuous zone is only about 3 km long. SR and RI are inferred from SRL and assumption of three pre-Holocene surface rupturing earthquakes.

20. EM-TP, Emigrant/Towne Passe. This fault is characterized as a northwest-dipping normal fault. Mw=7.02 for the maximum SRL=47. These values are revised from Plate 2 and discussion in Piety (1995). The Stovepipe Wells fault is included with EM. One early Holocene to latest Pleistocene offset of about 1 m, observed in the field by USGS staff, is also suggested in an oblique aerial photo by D.B. Slemmons (DBS), which shows about 1 to 2 m offset of a large Pleistocene or Holocene alluvial cone at Tucki Mountain. The date of the most recent event appears to be >10 ka, approximately RI=19 ka for latest Pleistocene, or 69 ka for late Pleistocene. The fault is not relevant unless it is coupled with the Towne Pass fault, which is shown in the longest fault option.

21. PRP, North Pahrump-Stewart Valley. This fault is characterized as a strike-slip fault. Mw=6.94 (based on SRL=40 km): Piety (1995) map. The 40-km-long fault joins the south end of the Amargosa River fault (AR) or Ash Meadows fault (AM) and the north end of the South Pahrump-Stateline fault system (SPRP); the earthquake scenarios include possibilities of either a single 40-km rupture, or two segments with half that length. Our interpretation is based partly on the conclusions of J. L. Hoffard (University of Nevada, Reno, written communication, 1991) and observations by DBS during many low-sun-angle aerial reconnaissance flights over the area. Hoffard showed the North Pahrump fault extending into the Stewart Valley half-graben, and observations and photographs by DBS indicate a distributed pattern of at least three Quaternary faults

extending into Amargosa Valley. The irregularities of faulting between Stewart Valley and the Amargosa River fault suggest that they may be strongly segmented and can be considered separate sources. The assessment partly is based on the prevalence of surface warping along faults that cross areas of shallow water table and late Pleistocene activity at paleosprings. There are Holocene scarps and vegetation lineaments. The youngest scarp of early Holocene age is 5 m high (just south of Highway 52). Aerial examination with LSA shows discontinuous Holocene or late Pleistocene scarps in the valley, partly from concealment by the extensive sand dunes along the fault escarpment; deformed terraces (late Wisconsin?) and tilted spring deposits also are observed along the fault traces. The activity includes an early Holocene event and two or three events assumed since 128 ka. If the fault is primarily strike-slip or oblique-slip, as would be expected from this orientation, the horizontal component should be greater than the vertical. Louie *et al.* (in press) obtained geophysical data that suggest a lateral offset of 18 m at 24 m depth, having no more than 1 m of vertical offset. They estimate a horizontal slip rate of 0.1 mm/yr for 100 to 150 ka, and a possible higher 1.8 mm/yr rate if the offset is 10 ka old. We judge the latter rate as too high, but the relationships strongly indicate that the fault is a strike-slip fault, with a high ratio of 10:1 or 20:1 for strike-slip to vertical-slip component.

22. WPR, West Pintwater. This fault is characterized as a west-dipping normal fault. M=71 based on L=56 km (Piety, 1995). Piety (1995) reports that Reheis (1992) notes "weakly expressed to prominent lineaments and scarps on surface of Quaternary (primarily) and Tertiary deposits and as faults that are in Quaternary and Tertiary (primarily) deposits and that were identified from previous mapping." The source model assumes that the 56-km-long fault can be subdivided into three segments; there is equal likelihood of rupturing as one, two, or three segments; and rupture is equally likely to occur at any part of the zone. We have no displacement data. Fault may extend north from the tectonically active Las Vegas Valley at Indian Springs.

23. PAN-HM, Panamint Valley-Hunter Mountain. This fault is characterized as a strike-slip fault. PAN fault zone is truncated on the south end by the Garlock fault (which has SR of about 8 mm/yr) and continues north to the Hunter Mountain fault zone and Saline fault zone: Note the interconnection with Hunter Pass fault, which makes it a relevant source,

and frontal faults along the west side of Saline Valley. The seismic source parameters used in our model are based on Zhang *et al.* (1990), as summarized in Piety (1995).

24. SPRP, South Pahrump-Stateline. This fault is characterized as a strike-slip fault. Total fault length of ca. 65 km is from U.S. I-15 to Hidden Hills Ranch near the intersection of California Valley and Pahrump Valley. The north end connects with the south end of North Pahrump-Stateline and West Spring Mountains fault (WSM). The south end appears to terminate near U.S. I-15, since the adjoining Ivanpah fault does not appear to displace middle Pleistocene alluvial deposits. A full rupture length leads to Mw=7.18 and AD=1.127 m (based on MD determined from Wells and Coppersmith [1994] regression; MD, multiplied by 0.38, determines AD). The preferred RI=39 ka and SR=0.05 mm/yr, as the fault appears to be nearly linear and unsegmented. Aerial reconnaissance suggests that this section is less active than the North Pahrump/West Spring Mountains fault zones. However, the weak geomorphic expression may be due to mainly strike-slip offsets, and there may be two or more events in the past 128 ka. If the fault is primarily strike-slip or oblique-slip, as would be expected from this orientation, the horizontal component should be greater than the vertical. This fault was considered to have a low rate of activity in our first assessment, but the recent study by Louie *et al.* (in press) shows "almost purely strike-slip motion at scarp 1" near the Old Spanish Trail Highway, south of Hidden Hills Ranch. The weightings of one-third each include a high SR model, based on about 0.1 mm/yr (J. Louie *et al.*, University of Nevada, Reno, written communication, 1997), a 0.05 mm/yr rate that is intermediate, and a very low rate of 0.002 mm/yr.

APPENDIX E

SEISMIC SOURCE AND FAULT DISPLACEMENT EXPERT ELICITATION SUMMARIES

The following seismic source and fault displacement team expert interpretations have received review by PSHA Review Panel members in accordance with quality assurance approved PSHA Project Plan requirements but have not been reviewed for conformity with Department of the Interior, U.S. Geological Survey standards.

ELICITATION SUMMARY

WALTER J. ARABASZ, R. ERNEST ANDERSON, AND ALAN R. RAMELLI

TABLE OF CONTENTS

TABLE OF CONTENTS

TABLES

FIGURES

TABLE OF CONTENTS

ELICITATION SUMMARY
WALTER J. ARABASZ, R. ERNEST ANDERSON, AND ALAN R. RAMELLI

1.0
TECTONIC MODELS

No single tectonic model yet proposed can serve as a predictive template for seismic hazards assessments at Yucca Mountain. The region comprises several tectonic domains, each having distinctive (and, in most areas, complex) internal structure and contrasting bounding structures (D. W. O'Leary, USGS, written communication, 1996). In our evaluation of tectonic models, we accept that Yucca Mountain is located in a specific tectonic domain, to which we attach fundamental tectonic importance. Following D. W. O'Leary (USGS, written communication, 1996), we refer to it as the Crater Flat domain (CFD). Any viable tectonic model must explain the structural development of the CFD, especially its Quaternary structural history. It must also be consistent with contemporary regional tectonics, especially with those of the domains adjacent to the CFD.

Before determining the appropriate tectonic models, we evaluate the processes that control the contemporary tectonics of the CFD. In particular, we distinguish between pure shear and simple shear processes, evaluate whether magmatism should be considered a controlling process, and, similarly, whether regional detachment faulting is a controlling process. We recognize that fault-related tilting is pervasive in the CFD, and that in much of the domain the tilting is complicated by steep-axis rotation. These tilts and rotations are incompatible with pure (irrotational) shear, leaving simple (rotational) shear as the only option leading into the front end of our logic tree (Figure AAR-1).

We recognize that silicic magmatism, and especially caldera-forming processes, may have played an important role in the early development of the CFD. But we conclude that contemporary deformation in the CFD is not controlled by caldera-forming magmatic processes, because there is no evidence that events related to such processes continued into the latest Tertiary and Quaternary. Because there is evidence for both Quaternary basaltic

volcanism in the CFD and a temporal association of faulting and volcanism, we recognize that future earthquakes could be associated with basaltic volcanic processes. In a separate section, we assess that likelihood. Based on the estimated low frequency of basaltic volcanic events and the relatively low magnitude of earthquakes typically associated with basaltic volcanism, we do not include in our logic tree a tectonic model controlled by basaltic volcanic processes.

A separate but related question concerns the percentage of extension across the CFD that might be accommodated by volcanic intrusion. Basaltic intrusions occurring as dike injections, rather than rising along vertical pipes, should accommodate some extension and reduce the occurrence of earthquakes (cf., Parsons and Thompson, 1991). Estimates of Quaternary extension across the CFD come from evidence of surface faulting, so the question is whether surface faulting is caused by extensional stresses induced by intruding dikes (if not, then any extension accommodated by volcanism would occur in addition to that accommodated by earthquakes). Paleoseismic data for the Yucca Mountain faults typically span time frames of hundreds of thousands of years. Over these periods, most faults show evidence of several earthquake cycles (recurrence intervals for the principal faults average about 50 ka). The only evidence of volcanism over this same time span is the Lathrop Wells basalt cone, which formed within a relatively narrow time window (possibly primarily during a single eruptive episode). We do not consider accommodation of extension by volcanism for two reasons: (1) surface faulting occurs much more frequently than volcanism; and (2) surface faulting occurs over a widespread area, with little direct spatial association with the Lathrop Wells cone. If basaltic intrusions that did not reach the surface occurred much more frequently and over a broader area than suggested by the Lathrop Wells cone, this interpretation could bear revision.

We conclude that contemporary deformation in the CFD is not controlled by a regional detachment fault of the type envisioned by Scott (1990) because: (1) extensive geologic mapping of Miocene and pre-Miocene rocks has failed to reveal it; (2) there is no evidence that Miocene volcanic features or cells of Miocene hydrothermal activity have been shifted laterally from their roots; and (3) no detachment-related breakaway zone and tectonically denuded footwall have been identified in areas east of the domain. Also, we do not consider a tectonic model controlled by a deep (12 to 15 km) detachment fault because extensive

geologic evidence (geobarometry on mylonitic rocks) indicates that yielding in subhorizontal high-strain zones at those depths is accommodated by crystal-plastic recrystallization processes. In such cases, seismicity is considered to be generated only from the higher-angle faults feeding into the ductile accommodation zone.

We consider deformation in the CFD to be controlled by a stress field created by superposed stresses of uncertain relative influence, chiefly: (1) WNW-ESE Basin and Range extension, along with possible combinations of (2) NW-SE dextral shear related to Pacific-North American relative plate motion and (3) general N basal traction and/or horizontal compression related to southerly mass movement from an elevated northern Great Basin lithosphere. We conclude that all viable tectonic models for the CFD must include an element of extension.

1.1 DEXTRAL SHEAR STRUCTURES

The first node of our logic tree (Figure AAR-1) addresses whether a NW-SE dextral shear influence is manifested by significant unrecognized or poorly characterized dextral shear structure(s). The branch for "no significant NW-SE dextral shear structure(s)" does not preclude an influence by regional dextral shear. The branch simply indicates that if there is such an influence, it is not manifested by right-slip faults of a size that would produce earthquakes having maximum magnitudes greater than that of our background source zone. We weight the two possibilities equally because the issue is unresolved. Hypothesized dextral shear structures are plausible (in particular, a fault paralleling Highway 95, as proposed by Slemmons, or a cross-basin fault as supported in a presentation by Pezzopane), but (1) their existence has not been established, and (2) they are not characterized sufficiently to conclude that they are potential sources of strong ground motion above a background source.

The nature of plausible NW-SE dextral shear structure(s) is treated at the second node of our logic tree. Here three branches consider the possibility of unrecognized or poorly characterized sources in addition to the CFD faults: a throughgoing regional dextral shear zone, a right-stepping shear zone that produces a pull-apart basin, and a right-stepping shear zone in which the pull-apart basin is underlain by a cross-basin, right-slip fault. We assign

the greatest weight to a pull-apart basin containing one or more bounding dextral faults, because the Highway 95 fault is the only proposed dextral shear structure for which evidence has been described (Slemmons, information distributed to SSC teams by R. Quittmeyer dated 3/4/97). We assign less weight to the existence of a cross-basin fault; such a structure could explain the structural discontinuity of CFD faults, but its existence is based on indirect evidence. We assign a very low weight to the existence of a throughgoing regional shear zone because no direct evidence for such a feature exists and we know of no analogs.

In the absence of significant dextral shear structures, the CFD faults accommodate extension independently, but such accommodation can be accompanied by both dextral shear and southerly directed tectonic displacement. The evidence for such accompanying deformation comes from the earthquake record (Rogers *et al.*, 1991) and the geologic record of strike-slip faulting and steep-axis bending (Fridrich *et al.*, SSC Workshop 3, handout dated 11/1/1996). This model has as its analog the Gale Hills north of Lake Mead, where N- to NE-striking, left-normal faults and the blocks bounded by them bend clockwise as they are traced southward toward the adjacent right-slip Las Vegas Valley shear zone (Sonder *et al.*, 1994). Rather than having formed by drag associated with dextral shear, the faulting and bending are best interpreted as resulting from south-directed tectonic collapse and to have involved distributed basal traction (Anderson *et al.*, 1996).

1.2 LOCAL DETACHMENT

The third node of our logic tree (Figure AAR-1) addresses the existence of a local detachment and outlines credible models in which a local detachment is conditionally favored or permissible. In no case is a detachment fault considered to be a controlling structural element. As interpreted by us, a local detachment fault could be a reactivated thrust or a gently dipping accommodation zone.

The depth of a local detachment is addressed at the fourth node of the logic tree where, conditional on its existence, we consider the probability that the detachment lies at a depth < 3 km, 3 to 10 km, or > 10 km. Based on the geophysical data, we preclude a depth less than 3 km. We give greatest credibility to the 3- to 10-km depth range, because narrow fault blocks such as the 3- to 5-km-wide major blocks of the CFD are more likely to maintain their

structural integrity to depths 1 to 2 times their width than to 3 to 4 times their width. Our assigned distribution for the depth (and relative weighting) of a detachment in the 3- to 10-km depth range is:

4.5 km (0.185), 7.0 km (0.63), 9.0 km (0.185).

Throughout, when we assess a three-point distribution, we follow Keefer and Bodily (1983) in assigning relative weights. Following their guidance for three-point distributions, we consistently attempt to estimate the median (i.e., 50th percentile value) together with either the 5th and 95th percentile values or the 10th and 90th percentile values. The appropriate weights then are 0.185, 0.63, and 0.185 to approximate the 5th, 50th, and 95th percentile values, respectively, and 0.3, 0.4, and 0.3 for 10th, 50th, and 90th percentile values. Thus, our use of these combinations of weights in any three-point distribution implicitly indicates the estimated percentiles to which the weighted values correspond.

If the detachment is deeper than 10 km, we consider its depth to have a uniform probability of being anywhere between 10 km and the maximum depth of the seismogenic crust (discussed in the next section).

We conclude that a local detachment, if it exists, has a low-likelihood of being seismogenic, because the data provide no evidence for earthquakes on such faults in the Basin and Range. Accepting the agreed use of this term in this PSHA project, "seismogenic" is defined as capable of generating earthquakes significant to ground motions ($M \geq 5$). For convenience, we use the notation P[S] for "Probability [Seismogenic]." For a local detachment fault, we attach a low probability, P[S] = 0.05, to such a fault being seismogenic.

We concluded that any local detachment beneath the CFD would not be active over the entire domain. It would, for example, be constrained in extent by the downdip projection of the Bare Mountain fault on the west and the downdip projection of the Paintbrush Canyon fault on the east. Our evaluation is the following: In the unlikely case that a local detachment were seismogenic, we account sufficiently for its rare earthquake by our local background source zone, which has a maximum magnitude of 6.3 ± 0.3. This range would encompass seismic slip on a detachment having a maximum rupture of 200 km^2 and a larger than normal

average displacement of 1 m. Accordingly, we do not include a local detachment in our inventory of seismic source zones.

2.0
DEPTH OF THE SEISMOGENIC CRUST

In assessing the maximum depth of the seismogenic crust, we distinguish between (1) the maximum thickness of the seismogenic layer as a control on downdip width (and hence area) of rupture, particularly for use with regressions of Wells and Coppersmith (1994), and (2) the maximum depth to which seismic rupture (and seismic energy release) may physically reach during larger earthquakes. The latter depth becomes important in estimating rupture area, RA, for use in the moment equation, $M_0 = : * RA * ®$ (see, for example, Youngs and Coppersmith, 1985, equation 2), where : is the rigidity or shear modulus (assigned the value 3×10^{11} dyne cm^{-2}), and ® is the average (subsurface) displacement over the slip surface.

Our assessed distribution for the maximum thickness (and relative weighting) of the seismogenic layer, called DMAX1, in the Yucca Mountain region is:

11 km (0.185), 15 km (0.63), 17 km (0.185).

We base our assessment of DMAX1 on the depth distribution of seismicity in the southern Great Basin (K.D. Smith presentation at SSC Workshop 2), the aftershock sequence of the 1992 Little Skull Mountain earthquake (Harmsen, 1994), and a review of how Wells and Coppersmith (1994) measured downdip rupture width, including values for the largest historical normal-faulting earthquakes in the Western United States.

Taking into account the tectonophysics of rupture dynamics (e.g., Yeats *et al.*, 1997, p. 49ff, and references therein) and observational studies of the coseismic slip distribution for the Borah Peak and Landers earthquakes (Mendoza and Hartzell, 1988; Wald and Heaton, 1994; Cohee and Beroza, 1994), we assess a separate distribution, called DMAX2, for the maximum depth of seismic rupture during some larger earthquakes in the Yucca Mountain region. The depths and their relative weights are:

14 km (0.185), 18 km (0.63), 22 km (0.185).

Simply put, the rupture surfaces of large earthquakes can "reach down" below the seismogenic layer into the brittle-plastic transition zone, resulting in greater rupture width (and area). We interpret descriptions of this phenomenon as implying that seismic moment (and high-frequency seismic radiation) is released from the part of the rupture surface that extends into the transition zone. There, material that behaves plastically at low strain rates fails in a brittle mode at the high strain rates that accompany the dynamic rupture of a large earthquake.

We apply DMAX2 in cases where the expected rupture length is 25 km or greater (discussed presently) and where we also intend to estimate maximum magnitude through rupture area, RA, by using only the moment equation. In our evaluation, there is an important distinction between an estimate of RA for use in the moment equation and one for use in the regression equation of Wells and Coppersmith (1994). In the first case, RA can appropriately be estimated by the product of rupture length and downdip width, constrained by DMAX1 or DMAX2. In the second case, however, Wells and Coppersmith (1994) based the use of RA as an estimator of moment magnitude primarily on the spatial extent of aftershock hypocenters, inherently reflecting the thickness of the seismogenic layer. Thus, when applying their regression equation for moment magnitude using RA, we use DMAX1 as the depth constraint on area, regardless of rupture length.

Our consideration of a buried regional strike-slip fault beneath the CFD was an important factor leading to our evaluation of DMAX2. We chose a rupture length of 25 km as the threshold for applying DMAX2 based on (1) the 26.5-km surface rupture length of the 1959 Hebgen Lake normal-faulting earthquake ($M_W = 7.3$) (Wells and Coppersmith, 1994), and (2) our reasoning that candidate ruptures for penetrating deeper than 15 km would have an aspect ratio of length to width that exceeded 1.5, whether for a vertical strike-slip fault or a 60°-dipping normal fault. Coincidentally, 25 km corresponds to a low point in our density distribution of expected rupture lengths for local fault sources. Ultimately, DMAX2 is applied to only two local fault sources, each of them a major dextral shear structure (the buried regional strike-slip fault and the Highway 95 fault, discussed in a later section).

3.0
REGIONAL FAULT SOURCES

The surface traces of 19 regional faults having known or suspected histories of Quaternary surface displacement, and trace lengths great enough to classify them as relevant to ground motion considerations at Yucca Mountain, are shown on Figure AAR-2. Fault acronyms correspond to those used by S. K. Pezzopane (USGS, written communication, 1996). With the exception of the West Specter Range fault, map traces are generalized from Piety (1996). The trace of the West Specter Range fault is generalized from Anderson *et al.* (1995a). Also, the southeast limit of the Pahrump fault is extended about 43 km beyond that shown by Piety (1996).

3.1 TABULATED PARAMETERS

Parameters for the seismic source characterization of each regional fault source are given in Table AAR-1. Note that the table includes parameters for two linked regional faults, the Death Valley-Furnace Creek and the Amargosa River-Pahrump. On the basis of a highly preferred rhombochasm tectonic model for Death Valley, where these faults are intimately related, we assign a probability of 0.8 to the linked configuration of the Death Valley-Furnace Creek faults versus 0.2 that they behave independently. For the Amargosa River-Pahrump faults, the probabilities are 0.1 for the linked configuration and 0.9 for independent behavior. This low probability of linkage for the AR/PSV faults is based on a lack of evidence for Quaternary faulting in the 15- to 20-km-long gap between Stewart Valley and the Amargosa Desert (Anderson *et al.*, 1995b).

Where three values for any parameter are entered in Table AAR-1, these indicate estimates corresponding to 10th, 50th, and 90th percentile values, with appropriate weights of 0.3, 0.4, and 0.3, respectively. Further explanation of the table follows.

Total Fault Length

Tabulated values for minimum, preferred, and maximum total fault length (TFL) are scaled from trace lengths on Figure AAR-2. Values for minimum, preferred, and maximum maximum rupture length (MRL) for 14 of the regional faults are the same as the values for

TFL. For the remaining five faults, the Rock Valley, West Spring Mountains, Belted Range, Kawich Range, and Pahrump faults, the MRLs are less than the TFLs because the faults are considered segmented. Because little or no paleoseismologic data pertaining to segmented behavior exist, we assume that the maximum rupture length can occupy any portion of the total fault length.

The MRL on the linked Death Valley-Furnace Creek fault is less by about 30 km than the combined TFLs of those two faults because the two faults overlap. If these two faults rupture together, the rupture would likely bypass the southeastern part of the Furnace Creek fault which extends beyond the Death Valley fault. If the overlap area did rupture, we interpret that displacements would be relatively minor and would not significantly contribute to the size of the event. Also, in the Last Chance Canyon area between the Fish Lake Valley fault and the Furnace Creek fault, there is little evidence of Quaternary faulting (R. E. Klinger and L. A. Piety, USBR, written communication, 1996) despite the high rates of activity along the major faults that lead away from that area. We interpret this relatively inactive zone as a persistent segment boundary and do not link the Fish Lake Valley fault with the Furnace Creek fault.

Minimum Distance to Repository

Tabulated values were taken from S.K. Pezzopane (USGS, written communication, 1996) or measured from Figure AAR-2.

Documented Quaternary Displacement

Quaternary displacement is documented for 14 of the 19 regional faults (indicated by y). Our decision to include some faults that lack documented Quaternary displacement (indicated by y?) is based on various criteria and reasoning. The Mine Mountain and Cane Spring faults are included because they form part of a northeast-trending zone of coherent, active deformation that includes: (1) the Rock Valley fault, which has the highest slip rate of any fault located closer to Yucca Mountain than 50 km (the distance to the Death Valley/Furnace Creek fault system); and (2) the epicenter of the Little Skull Mountain earthquake. The Keane Wonder fault is included because it is a range-bounding structure at the east margin of the highly active Death Valley region (R. E. Klinger and L. A. Piety, USBR, written communication, 1996). The Yucca Lake fault is included because it appears to form the

northeast margin of the potentially active Mine Mountain-Wahmoni-Cane Spring fault group. The Oasis Valley fault is included because it is the only fault Anderson *et al.* (1995a) studied within the relatively stable Goldfield sector of the Walker Lane, for which they equivocated about Quaternary displacement over a significant length of trace.

Style of Faulting

N = normal, L = left lateral, R = right lateral, O = oblique.

Fault Dip

There are no specific subsurface data (such as from mines, drill holes, or aftershock distributions) to constrain the overall dip of any of the regional faults. Minimum, maximum, and preferred dip values are assigned mainly on the basis of known or inferred fault slip characteristics with steep dips assigned to strike-slip faults, and moderate dips to dip-slip faults. For example, preferred dips of 90 degrees are assigned to the Rock Valley, Cane Springs, Amargosa, Pahrump, and Furnace Creek strike-slip faults whereas all of the major range-front normal faults are assigned preferred dips of 65 degrees. Maximum and minimum values are assigned on the basis of reasonable ranges of overall dip of faults typical of each slip-sense category.

Slip Rate and Recurrence Data

Published slip rate and recurrence data are available for only two of the nineteen regional faults: the Death Valley and Furnace Creek faults (R. E. Klinger and L. A. Piety, USBR, written communication, 1996). These parameters were estimated for the Rock Valley fault from data in Piety (1996) augmented by more recent thermoluminescence ages (Shannon Mahan, USGS, written communication, 2/20/97). For the west Spring Mountains fault, the parameters are estimated by assuming that events equivalent in displacement to the estimated displacement of the most recent surface faulting event were responsible for forming the largest scarp and by estimating an age range for alluvium on which the largest scarp is formed (Anderson *et al.*, 1995a). For the other regional faults, slip rates are estimated, but recurrence intervals are not.

Some estimates of slip rate are based on geomorphic data (primarily scarp-profile data) combined with an estimate of the age of the surficial deposits or alluvial surfaces that are

offset by the fault. An example is the Belted Range fault. Other slip rates are estimated by qualitative comparison of the fault orientation, location, fault-trace geomorphology, and tectonic setting to the faults in the region that have provided constraints on slip rate. For the Mine Mountain and Cane Spring faults, for example, maximum slip rates were taken to be α to 2, respectively, of the conspicuously more active Rock Valley fault. The Pahrump fault may have tectonic affinities with the strike-slip faults of the Death Valley system, but reconnaissance paleoseismic study shows that it is significantly less active than that system. It was assigned a maximum slip rate twice that of the relatively active Rock Valley fault because of its potential affinity to the Death Valley faults.

Probability of Being Seismogenic, P[S]

All the regional faults having documented Quaternary displacement are considered seismogenic, with P[S] = 1. These include the linked regional faults. For faults that lack documented Quaternary displacement, probabilities are assigned based on their orientation, tectonic setting, and relation to other seismogenic faults.

3.2 M_{max} APPROACH

For the regional fault sources, we use three approaches to estimate M_{max} in terms of moment magnitude M: (a) M estimated from surface rupture length SRL, using the relation from Wells and Coppersmith (1994) for all slip types; (b) M estimated from rupture area RA (SRL x downdip rupture width) using the relation from Wells and Coppersmith (1994) for all slip types; and (c) M estimated from SRL and slip rate S, using the relation from Anderson *et al.* (1996). We assign the following weights to the three approaches:

(a) (0.4), (b) (0.2), (c) (0.4).

Although M and RA are well correlated, we downweight approach (b) because the data Wells and Coppersmith (1994) used for RA were based on aftershock hypocenters; they are not a product of rupture length and width (see earlier section on "Depth of the Seismogenic Crust"). We also recognize the uncertainty in using SRL to estimate subsurface rupture length for calculating RA. Regarding approach (c), most of the preferred slip rates tabulated

for the regional faults in Table AAR-1 lie within the range of data regressed by Anderson *et al.* (1996), and the relation is straightforwardly applicable.

In Table AAR-1, total fault length is the length of the fault that is active, meaning the length along which seismic moment should be distributed given the slip-rate approach to recurrence (discussed below). The parameter used to estimate M_{max} is maximum rupture length (a measure of SRL), estimated in terms of minimum (mi), preferred (p), and maximum (m) values. When either the preferred or minimum value is selected for total fault length, weights for allowable maximum rupture length are renormalized.

3.3 RECURRENCE APPROACH

For the regional fault sources, we use two approaches for recurrence modeling: (1) a slip-rate approach and (2) a recurrence-interval approach. Weighting of these approaches is 0.6 and 0.4, respectively, for all the regional fault sources for which both slip-rate and recurrence-interval data are provided in Table AAR-1. Otherwise, the slip-rate approach is weighted fully.

Fault-specific recurrence relationships are generated from the slip rates using the methodology of Youngs and Coppersmith (1985) assuming constant moment rate. Whether using the slip-rate or recurrence-interval approach, we adopt the characteristic earthquake model with a weight of 0.7 and the "modified exponential" model (Youngs *et al.*, 1987) with a weight of 0.3. The exception is for the Death Valley and Furnace Creek faults. Because of their high slip rates the exponential model would lead us to expect many more moderate-magnitude earthquakes than have been observed. Given this, and the fact that the characteristic model was developed from observations for faults having high rates of activity, we give 1.0 to the characteristic model for the Death Valley and Furnace Creek faults. For both the characteristic and "modified exponential" models, M_{max} evaluated for a fault is assumed to be uniformly distributed in the range $M_{max} \pm 3$ magnitude unit, with $M_{max} + 3$ being the upper-bound magnitude, m^u.

Where recurrence intervals are provided, we use the method of Youngs and Coppersmith (1985) that assumes a constant frequency of earthquakes above some specified size. Given

M_{max} for a fault, the cumulative frequency for earthquakes of M_{max} - 3 is set equal to the inverse of the tabulated recurrence interval, which is interpreted to represent the frequency of characteristic-size events for the fault.

Based on seismicity recurrence calculations provided (Section 3.1 contains a description of the methodology used to calculate seismicity parameters) from diverse regional sources within 300 km of Yucca Mountain, our assessed distribution for the b-value (and relative weighting) for applying the methodology of Youngs and Coppersmith (1985) is:

0.80 (0.3), 1.00 (0.4), 1.20 (0.3).

4.0
LOCAL FAULT SOURCES

4.1 FAULTS CONSIDERED IN LOCAL ANALYSIS

The following faults are considered potential seismic sources within 20 km of Yucca Mountain, and are referred to in our analysis as local faults. Figures AAR-3 and AAR-4 show local faults included in our coalesced and independent models (discussed later in this section).

Paintbrush Canyon Fault (PBC)

PBC connotes the fault zone that bounds the west sides of Alice and Fran Ridges and Busted Butte. Activity extends at least from near Yucca Wash, where PBC has no obvious geomorphic expression (but where trench A1 reveals minor Quaternary offsets), to southwest of Busted Butte, where Holocene alluvium truncates a subtle scarp. Some map depictions (e.g., Simonds *et al.*, 1995) indicate a left step of about 0.7 km at Fran Ridge, suggesting possible segmentation. We do not segment PBC here because other depictions suggest greater continuity, and data do not require it; in any case, we would give this a low weight and consider it for only some events. Displacement and recurrence parameters for PBC are derived from chapter 4.4 of the Tectonics Synthesis Report (USGS, written communication,1996). With multiple exposures and an extensive record (~700 ka) at Busted

Butte, a value was calculated for the average displacement per event (Davg) that is less than the maximum displacement per event (Dmax).

Stagecoach Road Fault (SR)

As delineated on most maps, SR has a short length (about 4 km), despite prominent geomorphic expression and a relatively high rate of activity. SR commonly is considered linked as a single fault with PBC, with the intervening area masked by young alluvium; we favor this interpretation. At least one depiction suggests that SR could connect with the Mine Mountain fault to the northeast (Maldonado, 1985); this interpretation is not considered here because mid to late Quaternary alluvial surfaces east of Yucca Mountain lack geomorphic evidence of such a connection. The uncertainties in trench data possibly are larger for SR than for other Crater Flat Domain (CFD) faults because of: (1) the predominant loose sand encountered in the trenches, which are difficult materials to work with; (2) dating results that were inconsistent; and (3) significant hanging wall deformation in the trenches. Unless age estimates are grossly in error, which rough agreement suggests is not the case, SR is one of the most active CFD faults during the late Quaternary, although this is based on a relatively short record. Correlation of an 8 Ma tephra across SR (J.W. Whitney presentation at SSC Workshop 2) indicates substantial post-Rainier Mesa offset.

Bow Ridge Fault (BWR)

BWR has weak geomorphic expression of Quaternary activity for < 1 km along Exile Hill, and all data come from one cluster of trenches. Length and displacement thus are poorly constrained, but do not appear significantly underestimated given the lack of geomorphic expression elsewhere. The northward projection of BWR has been depicted alternatively as continuing with a northerly strike to near Yucca Wash (Scott and Bonk, 1984; Day *et al.*, 1996a) or curving to the northwest and connecting with the Sever Wash fault (Simonds *et al.*, 1995). We favor the former interpretation because BWR appears to control a north-trending linear drainage between Exile Hill and Yucca Wash. Trench A/BWR-3, excavated across the projection of BWR north of Exile Hill, showed no evidence of displacement in Q3 gravels (est. 100 to 200 ka), supporting a low rate of activity. BWR commonly is depicted as having a steep dip and connecting with PBC at a depth of a few km; however, projection to the Exploratory Studies Facility (ESF) (cross-section, R.C. Lung presentation at SSC Workshop

2 and handouts at SSC Workshop 3) indicates a dip of about 60 degrees, similar to that of the other block-bounding faults.

Ghost Dance Fault (GD)

There is evidence of minor Quaternary activity on GD, but the evidence is nondefinitive, geomorphic evidence constrains offset to be minor (at a detection threshold), and the possible displacements could be secondary. Map depictions suggest that GD connects with the Abandoned Wash fault, but considering them as a single fault indicates an extremely high aspect ratio (i.e., a long, small displacement fault), and the Abandoned Wash fault shows no evidence of Quaternary activity. GD is considered in the analysis because of its location, but we assign a low weight to the probability that it is seismogenic (P[S]=0.1), because activity is unproven and the possible small displacements could reflect secondary slip.

East Lathrop Cone Fault (ELC)

This is a NE-striking fault south of SR and east of the Lathrop Wells basalt cone (A. R. Ramelli and J. W. Bell, Nevada Bureau of Mines and Geology, written communication, 1996). It displays a small scarp (< 0.5 m high) in late Quaternary alluvial deposits (A.R. Ramelli presentation at SSC Workshop 3). The fault has not been studied in detail, so estimated parameters are poorly constrained. However, its small scarp, its moderate post-Tiva offset (Frizzell and Shulters, 1990), and its apparent short length all indicate that ELC is a minor fault. The fault is located well south of the controlled area. If considered part of a PBC/SR system (our preferred interpretation), ELC slightly increases the overall length of the system.

Solitario Canyon Fault (SC)

SC is taken to extend along a nearly continuous scarp projecting toward Lathrop Wells cone and the southern end of SR. A possible NE-striking connection between SC and SWW is not directly included here because of its weak geomorphic expression and unproven activity, but is included in the single west-side coalesced model. The southern end of SC is buried by young alluvium. SC has the longest continuous late Quaternary scarp of any Yucca Mountain fault, but trench results indicate a lower long-term rate of activity than for the other block-bounding faults (e.g., PBC, SR, SWW, SCF). Displacement and rate estimates are based on late Quaternary activity, which is considered more likely to be representative of the next 10^4

to 10^5 years. Our estimate for Davg is less than that for Dmax, based on the multiple trench sites and the fact that relatively large displacements are confined to a short section of the fault.

Iron Ridge Fault (IR)

IR strikes subparallel to SC, and is therefore considered a SC splay that obliquely connects to SR. IR has a nearly continuous bedrock scarp along much of its length. Results from a single trench site (SCF-T2) indicate Quaternary activity. The trench revealed massively cemented gravels (mid-Pleistocene in age) juxtaposed against bedrock, with permissible minor late Quaternary extensional opening. The lack of definitive late Quaternary offset indicates a low rate of activity and precludes significant rupture associated with late Quaternary events on SC or SR.

Fatigue Wash Fault (FW)

The FW scarp originally was referred to as part of the Windy Wash fault but actually connects with Scott and Bonk's (1984) Fatigue Wash fault. FW lies close to and interconnects with the Windy Wash fault, and the two are considered likely to make up a single fault system. This likelihood is incorporated in our linked and coalesced models (discussed below). The northernmost mapped extent of FW has minor bedrock offset and no evidence of Quaternary activity; it therefore is not considered in the analysis. Estimates for FW are based largely on a single, poorly sited trench (CF-1), one of the original trenches excavated for the Yucca Mountain program. CF-1 is adjacent to a drainage that flows parallel to the fault (perpendicular to the trench), providing a cross-sectional view of channelized deposits that form poor stratigraphic markers. The estimate of slip rate is adjusted to account for surface separations where FW crosses the Crater Flat road, as discussed in USGS (written communication, 1996).

South Windy Wash Fault (SWW)

This fault is considered to be separate from the North Windy Wash fault because the two are not directly connected. To the north, SWW abruptly terminates against the Central Windy Wash fault; its southern end is less well constrained. Paleoseismic data are derived from a trench site at the extreme north end of SWW. Displacements are assumed to be somewhat larger along its central part (south of FW splay), based on a 100-m offset of 3.7 Ma basalt.

The trench site is the best along SWW with respect to Quaternary stratigraphy. The best long-term rate for a principal Yucca Mountain fault is provided by offset of 3.7 Ma basalt. Total displacement along the central part of SWW is unknown.

North Windy Wash Fault (NWW)

This is the original Windy Wash fault of Scott and Bonk (1984). A small, nearly continuous bedrock scarp likely reflects some Quaternary activity, but field relations indicate this is largely a fault-line scarp formed by erosion of deposits on the downthrown side of the fault. Late Quaternary activity is minor at most. There are no trench data or other good constraints on activity, which is therefore assumed to be similar to northern SC and the Northern Crater Flat fault.

South Crater Flat Fault (SCF)

Offset of 3.7 Ma basalt on this fault is much smaller than that on SWW (about one-third). The fault projects toward CWW, and is considered a splay of the Windy Wash system. SCF is the best candidate for having activity that extends through the hills south of Crater Flat. Trench data are complicated by uncertain correlations across the fault, but they show progressively downthrown and buried soils, indicating repeated activity.

North Crater Flat Fault (NCF)

As described by the USGS (written communication, 1996), this fault is a system that includes at least three closely spaced, subparallel faults, each having probable small Quaternary scarps. Two trenches were located across its westernmost trace. Quaternary activity is documented at trench CFF-T2a, but late Quaternary activity is constrained to be minor based on lack of faulting in trench CFF-T2 (USGS, written communication, 1996).

Central Windy Wash Fault (CWW)

This down-to-the-east fault is distinguished from the down-to-the-west faults of the Windy Wash system (SWW and NWW); it abruptly truncates the north end of SWW and terminates near the south end of NWW. The scarp of CWW is modified along its central part because of drainage deflection, but unmodified scarps are present along both ends. Displacement and rate estimates are based on vertical separations of late Quaternary alluvial surfaces.

Central Crater Flat (CCF)

This down-to-the-east fault has a similar extent and position as CWW, although it is not as directly connected to down-to-the-west faults. Displacement and rate estimates are the same as for CWW, based on similar surface separations of the same alluvial surfaces.

Black Cone Fault (BC)

This down-to-the-east fault displays a system of NW-trending, mostly down-to-the-east scarps northeast of Black Cone, indicating minor late Quaternary activity. BC is inferred to connect with a north-striking fault southeast of Black Cone. The north-striking fault has a 0.5- to 1-m scarp in alluvium that deflects drainage and possibly offsets 3.7 Ma basalt near drillhole VH-2 (Simonds *et al.*, 1995; A. R. Ramelli and J. W. Bell, Nevada Bureau of Mines and Geology, written communication, 1996). Displacement and rate estimates are the same as for CWW and CCF, based on similar surface separations and provide the basis for our preferred rate.

Bare Mountain Fault (BM)

This down-to-the-east fault forms the western boundary of Crater Flat. Its southern end is poorly defined, with bedrock offset extending south into Amargosa Desert, but Quaternary activity apparently is confined to north of Black Diamond. BM has a slightly longer continuous Quaternary trace than does SC. It was the most active fault and had the largest throw within CFD during the Miocene. Its Quaternary rate is similar to the Yucca Mountain faults, suggesting reactivation under different conditions. The postulated higher rate for BM based on alluvial fan size (Ferrill *et al.*, 1996) is incorporated in our upper bound on slip rate, but trench data and surficial mapping are considered better constraints and provide the basis for our preferred rate.

Midway Valley (MWV)

MWV is a north-striking fault inferred from geophysical surveys and shallow borehole data. It is buried by unfaulted mid to late Quaternary alluvium. Estimates for this fault are based on activity at the threshold of resolution.

West Dune Wash #1 (WD1)

WD1 is a left step of about 0.3 km from the Ghost Dance fault. McKague *et al.* (1996) list it as a Type I fault, and Quaternary activity is suggested by bedrock scarps, vertical CaCO3-filled fractures, and linear drainage (Simonds *et al.*, 1995). Estimates for this fault are based on activity at the threshold of resolution.

West Dune Wash #2 (WD2)

WD2 is a north-northwest-striking fault listed as a Type I fault by H. L. McKague *et al.* (CNWRA, written communication, 1996), and Quaternary activity is suggested by bedrock scarps (Simonds *et al.*, 1995). Estimates for this fault are based on activity at the threshold of resolution.

East Busted Butte (EB)

EB is a down-to-the-east fault bounding the eastern sides of Busted Butte and Fran Ridge. Quaternary activity is indicated by arcuate, subtle scarps flanking Busted Butte (Simonds *et al.*, 1995; A. R. Ramelli and J. W. Bell, Nevada Bureau of Mines and Geology, written communication, 1996). Estimates for EB are based on small mid to late Quaternary offset reflected in its scarp. Topographic relief suggests extension of this fault along the east side of Fran Ridge, although no evidence of Quaternary activity has been described at that location.

4.2 NOTES ON LOCAL FAULT ESTIMATES (TABLE AAR-4)

Total Active Length

This is the surface length over which a fault has apparent Quaternary activity. It is scaled from mapped depictions and cross-checked against low-sun-angle aerial photographs: mininum = distance over which Quaternary fault scarps or other evidence of activity can be traced; preferred = preferred value from considerations of topography, mapped depictions, and burial by younger deposits; maximum = upper bound considering map depictions, fault intersections, topographic expression, and relative cumulative displacements.

Style

In the nomenclature used, ln = left-normal (dominantly normal with a left-oblique component). Slip vector is poorly defined for most faults, but available constraints (fault

striations, apparent offsets) suggest that most faults are dominantly normal with a left-oblique component. Where not documented, slip is assumed to be related to fault strike.

Fault Dip

For most faults, 60 degrees is the preferred estimate of dip based variously on well-constrained cross sections (e.g., the projection of BWR to the ESF), bedrock fault exposures (e.g., trench exposures along central SC), or geophysical data (e.g., BM). Reported dips from fault trenches and other surface exposures are consistently 10 to 15 degrees steeper and therefore are not used.

Total Displacement

In most cases, this measure is made from offset of the top of the Tiva Canyon member of the Paintbrush Tuff, which is estimated from cross sections or geologic maps (or topographic maps, where necessary). It was estimated for the part of a given fault where it appears largest. It generally is well constrained for faults in the north part of the basin, and less constrained in the southern part, where hanging walls are buried by thicker alluvium.

Displacement Per Event

Using data reported in individual chapters of the Tectonics Synthesis Report (USGS, written communication, 1996), the maximum displacement per event (Dmax) and the average displacement per event (Davg) are estimated for the part of a given fault where displacement appears largest (generally the central part of the fault). Maximum observed displacements, in some cases averaged for multiple events, are taken as best estimates of average displacement for faults for which there are single trench sites or multiple sites in nonrepresentative locations. Averages are derived from the largest displacements along a given fault for which there are multiple trenches deemed to be in representative locations, and/or from records of several events.

Slip Rate

Slip rates are based on data reported in individual chapters of the Tectonics Synthesis Report (USGS, written communication, 1996) and are estimated for the part of a given fault where they appear largest. For example, trenches CF-2 & CF-3 (Simonds *et al.*, 1995) are located at the extreme northern end of SWW and north of the intersection of SWW & FW, so a slip rate

derived from offset of basalt along the central part of the fault is assumed to be more representative.

Recurrence Interval

This is the average interseismic interval derived from paleoseismic data reported in individual chapters of the Tectonics Synthesis Report (USGS, written communication, 1996).

4.3 UNCERTAINTIES IN LOCAL FAULT ESTIMATES

Estimates of activity on local faults at Yucca Mountain involve large epistemic uncertainties. Estimates of length involve difficulties in recognizing remnants of small surface offsets, especially at the ends of ruptures, and they are sometimes complicated by burial by younger deposits. Measuring displacements is uncertain because there is a general lack of piercing points (and hence poorly constrained slip vectors), poor stratigraphic markers, uncertain correlation of units across a fault zone, and the common need to project geomorphic surfaces or stratigraphic units across a broad zone of deformation. Activity rates (slip rates and recurrence intervals) are highly uncertain because they depend on age estimates, which incorporate uncertainties in such things as analytical errors, unknown errors related to poorly understood processes and the experimental nature of most dating techniques, and indirect control (i.e., events typically are bracketed and not directly dated).

Subsurface fault geometry is poorly constrained because depths of fault penetration are unknown and fault dips are uncertain. Interpreting the number of events within the paleoseismic record is complicated by several factors: (1) The nature of fault interactions is uncertain (i.e., distributed events seem likely, but it is beyond our resolution to determine which faults rupture during individual events and how consistent such events have been). (2) Some displacements may have secondary or nontectonic origins. (3) Some events—especially small, older events—likely are unrecognized, as suggested by plots of event timing (e.g., S. K. Pezzopane *et al.*, USGS, written communication, 1996a). (4) Events are not necessarily recognizable at all sites because of factors such as variable offsets, bioturbation, and carbonate overprinting. (5) Not all fault traces have been studied.

Despite these many sources of uncertainty, our estimates of activity of the CFD faults appear to be reasonable and adequately accurate, and are internally consistent and in accord with generally low rates of regional strain. For example, comparing the minimum distances over which fault activity can be traced to conservative upper bounds on length suggests that length estimates are unlikely to be off by as much as a factor of two; displacement measurements are probably rarely off by more than 20% to 30%; and comparisons based on soils and geomorphology suggest that age estimates likely are accurate within factors of two to three.

We consider that current estimates of parameters for the CFD faults are reasonable approximations. To portray their approximate nature, most estimates are rounded to a single significant digit, and no adjustments are made that introduce additional significant digits. For example, cumulative displacements and numbers of events could be reduced to account for possible secondary or nontectonic offsets. However, we would expect such nonprimary displacements to occur as fracturing or small offsets, which generally are difficult to recognize. In no cases have fracturing events lacking discernable offset been factored into earthquake frequency. We estimate the contribution of small offsets to be less than 20% to 25%, and some small offsets may represent primary faulting associated with moderate-sized events or distributed rupture, so a correction factor would be no more than 10% to 15%. Current interpretations include more frequent occurrence of small offsets within relatively recent time periods, strongly suggesting that older small offsets have been obscured and are unrecognizable. To a first approximation, unrecognized small offsets might balance out consideration of a few secondary or nontectonic offsets as seismogenic events. In either case, any adjustment we might make would be a minor fraction of the one-significant-figure estimates.

4.4 NOTES ON ESTIMATES FOR BURIED/BOUNDING FAULTS

Postulated buried or bounding fault sources associated with dextral shear across the CFD (Figure AAR-5) are model-driven; no direct evidence of activity is available. Estimates are thus hypothetical, with bounds deemed to cover reasonable possibilities.

Total Active Length

The following subsurface lengths were deemed reasonable for the postulated structures. For the throughgoing, regional strike-slip fault, min = dimension required to extend beyond CFD and thus qualify as a throughgoing structure; pref = midpoint between min and max; max = approximate comparison to the longest historical strike-slip ruptures in the Basin and Range province (specifically 1872 Owens Valley). For the "Highway 95 fault," length estimates are based on a general comparison to historical Basin and Range surface-faulting events (e.g., 1932 Cedar Mountain) and on constraints posed by postulated segment boundaries (i.e., intersection with the Rock Valley fault and the extensional bend at Oasis Valley). For the cross-basin fault, min = approximate dimension required for a seismic event above the background source; pref = midpoint between min and max; max = constrained by dimensions of the CFD. The north-bounding strike-slip fault is inferred to have similar dimensions and activity as the cross-basin fault.

Style and Fault Dip

As conceptualized, all buried and bounding sources are strike-slip faults assumed to be nearly vertical.

Displacement per Event/Slip Rate

These parameters are based on historical analogs and comparisons to the CFD faults. For the throughgoing, regional strike-slip fault, the slip rate was estimated as that required to be a driving fault (i.e., approximately equal to the sum of slips on CFD faults). For the "Highway 95 fault," we estimated rates required for the fault to be a partially driving fault (i.e., somewhat less than the summed slip on CFD faults). For the cross-basin and north-bounding faults, we used historical analogs and comparison to CFD faults (i.e., approximately equal to CFD faults).

4.5 NOTES ON THE 52 FAULTS THAT NRC CONSIDERS IMPORTANT

The faults listed below, which H. L. McKague *et al.* (CNWRA, written communication, 1996) included as Type I faults, either were not considered or have designations that could lead to confusion. Reasons for not considering these faults and/or clarifications as to fault designation are given below.

Simonds #1 Fault

Included on Simonds *et al.* (1995) as a bedrock fault having an unknown age of movement; lack of geomorphic expression in bedrock is unsupportive of significant Quaternary activity; estimated Mw 5.6 (H. L. McKague *et al.*, CNWRA, written communication, 1996) is less than M_{max} for our background source zone.

Simonds #2 Fault

Included on Simonds *et al.* (1995) as a bedrock fault having an unknown age of movement; lack of geomorphic expression in bedrock is unsupportive of significant Quaternary activity; estimated Mw 7.28 (H. L. McKague *et al.*, CNWRA, written communication, 1996) is unsupportably high given the fault's 7-km length and is inferred to be a typographical error; estimated Mw should be less than M_{max} for our background source zone.

Simonds #3 Fault

Included on Simonds *et al.* (1995) as a bedrock fault having an unknown age of movement; lack of geomorphic expression in bedrock is unsupportive of significant Quaternary activity; estimated Mw 5.9 (H. L. McKague *et al.*, CNWRA, written communication, 1996) is less than M_{max} for our background source zone.

Simonds #4 Fault

Included on Simonds *et al.* (1995) as a bedrock fault having an unknown age of movement; lack of geomorphic expression in bedrock is unsupportive of significant Quaternary activity; estimated Mw 5.9 (H. L. McKague *et al.*, CNWRA, written communication, 1996) is less than M_{max} for our background source zone.

Simonds #5 Fault

Included on Simonds *et al.* (1995) as a bedrock fault having an unknown age of movement; lack of geomorphic expression in bedrock is unsupportive of significant Quaternary activity; estimated Mw 5.9 (H. L. McKague *et al.*, CNWRA, written communication, 1996) is less than M_{max} for our background source zone.

Simonds #7 Fault

Included on Simonds *et al.* (1995) as a bedrock fault having an unknown age of movement; lack of geomorphic expression in bedrock is unsupportive of significant Quaternary activity; estimated Mw 5.9 (H. L. McKague *et al.*, CNWRA, written communication, 1996) is less than M_{max} for our background source zone.

Simonds #8 Fault

Included on Simonds *et al.* (1995) as a bedrock fault having an unknown age of movement; lack of geomorphic expression in bedrock is unsupportive of significant Quaternary activity; estimated Mw 6.1 (H. L. McKague *et al.*, CNWRA, written communication, 1996) is less than M_{max} for our background source zone.

Simonds #9 Fault

Included on Simonds *et al.* (1995) as a bedrock fault having an unknown age of movement; lack of geomorphic expression in bedrock is unsupportive of significant Quaternary activity; estimated Mw 5.8 (H. L. McKague *et al.*, CNWRA, written communication, 1996) is less than M_{max} for our background source zone.

Simonds #10 Fault

Included on Simonds *et al.* (1995) as a bedrock fault having an unknown age of movement; lack of geomorphic expression in bedrock is unsupportive of significant Quaternary activity; estimated Mw 5.9 (H. L. McKague *et al.*, CNWRA, written communication, 1996) is less than M_{max} for our background source zone.

Simonds #11 Fault

Figure 1-2 of H. L. McKague *et al.* (CNWRA, written communication, 1996) depicts this fault as one we include as part of the No. Crater Flat fault system, whereas their Appendix A describes this as the Black Cone fault of Piety (1996), which we include as a separate fault.

Simonds #12 Fault

We include this fault as part of the North Crater Flat fault system, consistent with chapter 4.11 of the Tectonics Synthesis Report (USGS, written communication, 1996).

Boomerang Point Fault (BP)

Included on Simonds *et al.* (1995) as a bedrock fault having an unknown age of movement; lack of geomorphic expression in bedrock is unsupportive of significant Quaternary activity; estimated Mw 5.9 (H. L. McKague *et al.*, CNWRA, written communication, 1996) is less than M_{max} for our background source zone.

Note: For Simonds #13 to #19 faults, there is a discrepancy between Figure 1-2 and Appendix A of H. L. McKague *et al.* (CNWRA, written communication, 1996), with all faults apparently shifted one number (e.g., fault #13 on Figure 1-2 is fault #14 in Appendix A). The following fault names refer to their Figure 1-2.

Simonds #13 Fault

Simonds *et al.* (1995) depict evidence of possible Quaternary activity along the fault's southern part; as depicted, it is located within the controlled area; we include this fault as our West Dune Wash #1 fault (WD1).

Simonds #14 Fault

Geomorphic expression suggests possible Quaternary activity on this fault (Simonds *et al.*, 1995; Bell *et al.*, 1996), and it is located within the controlled area; we include this fault as our West Dune Wash #2 fault (WD2).

Simonds #15 Fault

Included on Simonds *et al.* (1995) as bedrock fault having an unknown age of movement; lack of geomorphic expression in bedrock is unsupportive of significant Quaternary activity; estimated Mw 5.8? (H. L. McKague *et al.*, CNWRA, written communication, 1996) is less than M_{max} for our background source zone.

Simonds #16 Fault

We include most of the depicted length of this fault as part of our South Windy Wash fault (SWW). North of where it merges with SWW, it has a length of about 4 km and has geomorphic expression (bedrock scarps) permissive of Quaternary activity. We interpret this as a secondary fault connecting the SWW and Solitario Canyon faults; we do not include it as a separate source.

Simonds #17 Fault

Included on Simonds *et al.* (1995) as bedrock fault having an unknown age of movement; lack of geomorphic expression in bedrock is unsupportive of significant Quaternary activity; estimated Mw 5.6? (H. L. McKague *et al.*, CNWRA, written communication, 1996) is less than M_{max} for our background source zone.

Simonds #18 Fault

This is the South Crater Flat fault, which we include.

4.6 COMPARISON OF QUATERNARY AND MIOCENE DEFORMATION

The plausible tectonic models we consider relevant to Quaternary activity within the CFD (Figure AAR-1) hinge in part on the similarities between Quaternary and Miocene deformation. For example, we consider it likely that an active detachment surface may have existed at shallow depths (i.e., less than 10 km) during the Miocene, when heat flow associated with the caldera systems likely reduced the effective brittle thickness of the crust. The relative deformations of the Paintbrush Tuff (primarily the broadly exposed Tiva Canyon member) and the Timber Mountain Tuff (primarily the Rainier Mesa member) clearly indicate that Quaternary faulting within the CFD generally has occurred along structures that were more active during the Miocene. However, stratigraphic constraints are insufficient to demonstrate whether Quaternary activity represents the waning stages of Miocene activity, as has been suggested by Fridrich (1996), or whether it represents reactivation of preexisting zones of weakness within the past 5 Ma or so (the period marking significant changes in Basin and Range tectonics, including rapid uplift of the Sierra Nevada and formation of Death Valley). Wholesale differences in Miocene and Quaternary deformation in the Sliver Peak area about 100 km northwest of the CFD were documented by Stewart and Diamond (1990), who found no relation between the Miocene Esmeralda basin and the current basin configuration. Although they describe differences between Miocene and Quaternary deformation that are much greater than in the CFD, both areas lie just east of the Death Valley/Owens Valley region within the Nevada Walker Lane and are likely to have some affinities.

Although difficult to prove, reactivation of Miocene faults during the past 5 Ma seems plausible given the regional tectonic changes, especially onset of major activity in the adjacent Death Valley region, and renewal of basaltic volcanism in the CFD. Aside from rate, Quaternary deformation appears generally similar to Miocene deformation, but several lines of evidence indicate potentially significant differences.

(a) **Relative activity of the Bare Mountain and Yucca Mountain faults.** Cumulative throw clearly is much larger on the Bare Mountain fault (BM) than on any of the Yucca Mountain (YM) faults, and estimated uplift rates suggest that BM was considerably more active during the primary phase of Miocene deformation. Paleoseismic data, on the other hand, suggest that at least two YM faults (SWW and SR) have higher Quaternary rates than does BM, and the estimated summed slip across the YM faults is several times that on BM. The apparent discrepancy in Miocene versus Quaternary rates is significantly larger than what we consider reasonable bounds on estimates of Quaternary activity for these faults.

(b) **Contrast in deformation of Miocene tuffs and 3.7 Ma basalts along So. Windy Wash fault.** Deformation of the tuffs involved extensive and highly variable tilting, including broad-scale, low-amplitude north-south warps, whereas the basalts are uplifted uniformly. This difference is compatible with the notion of a warmer, thinner, more-ductile crust during the main phase of deformation; it also begs the question as to what extent tilting and displacements are coeval.

(c) **Age of formation of hills bounding the south end of Crater Flat.** Parts of these hills are capped by slide blocks, which rest on 10.5 Ma basalts; therefore the hills have entirely formed post-10.5 Ma. This contrasts with the topography of Yucca Mountain, which must have largely formed before eruption of the Timber Mountain Tuff (assuming that tilts and major fault displacements were coeval).

(d) **Difference in state of stress.** From populations of fault striations, extension is interpreted to have rotated in a clockwise direction; it is inferred that during the primary phase of Miocene deformation it was WSW-ENE to nearly east-west, whereas during the Plio-Quaternary it has been NW-SE (H. D. Ander, Rice University, written communication, 1984; Frizzell and Zoback, 1987).

(e) **Relative activity of NE-striking and NW-striking bridging faults.** Northeast-striking, connecting faults show Quaternary activity in several locations, whereas northwest-striking ones rarely do. In one case (the northeast-striking connection between the Fatigue Wash and southern Windy Wash faults), Quaternary scarps

trend over a bedrock ridge, producing only minor bedrock offset, which suggests that they are post-Miocene features.

4.7 SYNCHRONOUS RUPTURES

To account for possible distributed (or synchronous) ruptures involving multiple faults, we define various models that group closely spaced and/or interconnected faults into coalesced or linked fault systems. In these models, slip at depth on a defined principal structure results in distributed and/or secondary surface rupture on the faults included in a given system. Linked faults imply along-strike connection of separately defined faults (e.g., a combined Paintbrush/Stagecoach Road fault). Aside from considering combined lengths, linked faults are treated the same as independent faults. Coalesced faults imply upward-splaying fault systems, with interconnection between subparallel faults.

At the outset, we make the following points regarding our consideration of synchronous ruptures.

- Completely independent behavior of the CFD faults (with the exception of the Bare Mountain fault) seems highly unlikely, given their similarities, close cross-strike spacing (generally < 2 km), and high degree of plan-view interconnection.

- The presence of basaltic ash within extensional openings along several faults is possible indication of synchronous rupture. Without such evidence, synchronous ruptures would be more speculative.

- Similarities in timing indicated by paleoseismic data are suggestive, but not compelling, evidence for synchronous ruptures, given many uncertainties.

- Synchroneity of paleo-ruptures is ultimately unprovable. Even under ideal circumstances (e.g., tightly-constrained events based on C14 dating or dendrochronology), synchroneity cannot be distinguished from occurrences close in time, as might occur from short-term triggering.

Two methods for grouping the CFD faults into "predicted" distributed ruptures during future surface-faulting earthquakes are: (1) defining scenarios (as done by S. K. Pezzopane *et al.*, USGS, written communication, 1996a) for past ruptures, allowable within the constraints of

paleoseismic data; and (2) defining distributed systems that incorporate the principal faults and a surrounding halo of lesser faults. Both methods capture a range of behavior.

Scenarios (S. K. Pezzopane *et al.*, USGS, written communication, 1996a) allow the most direct input of paleoseismic data. Assuming that distributed behavior occurs, the data can be viewed as documenting the minimum extent of events if one includes only those faults for which evidence has been described. As defined by Pezzopane (USGS, written communication, 1996), the scenarios can generally be divided into east- and west-side rupture events.

Defined distributed systems, in our judgment, have distinct advantages. They (1) allow grouping of the most directly connected faults; (2) allow inclusion of all faults; (3) are stable (i.e., they don't jump around, thus avoiding open-ended complexity); and (4) are controlled by parameters of the principal structures, with small contributions to displacement by lesser structures.

Methodology for Treating Possible Synchronous Behavior

First, we assign weights (Table AAR-5) to the likelihood of independent versus coalesced behavior (Figure AAR-6) for each of our 11 defined tectonic models depicted on Figure AAR-1. In summary, the tectonic model designations are based on the following structure of our logic tree: A = buried, throughgoing right-slip fault beneath CFD; B = shear couple across CFD with bounding structure(s), but no buried cross-basin fault; C = shear couple with bounding structure(s) and buried cross-basin fault; D = basin extension without significant dextral shear structures; 1 = shallow (3 - 10 km) detachment; 2 = deep (> 10 km) detachment; 3 = no detachment.

Notes:

(1) Examples: In Model B-1 there is a shear couple with no buried fault and there is a shallow detachment; in Model D-3 there is basin extension with no significant dextral shear structure(s) and without any detachment.

(2) "Detachment" implies a subhorizontal zone of decoupling, but not necessarily a seismogenic structure.

(3) For buried sources, we consider only those deemed potential sources of earthquakes larger than the maximum background earthquake of M 6.3 ± 0.3.

(4) Exception to detachment numbering: Model C-2 involves a buried cross-basin fault without a detachment. (Given a detachment >10 km, we exclude the possibility that a buried cross-basin fault would generate an earthquake larger than the maximum background earthquake.)

With one exception (model C2), the CFD faults are considered much more likely to rupture during distributed (coalesced) events than as completely independent faults (Table AAR-5) for several reasons, including the close fault spacing, anastomosing nature, similar event timing, and historical analogs. In model C2, higher weighting is assigned to independent behavior based on reasoning that an overlapping cross-basin fault likely would segment the CFD faults. Coalesced behavior is considered more likely in models containing a 3- to 10-km detachment, because such a feature would provide a straightforward mechanism for interconnection of overlying steep faults. Because most CFD faults appear to have similar dips, coalesced behavior is considered less likely with increasing depth of penetration; however, no distinction is made between models having $\geq$ 10 km detachment or no detachment because at those depths ruptures have extended through most of the seismogenic layer and possible mechanisms of interconnection are poorly understood.

We exclude the possibility of a third west-side system associated with an inferred major fault in central Crater Flat, because we have no evidence of Quaternary activity. We also exclude additional coalesced options on a "diminishing-returns" basis; additional options would quickly magnify the complexity of the interpretation without adding to its credibility.

Second, we define various linked and coalesced fault systems. The following CFD faults are considered in our linked and coalesced models:

WEST-SIDE FAULTS	EAST-SIDE FAULTS
SC - Solitario Canyon	PBC - Paintbrush Canyon
IR - Iron Ridge	SR - Stagecoach Road
SWW - So. Windy Wash	ELC - E. Lathrop Cone
FW - Fatigue Wash	MWV - Midway Valley
NWW - No. Windy Wash	BWR - Bow Ridge
SCF - So. Crater Flat	WD1 - West Dune Wash #1
NCF - No. Crater Flat	WD2 - West Dune Wash #2
CWW - Central Windy Wash	EB - E. Busted Butte
CCF - Central Crater Flat	
BC - Black Cone	
BM - Bare Mountain	

For cases of independent fault behavior, we make a further distinction whether some faults may be connected along strike (i.e., linked faults). Based on map patterns, we define two plausible linked systems, PBC/SR and WW/FW (Table AAR-6). PBC/SR is considered a somewhat more likely linked system than WW/FW because PBC/SR involves faults that are on line with each other, there is no obvious discontinuity in the possible linked trace, and coincident rupture during multiple events is suggested by paleoseismic data. WW/FW involves faults that do not have the same continuity, but are closely spaced and have direct splaying relations. In models that include 3- to 10-km detachment, relatively less weighting is assigned to linked behavior because a shallow detachment would result in unusually high aspect ratios (i.e., long ruptures, given their depth of penetration). In model C2, an overlapping cross-basin fault provides a mechanism for segmenting the faults, especially WW/FW, so lower weighting is assigned to linked behavior.

For cases of coalesced behavior, we divide the CFD faults into four coalesced systems (Figure AAR-4) as follows.

- **E-side**: Coalesced system including all faults on the east side of Yucca Mountain. The PBC/SR linked fault, with a slight extension to the south along ELC, forms the principal structure of the system, with all other faults secondary.

- **W-side #1**: Simple coalesced system comprising SC and IR: SC forms the principal structure, and IR is secondary. Paleoseismic studies indicate relatively low long-term rates on these two faults, so this system is the least significant in a three-system model; however, the late Quaternary rate for SC compels inclusion at a similar level.

- **W-side #2**: Coalesced system including all faults on the west side of Yucca Mountain except SC and IR. The linked SWW/FW/CWW/NWW fault forms the principal structure of the system, with all other faults secondary.

- **Bare Mountain fault (BM)**: Mostly a singular fault trace, but also includes some possible distributed faulting along its northern part. BM is considered more likely to behave independently because it lacks the close spacing and interconnection of the YM faults.

We then distinguish and assign weights to four models involving rupture of different combinations of the defined coalesced systems (Table AAR-7). The principal structures of the three Yucca Mountain systems appear to have similar fault dips, and therefore are interpreted to extend to sufficient depths to be considered separate seismogenic structures. For models in which multiple coalesced systems rupture synchronously (for example, in response to external forces), they are treated as simultaneous rupture of separate structures.

Weights are assigned on a relative basis, with a higher probability of comprising fewer systems (increased coalescence) assigned to models including: first, a buried dextral fault spanning the CFD (i.e., throughgoing or cross-basin fault), because displacement on such a structure should affect all of the overlying area; and second, a 3- to 10-km detachment, because such a feature would provide a straightforward mechanism for interconnection of steep, overlying faults. Coalescence is thus considered most likely given a buried dextral fault AND 3- to 10-km detachment, less likely given a buried throughgoing fault AND >10-km detachment or no detachment, even less likely given deep or no detachment AND no buried dextral fault, and least likely given a cross-basin fault AND no detachment (i.e., A1>C1>A2=A3>B1=D1>B2=B3=D2=D3>C2).

- **One system**—CFD faults, including BM, comprise a single coalesced system; this possibility is considered only in models that include BOTH a 3- to 10-km detachment AND a buried strike-slip fault (i.e., models A1 and C1).

- **Two system**—All YM faults comprise a single coalesced system, and BM is independent; again, this possibility is considered only in models including BOTH a 3- to 10-km detachment AND a buried strike-slip fault (i.e., models A1 and C1).

- **Three systems (E-W)**-PBC/SR/ELC/BWR/MWV/GD/WD1/WD2/EB comprise an east-side system; SC/IR/SWW/FW/NWW/SCF/NCF/CWW/CCF/BC comprise a single west-side system; and BM is independent.

- **Four systems (E-2W)**-PBC/SR/ELC/BWR/MWV/GD/WD1/WD2/EB comprise an east-side system; SC/IR comprise one west-side system; SWW/FW/NWW/SCF/NCF/CWW/CCF/BC comprise a second west-side system; and BM is independent.

Geometry of Coalesced Systems

The following factors are considered.

- The overall geometry is controlled by the geometries of principal structures,

- In general, we consider 60 degrees our best estimate of dip for the principal structures, as suggested by well-constrained cross sections (e.g., Bow Ridge), bedrock fault exposures (e.g., Solitario Canyon), or geophysical data (e.g., Bare Mountain),

- If fault curvature is considered, deeper penetration would equate to shallower dip, but we eliminate this because of uncertainties (i.e., uncertainty in amount of curvature and insensitivity, given range of estimates),

- Depth of penetration is model-dependent (truncation at detachment, fault intersection, or base of seismogenic zone).

Slip Rates of Coalesced Systems

To assess slip rates for the coalesced systems, we use a simple summation of rates across strike.

4.8 M_{max} DIMENSIONS

For the local fault sources, maximum rupture dimensions basically are constrained by rupture length and downdip rupture width, RW. In some cases, RW is constrained not only from below, but also from above. Measures of maximum rupture length are provided in Table AAR-4 under the heading "active length," meaning the total length along which either (a) rupture may extend during a single event or (b) seismic moment should be distributed as

part of the slip-rate approach to recurrence (discussed below). For each fault source, the three entries for active length represent 10th, 50th, and 90th percentile values, for which corresponding weightings are 0.3, 0.4, and 0.3. When either the 10th or 50th percentile value is selected for fault length, allowable maximum rupture length follows accordingly, and weighting is renormalized.

Constraints on RW for the local fault sources include DMAX1 or DMAX2, aspect ratio (fault length/downdip width), and scenarios of truncation by either a local detachment (if one exists), by the Bare Mountain fault, or by a W-dipping fault in the case of E-dipping faults considered antithetic. For the CFD faults (Table AAR-3), the first general rule is that RW is not allowed to exceed twice the maximum rupture length (i.e., the minimum allowable aspect ratio is 0.5), based on data for earthquake slip-surface aspect ratios (Nicol *et al.*, 1996). The second general rule for these faults is that their downdip extent is limited by a detachment, if one exists; otherwise, the lower limit is DMAX1 or DMAX2—or the plane of the Bare Mountain fault. Rules for the other local fault sources listed in Table AAR-2, including special cases, are described below.

For the "Highway 95 fault," RW is independent of any detachment, and limits on lower and upper depth are provided by DMAX2 and the Earth's surface, respectively. RW for the "No. bounding strike-slip (ss) fault" is also independent of any detachment. For this fault, we allow RW to extend from DMAX1 up to 3 km below the surface, based on the fault's lack of clear surface expression.

Four of the down-to-the-east faults listed in Table AAR-4 are considered to be antithetic to, and hence would have downdip projections truncated by, a nearby west-dipping fault. Specifically, the Black Cone (BC), Central Crater Flat (CCF), and Central Windy Wash (CWW) faults would be truncated by the Fatigue Wash (FW) fault. Similarly, the West Dune Wash 2 (WD2) fault would be truncated by the Paintbrush Canyon (PBC) fault.

Scenarios A-1, A-2, A-3

For the regional ss fault, the lower depth limit of RW, in all cases, is constrained by DMAX2. Its uppermost limit—and the lowermost limit of the other CFD faults—is either the depth of

the detachment (scenarios A-1 and A-2) or, where no detachment exists (scenario A-3), a decoupling level for which we assign a depth distribution (and relative weighting) as follows:

4.5 km (0.185), 7.0 km (0.63), 9.0 km (0.185).

Scenarios C-1, C-2

For the cross-basin fault, the lower depth limit of RW is constrained by DMAX1. In scenario C-1, its upper-most limit—and the lowermost limit of the other CFD faults—is the depth of the detachment. In scenario C-2 we allow RW for the cross-basin fault to extend up to 3 km below the surface, based on the fault's lack of clear surface expression. In this scenario, DMAX1 or other general truncating rules constrain the lower depth limit of RW for the CFD faults. We accept the possibility of intersections between the cross-basin fault and the other CFD faults as the former develops under the shear couple.

Multiple-structure Coalesced Systems

In the cases of "multiple-structure coalesced systems" (Table AAR-4), that is, coalesced systems of the local faults that are allowed to rupture simultaneously in parallel, RW is constrained by DMAX1 in all cases. Although the tabulated lengths for these sources is greater than 25 km, we use DMAX1 because the expected value of rupture length for any of the individual coalesced systems is less than 25 km.

4.9 M_{max} APPROACH

For the local fault sources, using the data in Table AAR-4, we use four approaches to estimate M_{max} in terms of moment magnitude M: (a) M estimated from the "active length" of a fault, using either the relation for surface rupture length SRL or subsurface rupture length RLD (more below) from Wells and Coppersmith (1994) for all slip types; (b) M estimated from rupture area RA ("active length" x downdip rupture width) using the relation from Wells and Coppersmith (1994) for all slip types; (c) M estimated from fault length and slip rate S, using the relation from Anderson *et al.* (1996); and (d) M calculated from seismic moment M_o, determined from the moment equation. Note that approach (d) was not used for the regional fault sources because necessary information for single-event displacement was not available.

We refer the reader to the section on "Depth of the Seismogenic Crust" for an explanation of the moment equation and other relevant background such as DMAX1, DMAX2, and our perspective on using RA in the moment equation and in the regression equation of Wells and Coppersmith (1994).

In approach (a), we take the "active length" of the local faults (Table AAR-4) to be equivalent to estimates of subsurface rupture length (RLD) in the case of the buried or bounding strike-slip faults and to surface rupture length (SRL) for all the other cases involving the CFD faults in Table AAR-4. The correspondingly appropriate regression relation from Wells and Coppersmith (1994) is then applied. For the moment-equation approach in which RLD must be estimated for the CFD faults, data of Wells and Coppersmith (1994, their Figures 2 and 3) can be used to relate "active length" (i.e., SRL) to RLD, which is expected to have a slightly larger value. For the range of ruptures being considered, we use their mean value of 0.75 for the ratio of SRL to RLD. We consider the extra length in the subsurface (RLD - SRL) to extend symmetrically from the surface trace lengths depicted in Figures AAR-3 and AAR-4.

In approach (b), DMAX1 is used in all cases for the maximum depth constraint on downdip rupture width. In approach (d), we estimate ®, the average (subsurface) displacement over the slip surface, by (MD + AD)/2, where MD and AD are the maximum and average surface displacements per event, respectively, tabulated in Table AAR-4.

Table AAR-8 outlines our weighting used for the M_{max} approaches. The weighting depends on expected rupture length and on the subsurface structure involved in some of the tectonic models. In the case of rupture length, we assign 25 km to be the threshold for large earthquakes whose downdip rupture may extend to DMAX2. Whereas the RA regression of Wells and Coppersmith (1994) is used (along with DMAX1) when expected rupture length is less than 25 km, it is not used when expected rupture length is 25 km or greater, and its weight is redistributed to the moment-equation approach. We downweight the rupture-length/slip-rate approach because many of the local faults have slip rates lower than the range of data regressed by Anderson *et al.* (1996). Given a local detachment at 3 to 10 km depth, we downweight the rupture-length approaches and redistribute weight to the moment-equation approach. For the cases of multiple-structure coalesced systems, for which slip-rate

information is not available, weight for the rupture-length/slip-rate approach is redistributed to the rupture-length approach.

4.10 RECURRENCE APPROACH

For the local sources, we use two approaches for recurrence modeling: (1) a slip-rate approach and (2) a recurrence-interval approach. These approaches are assigned weights of 0.6 and 0.4, respectively, for all the local fault sources for which both slip-rate and recurrence-interval data are provided in Table AAR-4. Where only slip-rate or recurrence-interval data are provided, the corresponding approach is weighted fully.

Fault-specific recurrence relationships are generated from the slip rates using the methodology of Youngs and Coppersmith (1985) and assuming constant moment rate. Whether using the slip-rate or recurrence-interval approach, we assign the characteristic earthquake model a weight of 0.7 and the "modified exponential" model (Youngs *et al.*, 1987) a weight of 0.3. For both the characteristic and "modified exponential" models, M_{max} for a fault is assumed to be uniformly distributed in the range $M_{max} \pm 3$ magnitude unit, with $M_{max} + 3$ being the upper-bound magnitude, m^u.

Where recurrence intervals are provided, we use the method of Youngs and Coppersmith (1985) that assumes a constant frequency of earthquakes above some specified size. Given M_{max} for a fault, the cumulative frequency for earthquakes of M_{max} - 3 is set equal to the inverse of the tabulated recurrence interval, which is interpreted to represent the frequency of characteristic-size events for the fault.

Based on seismicity recurrence calculations provided (Section 3.1 contains a description of the methodology used to calculate seismicity parameters) from diverse regional area sources within 300 km of Yucca Mountain, our assessed distribution for the b-value (and relative weighting) in applying the methodology of Youngs and Coppersmith (1985) are:

0.80 (0.3), 1.00 (0.4), 1.20 (0.3).

REGIONAL SOURCES AND LOCAL BACKGROUND SOURCE ZONES

5.1 CATALOG

For all calculations, we place full weight on Version 7 of the Yucca Mountain earthquake catalog, which consists of primary events derived using the declustering algorithm of Veneziano and Van Dyck (1985). We believe their algorithm is statistically rigorous and far superior to declustering approaches that use fixed space-time windows as a function of mainshock size, given that mainshocks are known to generate clusters having characteristics that differ greatly in space, time, and size—even in the same general area. Our judgment here is guided by substantial experience of one team member with the practical problems of declustering earthquake catalogs (W.J. Arabasz presentation at SSC Workshop 2).

Completeness intervals adopted for the 100-km-radius declustered catalog are those proposed by I.G. Wong (handout to team seismologists at SSC Workshop 4), based on the completeness technique of J. C. Stepp (NOAA, written communication, 1973). We examined "Stepp" plots specifically for the Version 7 catalog before adopting the intervals. The completeness intervals are: 2.5-2.99 (1979 to date), 3.0-3.49 (1979 to date), 3.5-3.99 (1961 to date), 4.0-4.49 (1934 to date), 4.5-4.99 (1934 to date), 5.0-5.49 (1924 to date), 5.5-5.99 (1924 to date), and 6.0-6.49 (1914 to date). Where seismicity is sampled from regions extending beyond 100 km, we gave approval to use the same completeness intervals, recognizing that any incompleteness at the lower magnitude end would simply require selecting a higher minimum magnitude in the recurrence modeling. For the 100-km-radius area, the minimum magnitude we accepted for recurrence modeling was 2.5, with a weight = 0.3, and 3.0, with a weight = 0.7.

To delimit seismicity induced by underground nuclear explosions (UNEs) in the Nevada Test Site, we eliminate from the catalog all seismic events that lie within a zone defined by Rogers *et al.* (1987, their Figure 2) that occurred post 1950.

5.2 BACKGROUND SOURCE ZONES COUPLED TO REGIONAL SOURCES

We define our background source zones to lie within a radius of 100 km of the repository site. Three alternatives in which background source zones are coupled to regional area sources are depicted on Figures AAR-7 to AAR-9. A fourth alternative, based on spatially smoothed seismicity, is discussed in the next section. For the first three scenarios, large regional sources are defined for capturing seismicity. Seismicity is first gathered from the entirety of each regional source (except the area of exclusion for UNEs and associated seismicity). It is then normalized per unit time and unit area and assigned to the corresponding sector of the area source that lies within 100 km of the repository site—including the 20-km-radius "host zone" (explained below).

In scenario I (Figure AAR-7), we depict three background source zones that form parts of an eastern California shear zone (1), a Nevada Walker Lane belt (2), and the northern Basin and Range (3A), respectively. In scenario II (Figure AAR-8), the Walker Lane belt is not considered distinct from the northern Basin and Range (3B). In scenario III (Figure AAR-9), the southern Nevada transverse zone (3C) (e.g., Rogers *et al.*, 1991) is taken as a distinct subarea of the northern Basin and Range, parts of which lie both to its north and south (forming zone 3D).

5.3 BACKGROUND SOURCE ZONE BASED ON SPATIALLY SMOOTHED SEISMICITY

Given the spatial variability of epicentral density in the declustered Yucca Mountain catalog, we also consider a background source zone based on spatial smoothing of declustered seismicity within 100 km of the repository site. Values for the kernel width, h (i.e., 2 the distance seismicity effectively can be smoothed away from its location), and corresponding weighting are as follows: 5 km (0.25), 10 km (0.5), 20 km (0.25) (Figure AAR-10b). Where a prior b-value is used, we use the same distribution (and weighting) described for the recurrence modeling of our regional and local fault sources: 0.80 (0.3), 1.00 (0.4), 1.20 (0.3).

5.4 HOST ZONE

We define a local background source region, with an M_{max} of 6.3 ± 0.3, as extending in a 20-km radius from the repository site, within which we are confident that we have identified all fault-specific sources capable of generating earthquakes larger than the background. This "host zone" is defined only for assigning its own M_{max}. Recurrence rates derive from the applicable scenario for the background source zone within which the host zone is embedded. We use data and the results of modeling presented by S. K. Pezzopane and T. E. Dawson (USGS, written communication, 1996) for the maximum background earthquake to assess the following distribution for M_{max} of the host zone (with corresponding weighting):

6.0 (0.3), 6.3 (0.4), 6.6 (0.3).

5.5 M_{max} FOR BACKGROUND SOURCE ZONES > 20 km

Beyond 20 km—and out to 100 km—we admit the possibility that there may be faults (buried, unrecognized, or not included in our inventory of fault sources because of an interpreted lack of Quaternary slip) that may be capable of generating earthquakes larger than M = 6.3 ± 0.3. An example would be the Gravity fault, for which a Quaternary displacement history is not established and which we interpret to be distinct from, but possibly related to, the Ash Meadows fault. Accordingly, we assign a higher M_{max} to our background source zones from 20 to 100 km radial distance from the repository site to account for these potential sources. The distribution also is used to model seismicity rates for the regional sources.

For our assessment of this M_{max} we used data from Table AAR-1 for regional fault sources within 100 km of Yucca Mountain (excluding the Death Valley and Furnace Creek faults and the linked case for the Amargosa River/Pahrump faults). From these data we constructed cumulative distributions of maximum rupture lengths (using preferred and maximum values only) and slip rates. Simply put, we use what can be seen as representative of what cannot be seen or has been missed. (Simultaneously, we considered dimensional arguments for possibly unrecognized intra-basin faults.)

Using the above data and the same weighted M_{max} approaches used for the regional faults, our resulting distribution for the generic M_{max} for all background sources > 20 km (with corresponding weighting) is:

6.6 (0.3), 6.9 (0.4), 7.3 (0.3).

5.6 WEIGHTING OF ALTERNATIVES FOR BACKGROUND SOURCE ZONES

Our weighting scheme for alternative background source zones takes into account the stationarity of seismicity vis-à-vis a 10,000-yr time frame. We give higher weight to scenarios in which seismicity rates near the site are similar to those in distinct regional zones in which regional seismicity (mainshocks per unit time and area) is interpreted to be representative of a stationary pattern over thousands of years. Thus, spatially smoothed seismicity, which reflects localization of seismicity from the short instrumental time sample, is down-weighted. In our section on Tectonic Models, we discuss the uncertain relative influence on the regional stress field of WNW-ESE Basin and Range extension, NW-SE dextral shear, and general N-S basal traction and/or horizontal compression. This uncertainty leads us to give equal weight to the three scenarios based on regional seismotectonics. Our weights, then, are:

0.3: Scenario I (Zones 1, 2, 3A)
0.3: Scenario II (Zones 1, 3B)
0.3: Scenario III (Zones 1, 3C, 3D)
0.1: Spatially Smoothed Seismicity.

5.7 NON-INCLUSION OF A VOLCANIC ZONE

We considered the need to account for seismicity associated with episodic volcanism in the Crater Flat domain and concluded that it is unnecessary to include a volcanic source zone in addition to a spatially coincident background source zone. Our reasoning is as follows: An appropriate M_{max} for volcanic-related seismicity in the Yucca Mountain region is M 5.0 to M 5.5 (Smith *et al.*, 1995, 1996). Given that the project definition of seismogenic implies the generation of earthquakes of $M \geq 5.0$, the question becomes, "How often are volcanic-related earthquakes of M 5.0 to M 5.5 likely to occur in the Crater Flat domain?"

According to (B. M. Crowe *et al.*, LANL, written communication, 1995, p. i), postcaldera basaltic volcanism in the Yucca Mountain region represents "one of the lowest eruptive rates in a volcanic field in the southwest United States." More specifically, estimates of the maximum or worst-case recurrence (minimum interevent time) for volcanic events in the Yucca Mountain region are 8.0×10^{-6} events yr^{-1} (1/N = 125,00 yr) using homogeneous Poisson models and 8.4×10^{-6} events yr^{-1} (1/N = 119,000 yr) using nonhomogeneous Poisson models (ibid., p. 7-2f).

We examined the recurrence rates for background seismicity in the Yucca Mountain region calculated for DOE's 1994 design study for the ESF (I.G. Wong presentation at SSC Workshop 3). The cumulative annual number of events per km^2 above $M_{min} = 2.5$ and with $M_{max} = 6.5$ is given by $\log N = -1.37 - 0.83M$. (We assume equivalency between M_L and moment magnitude for the magnitude range being considered.) From the above, the expected annual number of events per km^2 in the range $5.0 \leq M < 5.5$ is 1.8×10^{-6} events yr^{-1} km^{-2}.

For comparison, we provisionally considered a volcanic source zone in the southwestern part of the CFD that has an area of approximately 1.4×10^3 km^2 smaller (and hence containing more events yr^{-1} km^{-2}) than the area of potential volcanism considered by B. M. Crowe *et al.* (LANL, written communication,1995). The number of background seismic events in the range $5.0 \leq M < 5.5$ within our volcanic source zone would be 1.8×10^{-6} events yr^{-1} km^{-2} * 1.4×10^3 km^2 or 2.52×10^{-3} events yr^{-1} (1/N = 397 yr).

From the above, we compared the rate of background seismic events within our volcanic source zone (2.52×10^{-3} events yr^{-1}) to the estimated worst-case rate of volcanic events with which earthquakes would be associated—$(8.0\text{-}8.4) \times 10^{-6}$. The rate of volcanic events is two to three orders of magnitude lower than the rate of M5.0 to M5.5 background earthquakes within our volcanic source zone—beyond the precision with which background seismicity can be estimated.

Thus, we concluded that there is no need to define a volcanic source zone in addition a spatially coincident background source zone. Background earthquakes in the range of

M5.0 to M5.5 sufficiently represent, for probabilistic vibratory ground-motion hazard, the rare episodic occurrence of volcanic-related earthquakes in the same magnitude range.

6.0
FAULT DISPLACEMENT CHARACTERIZATION

6.1 GENERAL REMARKS

Our methodology for characterizing the potential for fault displacement at Yucca Mountain has been influenced greatly by the presentations and interactions at SSC Workshops 4, 5, and 6. In order to characterize, in a probabilistic way, the amount, frequency, and variability of future fault displacements at a point, we use two basic approaches: (i) an earthquake approach that builds on our seismic source characterization for ground-motion hazard and (ii) a displacement approach in which the observed geology guides the expectation of the long-term outcome.

From the outset, we have held the view — based chiefly on empirical observations and a substantial literature in structural geology (see, for example, the February-March 1996 Special Issue of the Journal of Structural Geology) — that scaling relationships variously involving single-event slip, fault dimension, and total cumulative displacement on a fault offer a practical way to characterize fault-displacement potential. This applies particularly to a displacement approach.

We recognize that any use of scaling relationships in the context of earthquakes and faulting can be expected to invite scrutiny and concern. There is ongoing debate about the scaling of earthquake slip with source dimensions, particularly as it relates to implications for underlying mechanics and the dynamics of rupture propagation (e.g., Bodin and Brune, 1996, and references therein). Controversy about scaling relations for large earthquakes is a notable case in point (Romanowicz and Rundle, 1993).

In our final methodology we have taken care to use only scaling relations that are empirically founded and defensible from documented observations in the Yucca Mountain region and/or by supporting reference to the published literature. We specifically avoid assumptions about